AEDC-TR-79-4

cy.2

COMPUTER PROGRAM FOR CALCULATION OF SEPARATED TURBULENT FLOWS ON AXISYMMETRIC AFTERBODIES INCLUDING EXHAUST PLUME EFFECTS

Gary D. Kuhn

NIELSEN ENGINEERING AND RESEARCH, INC
510 CLYDE AVENUE
MOUNTAIN VIEW, CALIFORNIA 94043

March 1979

Final Report for Period July 5, 1977 — September 5, 1978

Approved for public release; distribution unlimited.

Prepared for

ARNOLD ENGINEERING DEVELOPMENT CENTER/DOTR
ARNOLD AIR FORCE STATION, TENNESSEE 37389

NOTICES

When U. S. Government drawings, specifications, or other data are used for any purpose other than a definitely related Government procurement operation, the Government thereby incurs no responsibility nor any obligation whatsoever, and the fact that the Government may have formulated, furnished, or in any way supplied the said drawings, specifications, or other data, is not to be regarded by implication or otherwise, or in any manner licensing the holder or any other person or corporation, or conveying any rights or permission to manufacture, use, or sell any patented invention that may in any way be related thereto.

Qualified users may obtain copies of this report from the Defense Documentation Center.

References to named commerical products in this report are not to be considered in any sense as an indorsement of the product by the United States Air Force or the Government.

This final report was submitted by Nielsen Engineering and Research, Inc., 510 Clyde Avenue, Mountain View, California 94043, under contract F40600-77-C-0008, with the Arnold Engineering Development Center/DOTR, Arnold Air Force Station, TN 37389. Mr. E R. Thompson, DOTR, was the AEDC Project Engineer.

This report has been reviewed by the Information Office (OI) and is releasable to the National Technical Information Service (NTIS). At NTIS, it will be available to the general public, including foreign nations.

APPROVAL STATEMENT

This report has been reviewed and approved.

Elton R. Thompson
ELTON R. THOMPSON
Project Manager, Research Division
Directorate of Test Engineering

Approved for publication:

FOR THE COMMANDER

Robert W. Crossley
ROBERT W. CROSSLEY, Lt Colonel, USAF
Acting Director of Test Engineering
Deputy for Operations

REPORT DOCUMENTATION PAGE

READ INSTRUCTIONS BEFORE COMPLETING FORM

1 REPORT NUMBER: AEDC-TR-79-4	2 GOVT ACCESSION NO.
	3 RECIPIENT'S CATALOG NUMBER
4 TITLE (and Subtitle): COMPUTER PROGRAM FOR CALCULATION OF SEPARATED TURBULENT FLOWS ON AXISYMMETRIC AFTERBODIES INCLUDING EXHAUST PLUME EFFECTS	5 TYPE OF REPORT & PERIOD COVERED: Final Report - July 5, 1977 - September 5, 1978
	6 PERFORMING ORG REPORT NUMBER: NEAR TR 165
7 AUTHOR(s): Gary D. Kuhn	8 CONTRACT OR GRANT NUMBER(s): F40600-77-C-0008
9 PERFORMING ORGANIZATION NAME AND ADDRESS: Nielsen Engineering & Research, Inc. 510 Clyde Avenue Mountain View, CA 94043	10 PROGRAM ELEMENT PROJECT, TASK AREA & WORK UNIT NUMBERS: Program Element 65807F
11 CONTROLLING OFFICE NAME AND ADDRESS: Arnold Engineering Development Center/OIS Air Force Systems Command Arnold Air Force Station, Tennessee 37389	12. REPORT DATE: March 1979
	13 NUMBER OF PAGES: 130
14 MONITORING AGENCY NAME & ADDRESS (if different from Controlling Office)	15. SECURITY CLASS. (of this report): UNCLASSIFIED
	15a. DECLASSIFICATION DOWNGRADING SCHEDULE: N/A

16 DISTRIBUTION STATEMENT (of this Report)

Approved for public release; distribution unlimited.

17 DISTRIBUTION STATEMENT (of the abstract entered in Block 20, if different from Report)

18 SUPPLEMENTARY NOTES

Available in DDC

19 KEY WORDS (Continue on reverse side if necessary and identify by block number)

compressible flow
finite-difference methods
interaction methods
separated flow
computer programs
integral methods
turbulent boundary layers
transonic flow
inviscid flow
entrainment
exhaust plumes

20 ABSTRACT (Continue on reverse side if necessary and identify by block number)

A computer code for a turbulent boundary-layer, inviscid interaction method for axisymmetric configurations of the type used for isolated nozzle afterbody models is presented. The method is applicable to flows with subsonic free streams, including slightly supercritical flows and to bodies with either high pressure exhaust plumes or solid plume simulators. The method consists of an integral boundary-layer and plume-entrainment method and a finite-difference inviscid-flow method which are coupled iteratively

20. ABSTRACT (Continued)

through the boundary-layer displacement thickness. Both attached and separated boundary layers can be calculated. An option is provided for calculating two-dimensional boundary layers. The procedure for separated flows is to specify the displacement thickness of the boundary layer and calculate the free-stream velocity distribution from both the boundary-layer equations and the inviscid-flow equations. The separation point location and the angle of the displacement surface are found by an iterative procedure. Comparisons with experimental data indicate that the entrainment model and the viscous-inviscid iteration procedure provide an accurate engineering method for predicting boattail flow fields for moderately underexpanded exhaust flows, and for boattails with solid exhaust plume simulators. The equations programmed are presented along with detailed instructions for the preparation of input data, description of the program output and instructions for operation of the program on an IBM 370 computer. Sample cases are provided for a complete axisymmetric interaction calculation and for a two-dimensional boundary-layer calculation.

AFSI
Arnold AFS Tenn

PREFACE

The results reported herein were developed for the Arnold Engineering Development Center, Air Force Systems Command, by Nielsen Engineering & Research, Inc. under Contract F40600-77-C-0008. The Air Force Project Engineer for this contract was E. R. Thompson, AEDC/DOTR. This report covers the work done during the period July 5, 1977 to September 5, 1978. The reproducibles used in the reproduction of this report were provided by the author.

TABLE OF CONTENTS

TABLE OF CONTENTS (Concluded)

COMPUTER PROGRAM FOR CALCULATION OF SEPARATED TURBULENT FLOWS ON AXISYMMETRIC AFTER-BODIES INCLUDING EXHAUST PLUME EFFECTS

by Gary D. Kuhn

Nielsen Engineering & Research, Inc.
Mountain View, California

1.0 INTRODUCTION

One of the critical areas in the design of both aircraft and missiles is the interaction between propulsive jets and the external flow over the aerodynamic shapes from which they issue. The drag of the afterbody and exhaust nozzle can be a significant fraction of the total vehicle drag. In order to obtain knowledge of the afterbody and nozzle flow fields and their interaction as early as possible in the design procedure, it is desirable to have a fast computational method for accounting for the viscous flow over the afterbody including separation on the body and entrainment of the flow by the exhaust jet. Such a method should also account for the interaction between the external inviscid flow and the viscous flow.

This paper describes a method for predicting the viscous flow field about an axisymmetric body at zero angle of attack with a cylindrical sting or an exhaust jet. Several previous methods for calculating such flows have employed empirical or approximate methods of predicting the location of separation and the characteristics of the separated flow region (c.f. ref. 1 and 2). The method described herein uses insights from those methods to establish first approximations which are subsequently refined by iteration to satisfy the viscous-inviscid interaction more completely. The method combines a finite difference inviscid-flow method with integral methods for the boundary layer and exhaust plume mixing layer. An eddy viscosity is used to account for the Reynold's stresses.

The basic principle of the viscous-inviscid interaction calculation is to define a displacement surface for the viscous layer which forms an effective boundary for the inviscid flow and which is compatible with the resulting inviscid pressure distribution. When the boundary layer is separated, special techniques are needed to determine the appropriate boundary layer solution. In the case of a body with a solid sting, boundary layer theory is used for the entire viscous region. However, if the sting is replaced by an exhaust jet, the merging of the boundary layer with the exhaust plume mixing layer must be

accounted for. Thus, in this work, an entrainment model was developed which allows the viscous interaction between the separated boundary layer and the exhaust plume to be calculated.

Since the principle of the viscous-inviscid interaction is the same whether a sting or a plume exists downstream of the body, the elements of the calculative method will be described in the following order. First, the overall viscous-inviscid interaction method will be described in order to provide a framework for explaining the various individual components of the method. Next, the method used to calculate the external inviscid flow will be presented. That presentation will be brief since the method has been described in detail in other reports. Following the description of the external inviscid flow method will be the method used to calculate the inviscid exhaust plume flow. Next, the boundary layer calculative method will be presented, followed by the exhaust plume entrainment model. Finally, some comparisons with experimental data are shown, illustrating the capabilities of the method. The remainder of this report contains a description of the computer programs associated with the calculative methods followed by detailed instructions for the use of the programs. The composite computer program described herein contains the boundary-layer and entrainment programs developed for this work and an inviscid-flow program which is essentially the same as that described in reference 3. Both programs are incorporated as subprograms into a mainline program which performs iterations to calculate the flow for axisymmetric bodies of the type used for nozzle boattails.

The programs are written in the FORTRAN programming language for use on an IBM 370 computer. The boundary-layer program retains the capability to calculate two-dimensional flows as an option. Both the boundary-layer program and the inviscid-flow program can be used individually, without iterating if so desired.

2.0 VISCOUS-INVISCID INTERACTION METHOD

Separation is the result of an adverse pressure gradient causing reversal of the low-energy, low-momentum fluid near the wall in the boundary layer. The adverse pressure gradient is determined by the inviscid flow field and is the net result of the body shape and the displacement effect of the boundary layer. Thus, the viscous and inviscid flow fields are interdependent. Accounting for this interdependence with an interaction model is made difficult by the fact that the boundary-layer equations are parabolic and therefore cannot respond to disturbances downstream of local stations, while for subsonic and transonic flows the inviscid flow is elliptical and therefore subject to influence

by the entire flow field. In the method described herein, the viscous-flow and inviscid-flow methods are used alternately in an iterative scheme.

The major difficulty encountered in calculating viscous-inviscid interactions with boundary layer separation is the problem of obtaining a smooth surface for coupling the viscous and inviscid flows. It is well known that for both laminar and turbulent boundary layers, the usual boundary layer equations exhibit singular behavior at the point of zero skin friction when the pressure gradient is prescribed. The details of the method used to avoid this singular behavior will be described in Section 5 of this report, along with the description of the integral boundary-layer method. For the present discussion, it is sufficient to note that a method is available for calculating a smooth surface which represents the displacement effect of the boundary layer, or exhaust plume entrainment layer, including boundary layer separation. The surface is constructed in two parts. In regions of attached flow, or far downstream in the exhaust plume mixing layer, the surface shape is calculated from a solution of the viscous flow equations with the velocity at the edge of the boundary layer prescribed from a calculation of the external inviscid flow. This velocity will subsequently be called the "inviscid velocity." In regions of separated flow, the edge velocity is calculated from the viscous flow equations with the boundary layer displacement thickness prescribed. This velocity is called the "viscous velocity." An iteration is performed to determine the surface shape so that the "viscous velocity" matches the "inviscid velocity" from the inviscid flow calculation.

2.1 ESTIMATION OF BOUNDARY OF SEPARATED REGION

The first step in calculating the viscous-inviscid interaction is to calculate the inviscid flow over the plain body. The resulting distribution of the velocity at the boundary is then prescribed as the boundary-layer-edge velocity, u_e, for the boundary-layer calculation. If strong adverse pressure gradients exist, the boundary-layer calculation may exhibit a singularity where the skin-friction coefficient approaches zero and the numerical calculation can proceed no further with u_e prescribed. This point is not necessarily the true location of separation, however, since the interaction with the inviscid flow has not yet been accounted for. A first approximation to the separation point location, x_s is obtained by a method which will be described in Section 5, along with the detailed description of the boundary layer method.

At the separation point, x_s the boundary-layer calculation is carried on into the separated flow using a prescribed distribution of the boundary layer displacement thickness, δ^*. The result of that calculation is a solution for the boundary-layer-

edge velocity (the "viscous velocity") which may or may not agree with the "inviscid velocity" produced by the inviscid flow theory. An iterative procedure is used to find the particular variation of δ^* downstream of x_s for which the "viscous velocity" and the "inviscid velocity" agree.

A two-parameter analytical formulation is used to represent the effective displacement surface between separation and a point downstream of reattachment or in the plume entrainment region (fig. 1). Thus, the effective body shape is given by

$$r = r_w + \delta^* \quad \text{for} \quad 0 < x < x_s \quad \text{and} \quad x_p < x < \infty \tag{1}$$

$$r = (r_w + \delta^*)_s + (x - x_s)\tan\theta_s \quad \text{for} \quad x_s < x < x_p \tag{2}$$

A first approximation to the angle, θ_s, is obtained from an expression presented in reference 4.

$$\theta_s = \tan^{-1}[(r_w)_x] + 14.4 - 4.89M_s \quad \text{(degrees)} \tag{3}$$

Downstream of x_p the boundary-layer-edge velocity is again prescribed on the viscous flow calculation as the inviscid boundary velocity from the previous calculation.

2.2 ITERATION PROCEDURE

The method developed in this work consists of two iterations. One iteration is used to locate the separation point, x_s and determine the angle, θ_s, of a conical displacement surface. The second iteration calculates the best solution for the specific values of x_s and θ_s. The iteration procedure is described schematically in figure 2.

The iteration procedure consists of two cycles. In the inner cycle, the inviscid flow and the boundary layer are calculated alternately until the largest change in the δ^* solution between iterations becomes smaller than a specified percent of the nozzle radius and simultaneously, the inviscid calculation procedure converges to a specified tolerance. At each step of the cycle, the boundary-layer displacement thickness is used to calculate an augmented body shape by the relation

$$r_n = r_w + \alpha\delta_n^* + (1 - \alpha)\delta_{n-1}^* \tag{4}$$

where r_n is the effective body radius at iteration n, and α is a damping factor, usually equal to 0.5.

When the inner cycle has been terminated, the calculation is complete if no separation occurred. However, if separation is present, there exist two solutions for the boundary-layer-edge velocity as described previously. The next step of the procedure is to calculate the squared deviation between the two velocity solutions downstream of x_s at corresponding points. The accuracy of the matching of the two solutions is then indicated by the value of the rms error, s, where

$$s = \left[\sum_{1}^{N} \left(u_{e_V} - u_{e_I} \right)^2 / \left(u_{e_o}^2 N \right) \right]^{1/2} \tag{5}$$

where u_{e_V} is the "viscous velocity", u_{e_I} is the "inviscid velocity", and u_{e_o} is the free stream velocity. This quantity is then compared with the value from the previous iteration and if a minimum has not been found, x_s and θ_s are adjusted in an appropriate manner, the boundary layer is recalculated using the new values of x_s and θ_s and the calculation reenters the inner cycle. This process is repeated until a minimum of the rms error, s, is found or until the value of s is less than a specified amount. For practical purposes, a value of s of 0.01 or less is usually adequate.

The manner in which x_s and θ_s are adjusted will now be described. The first value of s (equation (5)) is calculated using the estimated values of x_s and θ_s. The next step is to change θ_s a small amount (.25 degree) and calculate a second value of s. The third step is to change x_s a small amount, keeping θ_s at the original value, to calculate a third value of s. With these three solutions, the gradient of s with respect to x_s and θ_s is calculated from

$$s_\theta = \frac{\partial s}{\partial \theta_s} = \frac{s_2 - s_1}{\Delta \theta_s} \tag{6}$$

$$s_x = \frac{\partial s}{\partial x_s} = \frac{s_3 - s_1}{\Delta x_s} \tag{7}$$

The maximum rate of decrease of s with respect to x_s and θ_s should be in the direction of the negative of the gradient. Therefore, both x_s and θ_s are adjusted according to

$$\Delta x_s = -k \left| \sin \alpha \right| \frac{s_x}{|s_x|} L \tag{8}$$

$$\Delta\theta_s = -k \cos \alpha \frac{s_\theta}{|s_\theta|} \tag{9}$$

where

$k = .003$

L = the length of the body

$\alpha = \tan^{-1}\left(\frac{s_x}{s_\theta} L\right)$

After the third iteration, both quantities are adjusted along the direction of the negative gradient until either the tolerance is met or a minimum value of s is reached. If a minimum is found without satisfying the tolerance, the sequence is restarted, calculating a new gradient direction, using half steps for each subsequent adjustment of x_s and θ_s. If this procedure does not produce a value of s less than the specified tolerance after four restarts, the sequence is terminated.

A third element in the iteration procedure is the calculation of the inviscid exhaust plume. In the theory to be presented subsequently, the entrainment of the boundary layer flow and the turbulent mixing between the external inviscid flow and the exhaust plume flow are assumed to take place along a boundary defined by the radius of the exhaust plume with all mixing neglected. This "inviscid reference surface" is calculated twice during the iteration process described previously. The first plume calculation is performed assuming a constant external pressure. This gives a first approximate jet boundary upon which the viscous-inviscid iteration can be initiated. After 4 cycles of the iteration, a new exhaust plume is calculated using the external pressure distribution that exists at that time as calculated by the inviscid theory. Tests in which the plume was calculated a third time using the final converged pressure distribution indicated that only a slight change in the plume occurred. The effect on the flow characteristics on the body was small. Thus, the solution is not sensitive to the exact shape of the jet mixing boundary.

3.0 INVISCID-FLOW MODEL

The inviscid-flow method employed herein is the method of South and Jameson described in reference 5. The computer program used is that described in reference 3 with minor modifications

to accommodate the iteration between the inviscid and viscous flows. The detailed derivation of the flow equations, the calculative method, and the computer program are contained in references 3 and 5 and will not be repeated here.

The inviscid-flow method calculates the flow field about axisymmetric bodies by a finite-difference solution of the exact equation for the disturbance potential for axisymmetric compressible flow. The only simplifying assumption that is used is that the flow is isentropic. Thus, the entire subsonic velocity range can be calculated, and slightly supersonic free-stream Mach numbers are permissible so long as entropy production by shock waves is negligible. In addition, blunt as well as slender bodies can be treated accurately. A general description of the program is summarized here from reference 3.

"One of the important considerations when trying to solve the full potential equation is the choice of a coordinate system. For complex three-dimensional shapes cartesian coordinates may be best; however, for simpler two-dimensional or axisymmetric shapes the use of a coordinate transformation such that the body lies along a coordinate line can greatly simplify the application of the exact boundary condition at the body surface. The program described in this paper uses a body-normal coordinate system for closed bodies. For open bodies (i.e., bodies with a sting or simulated wake) it uses a body-normal system on the forebody up to the first horizontal tangent and a sheared cylindrical coordinate system* aft of that point. This coordinate system is suitable for closed bodies which are blunt on both ends and convex and smooth over the entire body or for open bodies which are blunt-nosed and convex and smooth up to the first horizontal tangent. It is possible to treat pointed bodies and bodies with slope discontinuities but the coordinate system is not well suited for them and their solution may not be so accurate as the blunt-body solutions."

"A stretching is applied to both the normal and tangential coordinates such that the infinite physical space is mapped to a finite computational space. Thus, the boundary condition at infinity can be applied directly and there is no need for an asymptotic far-field solution. Details about the stretching functions are given in (reference 3) appendix A."

"The general method of solution is to replace the governing second-order partial differential equation with a system of

---

*The origin of the x, r, θ coordinate system is shifted from the body axis to the body surface in a parallel transformation.

finite-difference equations, including Jameson's rotated difference scheme at supersonic points. The difference equations are solved by a column relaxation method."

"The boundary condition at the body surface is applied through the use of dummy points inside the body. Details of this computation are given in (reference 3) appendix B."

4.0 INVISCID PLUME MODEL

The inviscid exhaust flow calculation method used in this work is the same as the Henson and Robertson shock-expansion/one-dimensional method (reference 6) with two exceptions:

1. Compressions are computed as reverse Prandtl-Meyer expansions rather than by means of Newtonian impact theory.

2. Flow areas are computed as plane areas normal to the nozzle centerline rather than as spherical areas (normal to the nozzle centerline and the local plume contour).

A diagram of the nozzle plume region is shown in figure 3. The plume shape is calculated in a series of straight line segments which approximate the curved shape of the plume. The external pressure is compared with the internal pressure at the exit plume boundary point and at each consecutive boundary point, and an expansion or compression turn is calculated depending on the comparison.

The expansion or compression at the nozzle exit is computed by means of the Prandtl-Meyer relationships from specified values of the nozzle expansion angle and the exhaust jet Mach number such that the local external pressure is matched. This calculation yields M_{12}, the Mach number at the upstream end of the first plume segment and the inclination of this segment (the local flow direction). The local flow angle is used to compute the radius at the next downstream point, r_2 from which follows the area, A_2. The Mach number at the downstream end of the segment, M_{21}, is then computed from the one-dimensional relationship

$$(A/A^*)_{21} = (A/A^*)_{12} \, A_2/A_1 \qquad (10)$$

The Mach number at the upstream end of the second segment, M_{22}, is then determined by matching the internal static pressure to the local external static pressure at point 2 by means of an expansion or compression beginning at a flow direction equal to that of the first segment and the Mach number M_{21}. The Mach

number at the downstream end of the segment, M_{31}, is then computed by applying equation (10) to the second segment. Successive segments are constructed in the same manner until the plume boundary becomes parallel with the nozzle centerline.

The plume boundary velocity, q_p, corresponding to each axial station is computed from isentropic relations with the specified nozzle stagnation conditions. Thus

$$q_{p_2} = a_t M_{22}\left[1 + \frac{1}{2}(\gamma_p - 1)M_{22}^2\right]^{-1/2} \tag{11}$$

where

a_t = The sound speed corresponding to the nozzle stagnation temperature

γ_p = The ratio of specific heats of the plume gas

In order to approximate the velocity distribution in each cross section of the plume, the flow is assumed to be locally source-like, so that the velocity components required at r_c, the inner boundary of the turbulent mixing layer are approximated by

$$u_c = q_p\left[1 + \left(\frac{r_c}{r_w}\frac{dr_w}{dx}\right)^2\right]^{-1/2} \tag{12}$$

$$v_c = u_c \frac{r_c}{r_w}\frac{dr_w}{dx} \tag{13}$$

5.0 DEVELOPMENT OF BOUNDARY-LAYER METHOD

The complete derivation of the governing equations for the boundary layer has been presented in reference 7. In this report the derivation is summarized and modified for the application of interest herein.

5.1 ASSUMPTIONS

The analysis is based on the following assumptions:

1. The governing equations are those for a compressible turbulent boundary layer.

2. The air behaves as an ideal gas.

3. The molecular viscosity, μ, is proportional to the temperature.

4. The specific heat of the gas is constant.

5. The wall is either two dimensional or axisymmetric, but can have an arbitrary profile in the direction of flow as long as the longitudinal radius of curvature of the wall is large compared to the boundary layer.

6. The pressure is constant through the boundary layer normal to the wall.

7. The wall temperature is constant.

5.2 BOUNDARY-LAYER EQUATIONS FOR COMPRESSIBLE TURBULENT FLOW

The basic notation and coordinate scheme are shown in figure 4. Note that the same symbols are used for the physical coordinates of both two-dimensional and axisymmetric configurations. Thus, r denotes the distance of a point from the axis of an axisymmetric configuration, x is the distance along the axis, measured from the nose and the dimension y is measured from the body surface normal to the axis. It is noted that these coordinates are not the usual boundary layer coordinates. They are employed to avoid difficulties at sharp concave corners such as a boattail-sting junction.

The governing equations describing the steady flow of a compressible turbulent boundary layer in these coordinates are:

$$(r\rho u)_x + \{r\rho[v - (r_w)_x u]\}_y = 0 \tag{14}$$

$$\rho u u_x + \rho[v - (r_w)_x]u_y = -p_x + (1/r)(r\mu\beta\, u_y)_y \tag{15}$$

$$\rho u S_x + \rho[v - (r_w)_x u]S_y = (1/r)(r\mu\beta S_y)_y \tag{16}$$

where ρ is the density, u and v are the x and y velocity components, β is the eddy viscosity factor, μ is the molecular viscosity, p is the pressure and

$$S = T_t/T_{t_e} - 1 \tag{17}$$

where T_t is the total temperature and e denotes the boundary layer edge. Both laminar and turbulent Prandtl numbers are assumed to be unity.

Equations (14), (15), and (16) are easily applicable to laminar, transitional and turbulent flow. In laminar flow,

substitution of $\beta = 1$ reduces the equations to those for a laminar boundary layer. Further, suitable variation of the eddy viscosity makes the equations applicable to the transition region.

5.3 TRANSFORMATION OF AXISYMMETRIC BOUNDARY-LAYER EQUATIONS

The Probstein-Elliott transformation is (ref. 8)

$$d\tilde{x} = [r_w(x)/L]^2 dx \tag{18}$$

$$d\tilde{y} = [r(x,y)/L] dy \tag{19}$$

where L is an arbitrary reference length, $r_w(x)$ is specified by the body shape and $r(x,y)$ is given by

$$r(x,y) = r_w(x) + y \tag{20}$$

The transformed continuity equation has the form

$$(\rho\tilde{u})_{\tilde{x}} + (\rho\tilde{v})_{\tilde{y}} = 0 \tag{21}$$

where

$$\rho\tilde{u} = \rho u \tag{22}$$

and

$$\rho\tilde{v} = \left(rL/r_w^2\right)\rho\left[v-(r_w)_x u\right] + \left(L^2/r_w^2\right)\tilde{y}_x \rho u \tag{23}$$

Applying the transformation to the momentum and energy equations (15) and (16) yields the transformed equations

$$\rho\tilde{u}\tilde{u}_{\tilde{x}} + \rho\tilde{v}\tilde{u}_{\tilde{y}} = -p_{\tilde{x}} + [(1 + kt\tilde{y})\mu\beta\tilde{u}_{\tilde{y}}]_{\tilde{y}} \tag{24}$$

$$\rho\tilde{u}S_{\tilde{x}} + \rho\tilde{v}S_{\tilde{y}} = [(1 + kt\tilde{y})\mu\beta S_{\tilde{y}}]_{\tilde{y}} \tag{25}$$

where t is the transverse curvature factor

$$t = 2L/r_w^2 \tag{26}$$

and, from equations (19) and (20),

$$\tilde{y} = (r_w/L)y + y^2/2L \tag{27}$$

For flows in which the transverse curvature is small, letting $k = 0$ in equations (24) and (25) produces the equations of a two-dimensional boundary layer. The transverse curvature terms may be negligible for an axisymmetric flow if the body radius is large compared to the boundary-layer thickness. The Probstein-Elliott transformation is thus a first-order correction of the approximate equations for the effect of transverse curvature, allowing the boundary-layer thickness to be of the same order as the body radius.

5.4 TRANSFORMATION OF THE COMPRESSIBLE BOUNDARY-LAYER EQUATIONS

The Stewartson transformation (ref. 9) along with the assumption that the viscosity varies linearly with the temperature and laminar and turbulent Prandtl numbers are unity, reduces the equations of the compressible boundary layer to those of an incompressible boundary layer.

$$U_X + V_Y = 0 \tag{28}$$

$$UU_X + VU_Y = (S + 1)U_e U_{e_X} + C\nu_{e_o}\left[(1 + kt\tilde{y})\beta U_Y\right]_Y \tag{29}$$

$$US_X + VS_Y = C\nu_{e_o}\left[(1 + kt\tilde{y})\beta S_Y\right]_Y \tag{30}$$

where the subscript o refers to reference conditions in the undisturbed free stream.

The coordinate $\tilde{y}$ is not transformed in the transverse curvature terms because integration of the equations across the boundary layer is anticipated and only corresponding values are needed in those terms. The Chapman-Rubesin parameter, C is a constant evaluated at the wall temperature; that is,

$$C = \left(\mu_w T_{e_o}\right)/\left(\mu_{e_o} T_w\right) = \left(T_w/T_{e_o}\right)^{1/2}\left(T_{e_o} + T_s\right)/\left(T_w + T_s\right) \tag{31}$$

where Sutherland's law is used to evaluate the viscosity, with T_s a constant.

In the remainder of this report, the solution of the energy equation (30) will be approximated for boundary layers by the Crocco relation

$$S = S_w(1 - U/U_e) \tag{32}$$

The density profiles are then related to the velocity profiles through the temperature.

$$\rho_e/\rho = T/T_e = T_t/T_e - u^2/(2gJc_pT_e) \tag{33}$$

but

$$c_p = \gamma R/(\gamma-1) \tag{34}$$

So

$$T/T_e = \left(T_t/T_{t_e}\right)\left(T_{t_e}/T_e\right) - u^2/(2gJ\gamma RT_e) \tag{35}$$

or

$$(\rho_e/\rho) = (T/T_e) = (S + 1)(1 + m_e) - m_e(u/u_e)^2 \tag{36}$$

where

$$m_e = \frac{1}{2}(\gamma-1)M_e^2 \tag{37}$$

Thus, the velocity profiles found to be valid for incompressible, two-dimensional turbulent boundary layers can be used by simply transforming the input quantities to the incompressible plane, performing the calculation for an equivalent incompressible boundary layer, and then transforming the results back to the compressible plane, and for an axisymmetric flow, back to the axisymmetric coordinates.

5.5 DEVELOPMENT OF INTEGRAL BOUNDARY-LAYER METHOD

5.5.1 Integral Equations

The integral method used herein was described in detail in reference 10. Families of integral equations are derived by eliminating V between the momentum and continuity equations (28) and (29), and then taking weighted integrals of the resulting equation across the boundary layer.

$$\int_0^{\delta_i}\{UU_X - U_Y\int_0^Y U_X d\eta - (S + 1)U_e(U_e)_X$$

$$- C\nu_{e_o}[(1 + kt\tilde{y})\beta U_Y]_Y\}f(Y)dY = 0 \tag{38}$$

In the present case, the functions

$$f = Y^n \quad ; \quad n = 0, 1 \tag{39}$$

produce the momentum and moment of momentum integral equations, respectively.

5.5.2 Velocity Profiles

The Y dependence of the integral equations is eliminated by substituting an appropriate parametric formulation for the velocity profiles. The function used for the present theory is a modification of the Coles family of profiles (ref. 11) with a laminar sublayer added and the wake function approximated analytically.

$$U = U_\tau[2.5 \ln(1 + Y^+) + 5.1 - (3.39Y^+ + 5.1)\exp(-0.37Y^+)] + U_\beta \sin^2 \frac{\pi}{2} \frac{Y}{\delta_i} \tag{40}$$

The parameter U_τ is the friction velocity

$$U_\tau = (C_f/|C_f|)U_e\sqrt{|C_f|/2} \tag{41}$$

The variable Y^+ is defined to account for the axisymmetry of the flow

$$Y^+ = (L/r_w)(|U_\tau|Y/\nu_{e_o}) \tag{42}$$

The other parameters in equation (40) are δ_i, the transformed boundary-layer thickness and U_β a wake velocity. The exponential terms and the additional unit in the logarithmic term provide a smooth transition from the turbulent flow to the wall through a laminar sublayer.

5.5.3 Eddy Viscosity

The eddy-viscosity model used in this work is an extension of the two-layer model used by Kuhn (ref. 7) including an intermittency function for the outer layer and a modification of the outer layer for adverse pressure gradients and separated flows. In the inner layer of attached flows, the eddy-viscosity parameter, β, is represented by an exponential expression based on the law of the wall. In the outer layer Clauser's expression, modified for adverse pressure gradients, is used along with an intermittency function giving

$$\beta = [0.013+0.0038 \exp(-\delta_k^* p_X/15\tau_w)]U_e\delta_k^*/[1+5.5(y/\delta)^6] \tag{43}$$

where

$$\delta_k^* = \int_o^\delta (1 - u/u_e)dy \tag{44}$$

For favorable pressure gradients, the exponential term in equation (43) is taken to be unity.

For separated flows, the eddy viscosity across the entire layer is represented by a relation based on the velocity profile above the $U = 0$ line.

$$\beta = 0.013[1 + 5.5(y/\delta)^6]^{-1}(U_e/\nu)\int_{Y_{u=0}}^{\delta} (1 - u/u_e)dy \tag{45}$$

5.5.4 Transitional Eddy Viscosity

Transition from laminar to turbulent flow is calculated by letting the eddy viscosity change from a laminar viscosity to a fully turbulent value over a short distance according to the relation (ref. 7)

$$\beta_t = \{1 - \exp[-\kappa(x - x_t)^2]\}(\beta_T - 1) + 1 \tag{46}$$

where κ has been chosen to provide a transition length of approximately ten boundary layer thicknesses, so that

$$\kappa = 0.0001/\delta_t^2$$

and δ_t is the value of δ at the beginning of transition, X_t. The location of X_t must be specified independently.

5.5.5 Equations Solved

Substitution of equation (40) into the two equations produced by equations (38) and (39) produces two ordinary differential equations for the variation of the variables U_τ, U_β, δ_i, and U_e with x. A third equation produced by evaluating equation (40) at $Y = \delta_i$ allows the elimination of U_β from the equations, leaving a set of two equations

$$A_{11}(U_\tau)_x + A_{12}\delta_{i_x} + A_{13}(U_e)_x = B_n \tag{47}$$

$$A_{21}(U_\tau)_x + A_{22}\delta_{i_x} + A_{23}(U_e)_x = B_2 \tag{48}$$

where the coefficients are integrals evaluated from the following definitions.

For n = 1 or 2

$$G_n = 2UY^{n-1} - (n-1)\int_0^Y U dY - \delta_i^{n-1} U_e + (n-1)\int_0^{\delta_i} U dY \qquad (49)$$

$$I_n = \int_0^{\delta_i} Y^{n-1} (S+1) dY \qquad (50)$$

$$J_1 = -CU_\tau |U_\tau| \overline{K} \qquad (51)$$

$$J_2 = -C\nu_{e_o} \frac{r_w}{L} \overline{K} \int_0^{\delta_i} (1 + kt\tilde{y})\beta \frac{\partial U}{\partial Y} dY \qquad (52)$$

with

$$\overline{K} = \frac{r_w}{L} \left(\frac{1 + m_e}{1 + m_{e_o}} \right)^{\frac{1-3\gamma}{2(\gamma-1)}} \qquad (53)$$

The A_{nj} and B_n of equations (47) and (48) become

For n = 1, or 2,

$$\left.\begin{aligned} A_{n1} &= \int_0^{\delta_i} G_n \frac{\partial U}{\partial U_\tau} dY \\ A_{n2} &= \int_0^{\delta_i} G_n \frac{\partial U}{\partial \delta_i} dY \\ A_{n3} &= \int_0^{\delta_i} G_n \frac{\partial U}{\partial U_e} dY - U_e I_n \\ B_n &= J_n - (r_w)_x \int_0^{\delta_i} G_n \frac{\partial U}{\partial r_w} dY \end{aligned}\right\} \qquad (54)$$

These integrals are evaluated numerically, using a simple 11-point trapezoidal integration. More sophisticated approaches were examined, but were not found to effect the calculations significantly. The simpler method was therefore chosen in the interest of speed and cost.

The coefficients A_{nj} and the term B_n are functions of the variables U_τ, δ_i, and U_e. The usual procedure for solving equations (47) and (48) for attached boundary layers is to prescribe the pressure distribution or the boundary-layer-edge velocity distribution, U_e. However, if separation occurs, the pressure distribution cannot be prescribed arbitrarily in the separated region. If an adverse pressure gradient is prescribed for an attached boundary layer, the value of U_τ can approach zero. When U_τ vanishes, the coefficients A_{11} and A_{22} in equations (47) and (48) also vanish, producing a singularity. The singularity can be removed by rearranging the equations so that U_τ is not a dependent variable. One method of accomplishing this is simply to rearrange the equations so that U_τ can be prescribed and U_e can be calculated as a dependent variable as shown in reference 10.

A different method of avoiding the singularity at $U_\tau = 0$ is used herein. The displacement thickness, δ^*, is expressed in terms of U_τ, δ_i, and U_e through the definition

$$\delta^* = \int_0^\delta (1 - \rho u/\rho_e u_e)(r/r_w)dy \tag{55}$$

The result is differentiated with respect to x, producing a third equation.

$$A_{31}(U_\tau)_x + A_{32}\delta_{i_x} + A_{33}(U_e)_x + A_{34}\delta^*_x = B_3 \tag{56}$$

where the A_{31} and B_3 are functions of U_τ, δ_i, and U_e, evaluated from the following definitions

$$G_3 = \frac{\partial}{\partial U}\left(\frac{\rho_e}{\rho}\right) - \frac{1}{U_e} \tag{57}$$

$$I_3 = -\frac{1}{U_e}\int_0^{\delta_i}\left(\frac{\partial}{U_e}\left(\frac{\rho_e}{\rho}\right) + \frac{U}{U_e^2}\right)dy - \frac{1}{U_e}\,\frac{\gamma + 1}{2}\,\frac{M_e}{a_e}\,\overline{K}\delta^* \tag{58}$$

and

$$J_3 = \frac{\delta^*}{r_w} (r_w)_x \left(\frac{1 + m_e}{1 + m_{e_o}}\right)^{-\frac{\gamma + 1}{2(\gamma-1)}} \tag{59}$$

With these definitions, the coefficients A_{3j} and the term B_3 are evaluated by equations (54) for $j = 1,2,$ and 3. The final coefficient, A_{34} is given by

$$A_{34} = -\frac{r_w}{L} \left(\frac{1 + m_e}{1 + m_{e_o}}\right)^{-\frac{\gamma + 1}{2(\gamma-1)}} \tag{60}$$

Like the coefficients A_{11} and A_{21}, the coefficient A_{31} also vanishes when $U_\tau = 0$. However, it can be shown that A_{11}/A_{31} and A_{21}/A_{31} are both finite when $U_\tau = 0$. This allows the three equations, (47), (48), and (56), to be reduced to two ordinary differential equations in the four dependent variables, U_τ, δ^*, δ_i, and U_e. The resulting equations are:

$$a_{11}\delta_{ix} + a_{12}(U_e)_x = b_1 \tag{61}$$

$$a_{21}\delta_{ix} + a_{22}(U_e)_x = b_2 \tag{62}$$

where, with $n = 1$ and 2 and $j = 1$ and 2

$$a_{nj} = (A_{n1}/A_{31})A_{3,j+1} - A_{n,j+1} \tag{63}$$

and

$$b_n = (A_{n1}/A_{31})(B_3 - U_e\delta^*_x) - B_n \tag{64}$$

The value of U_τ can be obtained directly from known values of δ_i, δ^* and U_e by solving the nonlinear relation (55).

Prescribing the distribution of δ^* in equations (61) and (62) and obtaining U_τ from equation (55) is equivalent to prescribing U_τ as described previously.

5.5.6 Method of Solution of Equations

The equations (47) and (48), or (61) and (62) are integrated numerically using the following procedure: If ϕ denotes any one of the variables δ_i, U_e, or U_τ, the value of $d\phi/dx$ at a particular x-station can be calculated from the equations as

functions of the variables themselves. The value of ϕ at the next x-station is then found by means of the elementary predictor-corrector scheme described by Nash and Hicks (ref. 12). Thus,

$$\left.\begin{aligned} \phi_{x+\Delta x/2} &= \phi_x + (d\phi/dx)_x \cdot \frac{\Delta x}{2} \\ \phi_{x+\Delta x} &= \phi_x + (d\phi/dx)_{x+\Delta x/2} \cdot \Delta x \end{aligned}\right\} \tag{65}$$

In the present work, Δx is taken to be 1/16th of each finite-difference step of the inviscid calculational mesh. This provides a fast, accurate method of solution.

5.6 CALCULATION OF SEPARATED BOUNDARY LAYERS

As discussed previously, it is well known that for both laminar and turbulent boundary layers, the usual boundary layer equations exhibit singular behavior at the point of zero skin friction when the pressure is prescribed (or, equivalently, when the boundary-layer-edge velocity is prescribed). Stewartson (ref. 13) suggests that if the boundary layer is to continue downstream of separation, the external stream must adjust itself so that the singularity cannot appear. Furthermore, he says that the solution downstream of separation is no longer specified uniquely by the boundary-layer-edge velocity and the velocity profile at the beginning of the boundary layer. This is another way of saying that the boundary-layer-edge velocity cannot be specified arbitrarily at the separation point, or in the separated flow region downstream. If the solution continued downstream of separation does not satisfy some downstream boundary condition, the separation point must move until the downstream condition is met. It has been observed by many authors (c.f. Cebeci et al, ref. 14 and Gerhart and Bober, ref. 15) that the use of the experimental pressure distribution from a separated flow in a solution of the boundary layer equations does not always produce a singularity. Often the skin friction will simply decrease to some minimum value and then increase, with the calculated boundary layer remaining attached in a region known from experiment to be separated! The reason for this is believed to be due to the neglect of the terms in the Navier-Stokes equations which respond to downstream perturbations, i.e., the normal stress terms and normal pressure gradient terms. On the other hand, the work of Newman (ref. 16) and Simpson (ref. 17) has shown that these terms are negligible a short distance away from separation even though they can be very significant in the immediate vicinity of the separation point.

The approach taken in the present work is an engineering approximation based on the following assumptions:

1. Upstream influences are transmitted predominantly through the external inviscid flow which is elliptical in nature for a locally subsonic flow.

2. Violations of the boundary layer assumptions such as significant normal pressure gradients associated with separation can be neglected on the grounds that they are only important in a small neighborhood of the separation point and have negligible effect on the rest of the flow.

3. The effective boundary which determines the external flow field is a smooth boundary. That is, discontinuities in body slope are smoothed out by the boundary layer.

The significance of assumption number 3 is that a calculative technique which allows singular behavior at the separation point cannot produce a smooth body shape and may lead to instabilities in the iteration between the viscous and inviscid flow calculations. The approach taken herein is to obtain information about the location of the separation point independently from the boundary layer calculation, and simply let the skin friction be zero at that point keeping the boundary-layer-edge velocity and the displacement thickness, δ^* continuous. This means that the variation of C_f upstream of the separation point is probably slightly in error, the amount depending upon the extent of the neglected upstream influence. Also, other important boundary layer quantities may be slightly in error in that region. For many practical cases, however, the errors are not expected to be significant.

As discussed previously, if strong adverse pressure gradients are prescribed in equations (47) and (48), the boundary-layer calculation may reach a point where the friction velocity, U_τ approaches zero and the numerical calculation can proceed no further with u_e prescribed. This point is not necessarily the true location of separation, since the interaction with the inviscid flow has not been accounted for.

A better approximation to the location of separation x_s can be found by computing the shape factor, H_i.

$$H_i = \int_0^{\delta_i} (1-U/U_e)dy \Big/ \int_0^{\delta_i} U/U_e(1-U/U_e)dy \tag{66}$$

For the velocity profiles given by equation (40) this parameter has a value of 4.0 when $U_\tau = 0$. However, experimental measurements indicate that separation actually occurs when H_i is approximately 2.0. This suggests that the present boundary-layer

formulation is not accurate in the vicinity of the separation point. This is not unexpected in the light of the previous discussion. The velocity profiles of equation (40) have been demonstrated to provide a reasonable approximation to both attached and separated boundary layers (ref. 18) but to be of questionable accuracy at the point of zero skin friction. However, the effect of this inaccuracy is believed to be confined to the immediate vicinity of the separation point for the kind of flows of interest here. In order to obtain a smooth solution the first approximation to the value of x_s is taken to be the location at which H_i equals a specified value for the inviscid velocity calculated for the plain body.

When a value of x_s is established, the boundary layer is calculated from the nose of the body to x_s with the distribution of u_e from the external inviscid flow calculation prescribed using equations (47) and (48). At x_s the velocity u_e and the displacement thickness, δ^* are assumed to be continuous (see figure 5). The friction velocity, U_τ, on the other hand, is assumed to be zero as the initial value for the integration into the separated region using equations (61) and (62) with δ^* prescribed. It must be noted that the calculation could be started with a positive value of U_τ and the calculation would proceed through the point where $U_\tau = 0$ for an appropriate δ^* distribution with no singularity. However, due to the approximations inherent in the theory in the vicinity of the separation point, as discussed previously, it is not possible to determine the correct positive values of U_τ approaching separation. It is known that U_τ is zero at x_s. It is the purpose of the iteration procedure discussed previously to find the correct location of x_s.

For bodies of the type of interest herein, the imposition of a conical displacement surface corresponds to an increasing δ^* to the end of the body (figure 5c). When the plume or the sting surface is reached, δ^* begins to decrease. Correspondingly, U_τ, beginning at zero at x_s becomes negative, and increases in magnitude until the end of the body is reached. For a sting, U_τ then moves back toward zero, and eventually becomes positive (reattachment). At some point after reattachment, the calculation procedure must be changed back to the u_e prescribed mode using equations (47) and (48). The determination of the point, x_p for this switch is based on the behavior of the velocity, u_e, produced by the boundary layer solution. As shown in figure 5, u_e becomes nearly constant in the increasing δ^* region between x_s and the end of the body. Then, as the boundary layer proceeds toward reattachment, u_e decreases, eventually reaching a minimum a short distance downstream of reattachment. If δ^* is prescribed beyond the point where the minimum velocity is reached, a singularity develops in the boundary layer solution. To avoid this

singularity, the minimum point is designated as x_p and the solution is switched back to the u_e prescribed mode (equations (47) and (48)) with a u_e distribution constructed by fairing the viscous velocity from the minimum value into the inviscid distribution.

The procedure just described was found to produce an effective body shape which allowed the viscous and inviscid velocity distributions to be approximately matched. However, to achieve a matching of the magnitude of the two velocities and locations of the minimum velocity on the sting, it was found to be necessary to adjust the value of U_τ at x_p. If the calculated value of C_f at that point is less than 0.001, the initial value of U_τ for the calculation downstream of x_p is adjusted to produce a value of C_f of 0.001.

6.0 EXHAUST PLUME ENTRAINMENT MODEL

The flow field of an exhaust jet mixing with a subsonic external flow and a separated boattail boundary layer is shown in figure 6. Two regions can be distinguished in the flow field. In region 1, the boundary layer merges with the mixing layer at the exhaust plume boundary and the exhaust plume contains a core of inviscid flow. In region 2, the turbulent mixing reaches all the way to the axis of the jet so there is no inviscid core flow. In this report, only the flow in region 1 is considered since for the kinds of flow conditions of interest the entrainment is expected to be essentially completed in the length of the inviscid core.

6.1 ASSUMPTIONS

The analysis is based on the following assumptions:

1. The flow is axisymmetric.
2. All gases obey the perfect gas law.
3. The usual boundary layer assumptions are applicable to the mixing layer.
4. The mixing layer is fully turbulent.
5. The turbulent Prandtl and Lewis numbers are unity.
6. The exhaust jet flow is supersonic at the nozzle exit.
7. Radial pressure gradients are negligible in the mixing layer.

8. Streamwise turbulent transport mechanisms are negligible.

9. The exhaust jet flow is isentropic.

6.2 EQUATIONS FOR COMPRESSIBLE TURBULENT MIXING LAYER

The mixing layer is assumed to develop about a surface defined by the radius the plume would have if it was completely inviscid and subject to the pressure distribution calculated from the external inviscid flow. The basic equations are assumed to be the same as those of a turbulent boundary layer. In cylindrical coordinates for axisymmetric flow, these equations have been presented previously as equations (14)-(16). For the entrainment layer, as for the boundary layer, the energy equation (Eq. 16) will be approximated by an assumed temperature-velocity relation.

6.3 DEVELOPMENT OF INTEGRAL METHOD FOR THE MIXING LAYER

6.3.1 Integral Equations

For the entrainment layer, two equations are derived by eliminating the radial velocity terms between the momentum and continuity equations (14) and (15) and integrating the resulting equation across the mixing layer in two strips. No compressibility or geometric transformations are used. Eliminating the $[v-u(r_w)_x]$ term between the momentum and continuity equations and integrating yields

$$\int_{r_c}^{r} \rho u r u_x dr - \int_{r_c}^{r} u_r \int_{r_c}^{\eta} (\rho u r)_x d\eta dr = -\frac{1}{2}\left(r^2-r_c^2\right) p_x + r\mu\beta u_r$$

$$- \rho_c r_c [v_c-u_c(r_w)_x](u-u_c) \qquad (67)$$

where it has been assumed that the shear stress term vanishes at r_c, the inner boundary of the mixing layer. Evaluating equation (67) at $r = r_w$ and $r = r_e$ yields the two independent integral equations

$$\int_{r_c}^{r_w} r[\rho(2u-u_w)u_x + u(u-u_w)\rho_x]dr = \frac{1}{2}\rho_e u_e\left(r_w^2-r_c^2\right)(u_e)_x$$

$$+ r_w\mu_w\beta_w(U_r)_w$$

$$- \rho_c r_c [v_c-u_c(r_w)_x](u_w-u_c) \qquad (68)$$

and

$$\int_{r_c}^{r_e} r[\rho(2u-u_e)u_x + u(u-u_e)\rho_x]dr = \frac{1}{2}\rho_e u_e\left[r_e^2-r_c^2\right](u_e)_x - \rho_c r_c[v_c-u_c(r_w)_x](u_e-u_c) \quad (69)$$

where the pressure has been eliminated by evaluating equation (15) at $r = r_e$.

The external boundary of the mixing region is defined as follows:

$$\text{If} \quad \delta_c < \delta_{u_1}$$

$$\text{then} \quad r_e = r_w + \delta_{u_1} \quad (70)$$

$$\text{but, if} \quad \delta_c > \delta_{u_1}$$

$$\text{then} \quad r_e = r_w + \delta_c \quad (71)$$

where δ_{u_1} is the thickness corresponding to the boundary layer profile at the end of the boattail, and δ_c is the thickness of the inner part of the mixing layer.

It will be recalled that the viscous-inviscid interaction between the boundary layer-mixing layer and the external inviscid flow requires the calculation of an effective boundary shape for the inviscid flow. For the boundary layer, the effective shape is defined by the body radius plus the boundary layer displacement thickness, equation (55). In a similar manner, a displacement thickness is defined for the exhaust jet. For purely inviscid flow, the boundary of the exhaust jet is a streamline separating the nozzle efflux from the external flow. With entrainment and turbulent mixing, this line is no longer a streamline. However, in order to produce a continuous and smooth surface for the external inviscid flow, it is postulated that the effective boundary may be defined by a displacement from the inviscid plume boundary in the same manner as for a solid boundary. Thus, an additional equation is derived by defining

$$\delta^* = \int_{r_w}^{r_e} (1-\rho u/\rho_e u_e)(r/r_w)dr \quad (72)$$

Differentiating equation (72) yields a third integral equation

$$\int_{r_w}^{r_e} (r/r_w)(\rho u/\rho_e u_e)_x dr = -\delta^*_x - (r_w)_x (1-\rho_w u_w/\rho_e u_e+\delta^*/r_w) \quad (73)$$

6.3.2 Velocity Profiles

It has been experimentally observed that the velocity and temperature profiles in jets in the absence of entrainment effects exhibit self-similar behaviors. That is, appropriate combinations of the radial and axial coordinates will reduce these profiles to functions of a single variable to a high degree of accuracy. In the present case, it is assumed that such a condition exists at a large distance from the nozzle. Near the nozzle, the flow profiles are assumed to be composed of a linear combination of functions representing the boundary layer profile at the nozzle exit and the equilibrium jet boundary profile far downstream. Thus,

$$u = (1-K)u_n + Ku_s \quad (74)$$

where

u_n is a velocity profile proportional to the boundary layer profile at the nozzle exit station (both internal and external boundary layers)

u_s is a velocity profile function representing the downstream profile

and

K is a factor to be determined.

The velocity profiles in this relation are defined as follows:

For $r < r_w$:

$$u_n = \left(\frac{r_w-r}{\delta_c}\right)^{1/7} u_c = \left(\frac{-y}{\delta_c}\right)^{1/7} u_c \quad (75)$$

where $y = r - r_w$

For $r > r_w$:

$$u_n = (u/u_e)_n u_e \tag{76}$$

where $(u/u_e)_n$ is the profile of the external boundary layer at the end of the body. A family of profiles of u for several values of K and δ_c/r_w is shown for illustration in figure 7. The similarity behavior of the downstream profile is assumed to be approximated by a sine function.

Thus, for $r_w - \delta_c < r < r_w + \delta_c$

$$u_s = u_c + \frac{1}{2}(u_e - u_c)[1 + \sin(\pi y/2\delta_c)] \tag{77}$$

and, for $r > r_w + \delta_c$

$$u_s = u_e \tag{78}$$

With these definitions, five quantities must be determined to describe the flow. Two of the required quantities, r_w and u_c are determined by the approximate model of the flow in the inviscid exhaust jet. The remaining three quantities, u_e, δ_c and K will be calculated from solutions of equations (68), (69) and (73) combined with the inviscid external flow in the same manner as described previously for boundary layers.

6.3.3 Temperature-Velocity Relationship

At the end of the boattail, the temperature parameter, S is that of the boundary layer as described previously. For the external flow, a function S_n is thus defined

$$S_n = [1 - (u/u_e)]S_w \tag{79}$$

Inside the nozzle, a different relation is needed to accommodate the different jet total temperature. Assuming the linear relation between the total temperature and the velocity also exists inside the nozzle boundary layer, the following relation is proposed for $r < r_w$:

$$S_n = [1 - (u/u_c)]S_w + S_c\ (u/u_c) \tag{80}$$

For fully developed plume mixing layers, the following temperature profile was derived by Nielsen et al (ref. 19)

$$\frac{T_t - T_{t_e}}{T_{t_c} - T_{t_e}} = \frac{u_s - u_e}{u_c - u_e} - \frac{DC_c^2}{1 - T_{t_e}/T_{t_c}} \left[\frac{u_s - u_e}{u_c} \left(1 - \frac{u_e}{u_c}\right) - \left(\frac{u_s - u_e}{u_c}\right)^2 \right] \quad (81)$$

where

$$C_c^2 = \frac{m_c}{1 + m_c} \quad (82)$$

The value of the parameter D has the following effects:

- $D = 0$ gives linear T_t-u relation and quadratic T-u relation.
- $D = 1$ gives quadratic T_t-u relation and linear T-u relation.

In this work, $D = 0$ is used for calculative examples.

In order to express all terms of the equations in terms of a single reference quantity, equation (81) is rewritten using the external flow reference conditions. Thus, the similarity form of the temperature function S becomes

$$S_s = S_c \frac{u_s - u_e}{u_c - u_e} + D \frac{m_e}{1 + m_e} \left(\frac{u_s}{u_e} - 1\right)\left(\frac{u_s}{u_e} - \frac{u_c}{u_e}\right) \quad (83)$$

For the region immediately downstream of the nozzle exit, a transitional model of the temperature profiles is defined. Thus,

$$S = (1 - K)S_n + KS_s \quad (84)$$

The density profiles are related to the velocity profiles through the temperature in the same way as for the boundary layer. It is assumed that the mixing in the entrainment region is dominated by the external flow, since for separated flow, the boundary layer on the body is expected to be much thicker than the boundary layer inside the nozzle. With this assumption, the ratio of specific heats of the mixing layer is taken to be that of the external flow. The density profiles are then obtained from

$$\rho_e/\rho = (S+1)(1+m_e) - m_e(u/u_e)^2 \quad (85)$$

6.3.4 Turbulent Shear Stress

Recalling equations (68) and (69), it is noted that a relation is required for the shear stress along the inviscid reference line, $r = r_w$. In equation (68) it has been assumed that the shear stress is related to the radial velocity gradient through an eddy viscosity in the same manner as for the boundary layer on the body. Also, only the value of the shear at the boundary, $r = r_w$ is needed.

As for the velocity and temperature profiles, the eddy viscosity for a shear layer such as the jet boundary far downstream of the nozzle is found in the literature to have a specific form different from that of the boundary layer. In the present work, the eddy viscosity was assumed to undergo a transition from the value on the body to a value determined for the downstream flow in the same manner as for the velocity and temperature profiles, namely,

$$\varepsilon = (1-K)\nu_{e_o} + 2K\bar{\varepsilon}\left[\left(\frac{1+m_e}{1+m_c}\right)\left(\frac{u_{max}+u_{min}}{u_{max}-u_{min}}\right)\right]^{0.9}\delta_c(u_{max}-u_{min}) \qquad (86)$$

The value of the constant $\bar{\varepsilon}$ used in this work was

$$\bar{\varepsilon} = 0.0009$$

This value corresponds to the correlation of Nielsen et al (ref. 19) for mixing of two supersonic streams.

It is noted that the shear stress term in equation (68) contains the radial velocity gradient as well as the eddy viscosity. Differentiating equation (74), the gradient is

$$U_r = (1-K)(U_n)_r + K(U_s)_r \qquad (87)$$

The gradient of the similarity function u_s is well defined. However, the gradient of the initial boundary layer function is not well defined. The boundary layers developing on the boattail surface and the nozzle interior surface cannot be expected to have a continuous gradient at the nozzle exit. However, immediately downstream of the nozzle, a continuous gradient must exist as the two flows begin to merge. Since the jet velocity is expected to be much greater in magnitude than the velocity in the recirculating region over the boattail, an approximation for the velocity gradient at the inviscid reference line was derived by assuming that the velocity near the boundary $r = r_w$ is describable by a sine function in a similar manner to the downstream similarity function. To maintain continuity of the

velocity profile, the parameters of the function were evaluated by requiring the magnitude and gradient of the velocity profile to be continuous at $r_w - r/\delta_c = 0.1$. The resulting gradient at $r = r_w$ is

$$(u_r)_{r_w} = -3.39331\pi u_c/\delta_c \tag{88}$$

Calculations have indicated that this relation provides a reasonable approximation. The solution of the flow equations does not appear to be very sensitive to errors in this term.

6.3.5 Equations Solved

The integrands of equations (68), (69), and (73) contain the axial derivatives of u and ρ which must be expressed in terms of the variables u_e, δ_c, and K of the formulation. The quantities u and ρ are considered to be functions of x and the mixing layer variable $y = r - r_w$. However, the axial functional relationship is implicit in the variation of the other parameters of equations (41)-(44) so that

$$u(x,y) = u(u_e,\delta_c,K,y) \tag{89}$$

$$\rho(x,y) = \rho(u_e,\delta_c,K,y) \tag{90}$$

Then

$$u_x = \frac{\partial u}{\partial u_e}(u_e)_x + \frac{\partial u}{\partial \delta_c}(\delta_c)_x + \frac{\partial u}{\partial K}K_x \tag{91}$$

$$\frac{\partial \rho}{\partial x} = \frac{\partial \rho}{\partial u_e}(u_e)_x + \frac{\partial \rho}{\partial \delta_c}(\delta_c)_x + \frac{\partial \rho}{\partial K}K_x \tag{92}$$

The parameters r_w and u_c found in equations (75)-(78) are assumed to be related to the external flow velocity, u_e and do not appear explicitly in these relations. For convenience, the density expression is rewritten in terms of the density ratio of equation (85). Thus,

$$\rho_x = (\rho/\rho_e)(\rho_e)_x - \rho_e(\rho/\rho_e)^2(\rho_e/\rho)_x \tag{93}$$

and

$$(\rho_e/\rho)_x = \frac{\partial}{\partial u_e}\left(\frac{\rho_e}{\rho}\right)(u_e)_x + \frac{\partial}{\partial \delta_c}\left(\frac{\rho_e}{\rho}\right)(\delta_c)_x + \frac{\partial}{\partial K}\left(\frac{\rho_e}{\rho}\right)K_x \tag{94}$$

where it can easily be shown that

$$(\rho_e)_x = -\frac{2\rho_{e_o}}{\gamma-1}\left[\frac{1+m_e}{1+m_{e_o}}\right]^{-\frac{\gamma}{\gamma-1}}\frac{m_e}{u_e}(1+m_e)(u_e)_x \tag{95}$$

Due to the iterative nature of the solution procedure, an exact relation cannot be derived between the external flow velocity, u_e and the inviscid plume parameters, r_w and u_c. However, the relationship is approximately accounted for by use of the assumption that the solution is not very far from convergence so that both the external and the plume inviscid flows are subject to the same pressure distribution, p_e. The external flow is isentropic so that

$$\frac{\partial u_e}{\partial p_e} = -\frac{1}{\rho_e u_e} \tag{96}$$

Also, for an inviscid plume which is nearly uniform and axial, the Bernoulli equation gives

$$p_e + \frac{1}{2}\rho_c u_c^2 = p_{tc} \tag{97}$$

so that

$$\frac{\partial u_c}{\partial p_e} = -\frac{1}{\rho_c u_c} \tag{98}$$

and

$$\frac{\partial u_c}{\partial u_e} = \frac{\partial u_c/\partial p_e}{\partial u_e/\partial p_e} = \frac{\rho_e u_e}{\rho_c u_c} \tag{99}$$

with these relations and the definitions of equations (75)-(78), the required derivatives of u can be obtained as follows

$$\frac{\partial u}{\partial K} = u_s - u_n \tag{100}$$

$$\begin{aligned}\frac{\partial u}{\partial \delta_c} &= 0 \qquad \text{for} \qquad r > r_w + \delta_c \qquad \text{when} \qquad \delta_c < \delta_u \\ &= (1-K)\frac{\partial u_n}{\partial \delta_c} + K\frac{\partial u_s}{\partial \delta_c} \qquad \text{for} \qquad r_w - \partial_c < r < r_w + \delta_c\end{aligned} \tag{101}$$

where

$$\frac{\partial u_s}{\partial \delta_c} = -\frac{\pi}{4}\,(u_e - u_c)\,\frac{r - r_w}{\delta_c^2}\cos\left(\frac{\pi}{2}\,\frac{y}{\delta_c}\right) \tag{102}$$

and

$$\left.\begin{aligned} \frac{\partial u_n}{\partial \delta_c} &= \frac{1}{7}\,u_c\left(y/\delta_c^2\right)\left(-y/\delta_c\right)^{-6/7} \quad \text{for} \quad r_w - \delta_c < r < r_w \\ &= 0 \quad \text{for} \quad r > r_w \quad \text{and} \quad \delta_c < \delta_{u_1} \\ &= -\left(y/\delta_c^2\right)u_e\left(\frac{u}{u_e}\right)' \quad \text{for} \quad r > r_w \quad \text{and} \quad \delta_c > \delta_{u_1} \end{aligned}\right\} \tag{103}$$

where $(u/u_e)'$ denotes differentiation with respect to y/δ_c. Continuing,

$$\left.\begin{aligned} \frac{\partial u}{\partial u_e} &= (1-K)(u/u_e) + K\,\frac{\partial u_s}{\partial u_e} \quad \text{for} \quad r > r_w \\ &= (1-K)(u/u_c)\,\frac{\partial u_c}{\partial u_e} + K\,\frac{\partial u_s}{\partial u_e} \quad \text{for} \quad r < r_w \end{aligned}\right\} \tag{104}$$

where

$$\left.\begin{aligned} \frac{\partial u_s}{\partial u_e} &= 1 \quad \text{for} \quad r \geq r_w + \delta_c \\ &= \frac{1}{2}\left[1 + \sin(\pi y/2\delta_c)\right]\left(1 - \frac{\partial u_c}{\partial u_e}\right) + \frac{\partial u_c}{\partial u_e} \\ &\qquad \text{for} \quad r_w - \delta_c \leq r \leq r_w + \delta_c \end{aligned}\right\} \tag{105}$$

Using equation (85) in equation (94)

$$\frac{\partial}{\partial u_e}\left(\frac{\rho_e}{\rho}\right) = (1+m_e)\frac{\partial S}{\partial u_e} - \frac{2m_e}{u_e}\left[\frac{u}{u_e}\frac{\partial u}{\partial u_e} - (S+1)(1+m_e) - (1-m_e)\left(\frac{u}{u_e}\right)^2\right] \tag{106}$$

$$\frac{\partial}{\partial \delta_c}\left(\frac{\rho_e}{\rho}\right) = (1+m_e)\frac{\partial S}{\partial \delta_c} - 2\frac{m_e}{u_e}\frac{u}{u_e}\frac{\partial u}{\partial \delta_c} \tag{107}$$

$$\frac{\partial}{\partial K}\left(\frac{\rho_e}{\rho}\right) = (1+m_e)\frac{\partial S}{\partial K} - 2\frac{m_e}{u_e}\frac{u}{u_e}\frac{\partial u}{\partial K} \tag{108}$$

where

$$\frac{\partial S}{\partial u_e} = (1-K)\frac{\partial S_n}{\partial u_e} + K\left(\frac{\partial S_s}{\partial u_s}\frac{\partial u_s}{\partial u_e} + \frac{\partial S_s}{\partial u_e}\right) \tag{109}$$

$$\left.\begin{aligned}\frac{\partial S_n}{\partial u_e} &= (S_w - S_c)\frac{u}{u_c}\frac{1}{u_c}\frac{\partial u_c}{\partial u_e} && \text{for } r < r_w \\ &= \frac{S_w}{u_e}\frac{u}{u_e} && \text{for } r > r_w\end{aligned}\right\} \tag{110}$$

$$\frac{\partial S_s}{\partial u_e} = -S_c\frac{u_c - u_s}{(u_c-u_e)^2} + D\frac{m_e}{1+m_e}\frac{1}{u_e}\left[\left(\frac{u_c}{u_e} - \frac{u_s}{u_e}\right)\left(1 - 4\frac{u_s}{u_e}\right)\right] + \frac{\partial S_s}{\partial u_c}\frac{\partial u_c}{\partial u_e} \tag{111}$$

$$\frac{\partial S_s}{\partial u_s} = \frac{S_c}{u_c - u_e} - D\frac{m_e}{1+m_e}\frac{1}{u_e}\left(1-2\frac{u_s}{u_e} + \frac{u_c}{u_e}\right) \tag{112}$$

and

$$\frac{\partial S_s}{\partial u_c} = -S_c\frac{u_s - u_e}{(u_c-u_e)^2} + D\frac{m_e}{1+m_e}\frac{1}{u_e}\left(1 - \frac{u_s}{u_e}\right) \tag{113}$$

Also,

$$\frac{\partial S}{\partial \delta_c} = K \frac{\partial S_s}{\partial u_s} \frac{\partial u_s}{\partial \delta_c} + (1-K) \frac{\partial S_n}{\partial \delta_c} \tag{114}$$

where

$$\left.\begin{aligned} \frac{\partial S_n}{\partial \delta_c} &= 0 \quad \text{for } r > r_w \text{ and } \delta_c < \delta_{u_1} \\ &= \frac{1}{7} \frac{y}{\delta_c^2} \left(\frac{-y}{\delta_c}\right)^{-6/7} (S_c - S_w) \quad \text{for } r \le r_w \\ &= S_w \frac{y}{\delta_c^2} \left(\frac{u}{u_e}\right)' \quad \text{for } r > r_w \text{ and } \delta_c > \delta_{u_1} \end{aligned}\right\} \tag{115}$$

Finally,

$$\frac{\partial S}{\partial K} = S_s - S_n$$

Equations (68), (69), and (73) can now be written, after some algebra, in the form

$$A_{n1} K_x + A_{n2}(\delta_c)_x + A_{n3}(u_e)_x = B_n \tag{116}$$

with n = 1, 2 or 3

where the coefficients are integrals evaluated from the following definitions:

$$R_1 = r \frac{\rho}{\rho_e} (2u - u_e) \tag{117}$$

$$R_2 = r \frac{\rho}{\rho_e} (2u - u_w) \tag{118}$$

$$R_3 = \frac{\rho_{e_o}}{\rho_e} \frac{r}{r_w} \frac{\rho}{\rho_e} \frac{1}{u_e} \tag{119}$$

$$P_1 = ru \left(\frac{\rho}{\rho_e}\right)^2 (u - u_e) \tag{120}$$

$$P_2 = ru \left(\frac{\rho}{\rho_e}\right)^2 (u - u_w) \tag{121}$$

$$P_3 = \frac{\rho_{e_o}}{\rho_e} \frac{r}{r_w} \frac{u}{u_e} \left(\frac{\rho}{\rho_e}\right)^2 \tag{122}$$

$$\left.\begin{aligned} G_1 &= G_2 = (2m_e/u_e)(1+m_{e_o})/(\gamma-1) \\ G_3 &= 1/u_e \end{aligned}\right\} \tag{123}$$

Thus, for n = 1, 2 or 3

$$A_{n1} = \frac{\rho_e}{\rho_{e_o}} \int_{r_c}^{r_e} \left[R_n \frac{\partial u}{\partial K} - P_n \frac{\partial}{\partial K} \left(\frac{\rho_e}{\rho}\right)\right] dr$$

$$A_{n2} = \frac{\rho_e}{\rho_{e_o}} \int_{r_c}^{r_e} \left[R_n \frac{\partial u}{\partial \delta_c} - P_n \frac{\partial}{\partial \delta_c} \left(\frac{\rho_e}{\rho}\right)\right] dr \tag{124}$$

and

$$A_{n3} = \frac{\rho_e}{\rho_{e_o}} \int_{r_c}^{r_e} \left[R_n \frac{\partial u}{\partial u_e} - P_n \frac{\partial}{\partial u_e} \left(\frac{\rho_e}{\rho}\right) - GP_n \frac{\rho_e}{\rho}\right] dr + A'_{n3}$$

where

$$\left.\begin{aligned} A'_{13} &= -\frac{1}{2}\left(r_e^2 - r_c^2\right)(\rho_e/\rho_{e_o})u_e \\ A'_{23} &= -\frac{1}{2}\left(r_w^2 - r_c^2\right)(\rho_e/\rho_{e_o})u_e \\ A'_{33} &= 0 \end{aligned}\right\} \tag{125}$$

Also,

$$\left.\begin{aligned}
B_1 &= -r_c\rho_c(u_e - u_c)[v_c - u_c(r_w)_x] \\
B_2 &= -r_c\rho_c(u_w - u_c)[v_c - u_c(r_w)_x] + \Bigg\{(1-K)(\rho_e/\rho_{e_o})\nu_{e_o} \\
&\quad + 2K\bar{\varepsilon}\left[\frac{1+m_e}{1+m_{e_o}}\left(\frac{u_{max} + u_{min}}{u_{max} - u_{min}}\right)\right]^{0.9}\delta_c(u_{max}-u_{min})\Bigg\} r_w(u_r)_{r_w} \\
B_3 &= (\rho_w u_w/\rho_e u_e - 1 - \delta^*/r_w)(r_w)_x - \delta^*_x
\end{aligned}\right\} \quad (126)$$

The integrals in these equations are evaluated using a 21-point trapezoidal integration, with the intervals r_c to r_w and r_w to r_e each divided into 10 equal segments. It is noted that equations (116) are similar in form to the equations solved for the boundary layer over the body. Indeed, a similar approach is taken to solving the entrainment equations as was used for the boundary layer equations. At the end of the body (the beginning of the entrainment region), the value of δ^* is known, along with δ_{u_1} and u_e. A value of δ_c is determined from a nozzle boundary layer calculation. The value of K is assumed to be zero. The variation of δ^* is specified continuously from the boundary layer into the entrainment region, while u_e, δ_c and K are calculated by solving equations (116). To accomplish this calculation, the first two of equations (116) are reduced to two equations in the derivatives of δ_c and u_e by eliminating the derivative of K with the third equation. The value of K is determined at each step of the integration of the solution by solving equation (72) directly. When the point of minimum u_e is reached downstream of the nozzle, the need for prescribing δ^* is eliminated. From that point to the end of the calculation, u_e is prescribed as for the boundary layer on a sting and the values of K and δ_c are calculated from the first two of equations (116).

7.0 RESULTS

In this section, the theory is compared with experimental results on axisymmetric boattail-sting and boattail-exhaust plume configurations. In all cases, the boundary-layer was initialized as a laminar boundary-layer near the nose of the forebody with transition specified shortly downstream of the initial point. Initial boundary-layer quantities U_τ and δ_i were obtained from a similarity solution transformed to conical coordinates (see section 10.4).

7.1 CIRCULAR ARC BOATTAILS WITH SOLID PLUME SIMULATORS

Wind tunnel studies of the configuration shown in figure 8 were described in reference 20. The configuration is a cone-cylinder, with a circular arc boattail. Two of the boattails are examined here to illustrate the capabilities of the calculative method. The first example is for a boattail (configuration 2 in figure 8) for which no separation is evident experimentally at the Mach numbers of the tests. Surface static pressure distributions were measured along the boattail and along the sting for free-stream Mach numbers from 0.4 to 1.2. Boundary-layer transition was tripped at $x/D = .167$. Calculations for Mach numbers of 0.6, 0.8, and 0.9 were initialized as described previously. On the first iteration of each calculation for the $M_o = 0.6$ and 0.8 cases, a separation point was indicated on the boattail. On subsequent iterations, the separation point moved aft on the boattail until it eventually moved off the boattail and the calculation subsequently converged as an attached flow. The calculation for $M_o = 0.9$ converged without separation. Comparisons between the theory and measured results for the pressure coefficient distributions at Mach numbers of 0.6, 0.8, and 0.9 are presented in figure 9. The theory is seen to be in good agreement with the data for all three cases.

It will be recalled from section 5.6 that the initial estimate of the separation point location is obtained from the application of the plain-body (the body with no boundary layer) inviscid-flow solution to the boundary-layer calculation, with the separation point taken to be at the point where the transformed shape factor H_i reaches a specified value in the adverse pressure gradient on the boattail. The present case illustrates that the calculative method also has the capability to calculate attached flows. However, for such flows a separation point is often found on the first iteration because of the steep pressure gradients associated with the inviscid flow on the plain body. Whether the subsequent calculations actually proceed to move the separation point off the boattail, for a case in which that is the correct result, depends somewhat on the initial value of x_s, or on the initial value of H_i. If the initial value of x_s is too far forward, the calculation may not converge at all. To move the initial value of x_s back, the input value of H_i is increased. For the cases shown in figures 9a and 9b, a value of H_i of 1.3 was appropriate, while for the case shown in figure 9c, a value of 1.5 was required. The decision as to whether the solution is converged is based primarily on the magnitude of the rms errors. If the best value of s produced by the iteration is significantly greater than 1.0 percent (.01), the solution can generally be improved by adjusting H_i.

The second example is for a boattail (configuration 1 in figure 8) that has an extensive region of separated flow for all Mach numbers. This is evidenced by the pressure distribution which is typical of separated flows on such configurations and has been corroborated by oil flow studies described in reference 21. Comparisons between the theory and measured results for the pressure distributions at $M_o = 0.6$, 0.8, and 0.9 are presented in figure 10. For the two lowest Mach numbers, the theory is seen to be in excellent agreement with the data on the boattail, with a slight discrepancy on the solid plume simulator. Also, the calculated location of the separation point agrees exactly with the oil flow determination of reference 21 for the $M_o = 0.6$ case of figure 10a, with a small error noted for the $M_o = 0.8$ case of figure 10b. For the $M_o = 0.9$ case of figure 10c, the agreement is not so good. A fairly large discrepancy is noted in the pressure coefficient over the entire boattail, and a larger error occurs in the prediction of the separation location. For that case, supersonic flow occurs over the beginning of the boattail, with a shock of Mach number approximately 1.25 just ahead of the separation point. Abeyounis (ref. 21) suggests that for this configuration, the separation for free-stream Mach numbers above 0.8 probably occurs at the shock. Thus, the discrepancies noted in figure 10c are probably due to the fact that the present theoretical model assumes separation occurs behind the shock. Another measure of the accuracy of the solution is the degree of convergence of the calculated viscous-inviscid interaction. For the calculations of figures 10a and 10b, the iteration converged to an rms error of 1.0 percent, which has been found to yield generally good results, while results shown in figure 10c had an rms error of 2.3 percent.

As for the unseparated flows, the separated flows were also found to be somewhat dependent on the value of H_i for determining the outcome of the iterative calculations. In the two subsonic cases of figures 10a and 10b, a value of H_i of 1.15 was used, while for the transonic case of figure 10c a value of 1.0 was used. For other values of H_i the iteration either did not converge to a sufficiently small rms error, or developed numerical difficulties which subsequently stopped the calculations. A value of $H_i = 1.3$ is usually used to start calculations when nothing is known of the solution. Experience indicates that if the iteration procedure does not lead to a solution with an rms error of 1.0 percent or less, it may be possible to reduce the error by adjusting the initial value of H_i and starting a new iteration sequence.

Although no data were available for comparison, other boundary-layer quantities of interest are shown in figure 11. The velocity corresponding to the pressure of figure 10b is shown in figure 11a. The displacement thickness, also shown in figure 11a, is smooth and continuous, with an abrupt reversal of slope at the end of the boattail, consistent with the prescribed conical surface of the effective body as shown in figure 11b. In figure 11c, the skin-friction coefficient on the boattail and sting is shown. As described in section 5.6, the skin friction is negative in the region between x_s and reattachment, and undergoes an adjustment at x_p, with u_e and δ^* continuous.

The integrated pressure drag on the boattails is shown in figure 12. The calculated values at $M_o = 0.6$ and 0.8 are in excellent agreement with the data for the separated flow (figure 12a). For higher Mach numbers, the agreement is not so good, as would be expected from the pressure coefficient comparisons and the previous discussion. Even so, the calculations for $M_o = 0.9$ and an additional calculation at $M_o = 0.96$ indicate the method predicts the transonic drag rise with fair accuracy.

The integrated pressure drag on the unseparated boattail is shown in figure 12b. The error in the calculated drag is fairly large for the $M_o = 0.6$ case, but improves considerably for the higher Mach numbers.

7.2 CIRCULAR ARC BOATTAILS WITH COMPRESSED AIR PLUMES

Some of the wind tunnel tests of reference 20 were conducted with the exhaust plume simulated with high pressure air. Comparison between the theory and data for the pressure coefficient distribution on the boattail of configuration 1 (figure 8) is presented in figure 13 for exhaust nozzle total pressure ratios of 2.0 and 4.0 at a free-stream Mach number of 0.8 and for a nozzle pressure ratio of 2.0 for a Mach number of 0.6. The agreement between the theory and data for a pressure ratio of 2.0 and $M_o = 0.8$ is good as shown in figure 13a even though there is some error in the predicted separation point location. The rms error of the calculated viscous and inviscous solutions was 1.6 percent.

The comparison for a nozzle pressure ratio of 4.0 and $M_o = 0.8$ shown in figure 13b indicates good agreement for the pressure coefficient distribution and somewhat better agreement for the separation point location than the previous case. The rms error of that calculation was 1.1 percent.

The comparison for a nozzle pressure ratio of 2.0 and $M_o = 0.6$ shown in figure 13c indicates fair agreement for the pressure coefficient distribution and the separation point location. The rms error of that calculation was 1.66 percent.

Plots of the important entrainment region parameters for the $M_o = 0.8$ case are presented in figure 14. The case with exhaust total pressure ratio of 4.0 is presented in figure 14a. The plume inviscid reference surface represented by r_w is seen to expand slightly as it leaves the nozzle, reaching an essentially cylindrical shape in approximately 2 nozzle diameters. The inner boundary of the mixing region, represented by r_c, requires more than 6 nozzle diameters to reach the axis of the plume. The entrainment parameter, K increases rapidly at first and then more gradually after x_p is reached and the calculation switches from prescribed δ^* to prescribed u_e. Another change in the behavior of K occurs further downstream, associated with the change in the definition of the outer edge of the mixing layer, r_e, as defined by equations (70) and (71). The entrainment reaches completion ($K = 1.0$) asymptotically, but is effectively complete in less than 6 nozzle diameters.

The entrainment parameters for the exhaust pressure ratio of 2.0 are presented in figure 14b. The inviscid plume boundary, r_w is cylindrical for the entire plume, reflecting the fact that the plume is only very slightly underexpanded. Entrainment appears to proceed at a faster rate than for the higher pressure ratio as evidenced by the fast initial rise of the entrainment parameter, K. However, the entrainment calculations were terminated after approximately 2 nozzle diameters when the value of K reached a maximum and began to decrease. The reason for this behavior is not fully understood, although it is believed to be related to the fact that the jet velocity and the external flow velocity are nearly equal. For velocity ratios, u_c/u_e close to 1.0, it is expected that numerical calculations would encounter difficulties as K approached 1.0. For $K = 1.0$ and $u_c/u_e = 1.0$, the velocity profiles (Eqs. (74)-(78)) become constant with radius, and the equations (68) and (69) are redundant. The ratio u_c/u_e for the case shown in figure 14b is approximately 1.2.

Boattail drag coefficients calculated from the measured and calculated pressure coefficient distributions of figure 13 are shown in figure 15. The theoretical drag coefficients for the pressure ratios of 2.0 and 4.0 at $M_o = 0.8$ are in excellent agreement with the data (figure 15a). A third case, for an exhaust total pressure ratio of 5.0 has a calculated drag coefficient slightly higher than the data. The rms error for that case was 3.2 percent. The theoretical drag coefficients for the $M_o = 0.6$ case shown in figure 15b are in good agreement for a pressure ratio of 4.0 but the agreement for lower pressure ratios is poor. The rms error of the solutions shown in figure 15b was 0.77 percent for $p_{t_j}/p_o = 4.0$, 1.39 percent for $p_{t_j}/p_o = 3.0$ and and 1.66 percent for $p_{t_j}/p_o = 2.0$.

7.3 SUMMARY OF RESULTS

The calculative method has been found to be applicable to both attached and separated flows on boattails with solid plume simulators and with high pressure jets. The viscous-inviscid iteration procedure is somewhat sensitive to the first approximation to the separation point location, x_s, and the angle, θ_s, in that the iteration will not converge to the smallest possible error unless the initial values are close to the correct values. This does not appear to be a major limitation, since adequate starting conditions can usually be determined by trial and error in a few trials. Comparisons with experimental data indicate that the entrainment model and the viscous-inviscid iteration procedure provide an accurate engineering method for predicting boattail flow fields for moderately underexpanded exhaust flows, and for boattails with solid exhaust plume simulators.

8.0 COMPUTER PROGRAM ORGANIZATION

In this section, the general organization of the programs will be described. Specific information on data required for input and data developed for output will be described in sections 9, 10, and 11. Sample Job Control Card decks for a typical IBM 370 installation are presented in section 12.

The overall program consists of a mainline program (program 1) and three main subprograms each consisting of several subroutines. The first main subprogram is the inviscid-flow program (program 2). It is a modified version of the program described in reference 3. The second main subprogram is the boundary-layer-entrainment-layer program (program 3). It is based on the integral theory described previously. The third subprogram is the inviscid exhaust plume program (program 4). The mainline program controls the iteration between the other three programs. Either of the first two subprograms may be used separately, without iterating by appropriate choice of the input parameters.

Both the viscous-flow program and the inviscid-flow programs require some punched card input and may require some input data from disc or tape data files. The data files must be identified by specific Logical Unit numbers. Each program in turn produces new data files and printed output. The general relationship of the programs and the various data files are shown in figure 8. The specific Logical Unit numbers required for input and output are listed in Table I. Two Logical Unit numbers are associated with each data file shown in figure 16. One unit is used for input, the other for output.

Program 2 requires initially data from cards describing the free-stream conditions, the computational mesh and the body shape. Alternately, the program can accept the input body shape from data file 1. It can also accept an initial solution for the perturbation velocity potential from another data file (data file 2). Program 2 produces printed output lists of the appropriate flow field quantities, quantities describing the configurations and the computational mesh and several data files. Data file 2 is rewritten using the new solution for the potential. A third file (data file 3) is written containing the distribution of the axial velocity component at the inviscid boundary for use by the viscous flow program.

Program 3 requires initially the free-stream conditions and gas constants as well as parameters describing the shape of the surface over which the boundary layer is flowing. On the first iteration of a viscous-inviscid interaction, the surface shape is the same as that for program 2. On subsequent iterations, the body shape for the boundary-layer program remains the same, except when it is modified by the calculation of a new plume shape, while that for the inviscid flow is modified by the addition of the boundary layer. Program 3 can also accept data from data files as optional input. The boundary-layer-edge velocity distribution, u_e, can be input from data file 3, produced by program 2. The distribution of the body shape augmented by the displacement thickness can be input from data file 4. That file differs from data file 1 because it contains the raw data for $\delta^* + r_w$ versus x as calculated by the boundary-layer program while data file 1 contains the shape adjusted according to equation (4) and interpolated to the x stations of the original input shape. If program 3 is being used separately from program 2 (i.e., without iterating), two additional options are available for card input. Either the boundary-layer-edge velocity, u_e, can be input as mentioned previously, or the displacement thickness, δ^*, may be input. These options are described more fully in sections 10.1 and 10.2.

Program 3 produces as output lists of the boundary layer and flow quantities as they are calculated along the body. In addition, program 3 produces an updated version of data file 4 and the augmented body shape (data file 1) required by program 2. Data file 4 also contains a list of the velocity ratio u_e/u_{e_o} corresponding to the boundary layer.

Program 3 can be used in a two-dimensional boundary layer mode if desired. However, calculation of a viscous-inviscid interaction or exhaust plume entrainment can only be done for axisymmetric cases with the present inviscid program.

All card input pertaining to programs 2 and 3 is input through an input subroutine called by program 1. Program 1 also produces a file of the quantities needed to restart and continue the calculation if the calculation should terminate before all iterations are completed. These data are stored on data file 5. Detailed instructions regarding restarting are presented in sections 12.2.3 and 13.2.

9.0 INPUT TO THE PROGRAMS

The data required by the programs generally fall into three categories: (1) geometrical data; (2) flow field data; and (3) control parameters. The control parameters are indices for specifying options and iteration counters. It will be noted by comparison with reference 3 that a number of input quantities required for the inviscid-flow program have been eliminated in the present version. This has been done by incorporating the calculations required to obtain some of the quantities into the present code or by simply defining fixed values which have been found to be successful. Specifically, a value of 1.4 is used for the initial value of the subsonic relaxation factor, a value of 0.1 is used for the initial value of the supersonic relaxation factor and a value of 1.3 is used for the exponent in the normal coordinate stretching function. Also, it is assumed that the computational grid has equal step sizes in both coordinate directions at the nose of the body. Finally, the number of relaxation steps allowed in the inviscid program is fixed at 20 for the first four interaction iterations and is changed to 40 and 80 after four and eight iterations, respectively.

The general requirement of the input data is that the tabular lists of the various distributions required represent smooth curves. This is especially true of the list of body shape coordinates. The inviscid program uses cubic splines to fit the input coordinates, so those coordinates must accurately represent a smooth curve with continuous second derivatives.

9.1 TABULAR FORM

The input data required for calculating transonic viscous, inviscid-flow interactions consist of several punched cards containing parameters describing the free-stream flow conditions, the computational mesh for the inviscid calculation, initial values for the viscous flow calculation, and certain options that are available in the program. A dictionary of the input data is presented in the next section. Table II shows the input variables as they are to be punched on the data cards. More detailed explanation of the requirements for the inviscid-flow program (program 2) are presented in ref. 3 and are not repeated herein.

9.2 DICTIONARY OF INPUT VARIABLES

The variables required for input on punched cards are defined in this section in the order in which they are required. Additional details on the format of the punched data are given in Table II. The first three cards of any input data deck contain a description of the case being calculated. Any or all of these three cards may be blank, but all three are required. The remaining variables in Table II are as follows:

NRSTRT Integer indicating whether calculation is being restarted to continue a previous calculation. Only valid for interaction calculations (LPROG = 0. See below)

- = 0 Start from zero. Input all quantities on cards or data files as required.
- > 0 Restart. Input data file 5 (Logical Unit 11) containing data from previous iteration plus all other input data files plus other card data as indicated in Table II.

NPRINT Integer indicating quantity of output to be printed (see section 11.1).

- = 0 Minimum output.
- = 1 All output.

N3 Integer indicating whether restart is to begin with new values of x_s and θ_s (see section 13.2).

ILIM Integer number of seconds corresponding to estimated length of calculation. When the time from the beginning of the calculation is within 30 seconds of this limit, the final restart files will be written. This assures that the job will not terminate while writing such files.

IITER Integer determining size of perturbation of x_s and θ_s. The initial step sizes used will be those given by equations (8) and (9) divided by IITER.

LPROG Integer indicating level of calculation.

- = -1 Inviscid flow only.
- = 0 Viscous-Inviscid interaction.
- = 1 Boundary layer only.

N1 Integer iteration counter for inner viscous-inviscid iteration.

N2 Integer iteration counter for x_s-θ_s iteration presently limited to a maximum of 20.

IBL Integer indicating how interaction calculations are to begin.

= 3 Start with inviscid flow.

= 0 Start with boundary layer.

IUNIT Integer indicating which value of the gas constant, RGAS, and the constants in Sutherlands temperature-viscosity relation are to be used. The choice depends on whether air is the gas being calculated and the units of the input quantities.

= 1 Input units must be pounds, feet, seconds, and °R.

= 2 Input units must be pounds, inches, seconds, and °R.

= 3 Input units must be newtons, meters, seconds, and °K.

For another gas, or other units, put in anything for IUNIT and put in nonzero values of VISC, RGAS, and SCON. Any units are allowed. The basic rule is that all input quantities must be consistent with regard to units.

MIT Number of relaxation cycles allowed for the inviscid-flow program (Program 2). If a value of zero is input, a value of 20 is used. Otherwise, the input value is used.

GAM Ratio of specific heats of the external inviscid flow.

AMINF Free-stream Mach number.

IXY Integer number of values of coordinate pairs, XO,YO, to be input for inviscid body shape. If IXY = 0, the required shape must be input from data file 1 (Logical Unit 14). Maximum value is 200.

XO,YO Axial and radial coordinates of body shape for inviscid-flow calculation, 2 per card.

The next series of variables, items 7 and 8 in Table II, are for the inviscid-flow program (Program 2). Detailed information on how these data are to be obtained is contained in reference 1.

IMAX Number of grid lines in the tangential direction; I = 1 is the forward stagnation line, I = IMAX is the rear stagnation line for closed bodies and downstream infinity for open bodies. For each grid refinement IMAX is increased such that $IMAX_{NEW} = 2(IMAX_{OLD}) - 1$. The present limit on IMAX is 81. Instructions for changing this limit appear as comments in the program listing (subroutine ONE0). The grid refinement option is generally not used for viscous-inviscid interaction calculations.

JMAX Number of grid lines in the normal direction; J = 1 corresponds to an infinite distance from the body and J = JMAX is on the body. The same formula and limit that apply to IMAX also apply to JMAX.

MHALF Number of grid refinements to be done. For interaction calculations a value of zero should be used with a grid fine enough for adequate resolution.

KLOSE Body type.

= 0 Open body (i.e., one with a sting or wake).

= 1 Closed body.

LREADP Integer indicating whether initial estimate of potential distribution is to be input from data file 2 (Logical Unit 13).

= 0 No.

= 1 Yes.

If any one, or all of the next four input quantities are input as zero, the pre-programmed values are used.

DNDZO Step size of the normal coordinate at the body. The pre-programmed value is 7 percent of the maximum body diameter.

XIXM Value of the computational coordinate, X, at the matching point of the two stretching functions used in the finite-difference scheme (see ref. 3), for open bodies only. Since X varies from zero to one, XIXM is the fraction of the total number of grid points which will be in the first stretching region (ahead of x_m). The pre-programmed value is 0.75.

XM Axial location, x_m, (in physical coordinates) of the junction (or matching point) between the two tangential stretching functions, for open bodies only, see reference 3. Must be less than XO(IXY). This parameter is used to concentrate computational mesh points in a certain region. The usual approach for interaction calculations (the pre-programmed value) is to let x_m be equal to the length of the body to the beginning of the sting, or plume, XBT.

DSDXIM Step size of the tangential coordinate at the junction between the two tangential stretching functions. The pre-programmed value is 8 percent of the length of the afterbody (XBT-XZNEW).

XBT Length of the body.

DMAX Maximum body diameter.

XZNEW Length of forebody. Also, this is the axial location at which boundary-layer calculations will begin after four iterations have been calculated. The usual procedure is to start the boundary-layer calculations close to the nose of a long body at XZ (see item 17 in Table II) and then after four iterations move the starting point to XZNEW (XZNEW > XZ). In subsequent iterations, the boundary layer does not change for X < XZNEW. For long slender bodies with boattails, XZNEW should be the beginning of the boattail.

PLUMIN Logical variable indicating whether an exhaust plume is being calculated.

GAMAP Ratio of specific heats of exhaust gas.

PTPPFS Ratio of nozzle total pressure to free stream static pressure.

AMP Nozzle exit Mach number.

THETAP Nozzle exit divergence angle.

TTP Nozzle total temperature.

GMP Ratio of gas constant of air to that of the exhaust gas.

DELCZ Thickness of nozzle internal boundary layer at the nozzle exit.

The remaining input variables are related to the boundary-layer program alone or to the viscous-inviscid interaction method.

LSEP Logical variable indicating whether the location of separation (XSEP) is known (TRUE) or not (FALSE).

XSEP Axial location of separation. Put in only if LSEP = TRUE.

THETS Angle of δ^* surface with the boattail tangent at x_s. Put in only if LSEP = TRUE. A value of 0.0 will cause the program to calculate a value using equation (3).

IOPT Integer indicating the mode of the calculation.

= 1 u_e is to be input.

= 2 δ^* is to be input.

Put in a value of 1 for starting an interaction calculation.

K Integer indicating whether flow is axisymmetric.

= 0 Two dimensional.

= 1 Axisymmetric.

LVAR1 Integer indicator for method of input of u_e when IOPT = 1.

= 0 Input u_e (dimensional) on cards.

= 1 Input u_e/u_{e_o} on cards.

= 2 Input u_e/u_{e_o} from data file 3 on Logical Unit 12.

LSHAPE Integer indicating option for calculating all initial conditions (I.C.) except u_e (see section 10.4).

= 0 Input initial values per LIC.

= 1 Calculate I.C. for flat plate.

= 2 Calculate I.C. for cylinder.

= 3 Calculate I.C. for cone.

LIC Integer indicating initial condition options for IOPT = 1 and LSHAPE = 0.

= 1 Put in CFC1 and DELTA1.

= 2 Put in CFC1 and DELST1.

LDSTAR Integer indicating whether a file of $\delta^* + r_w$ is to be input.

= 0 No input.

= 1 File of $\delta^* + r_w$ versus x is required on Logical Unit 15 (data file 4).

LSHPBL Integer indicating whether body shape is to be input for boundary-layer calculations.

= 0 XRL and RL are assumed to be the same as XO and YO. This is usually the case when starting an interaction calculation.

= 1 XRL and RL will be required.

NOTE: The next three variables, NVAR, XVAR, VAR, are only required on cards if LPROG = 1 and LVAR1 = 0 or 1.

NVAR Integer indicating the number of values to be input for the prescribed variable (u_e or δ^*). Maximum value is 100.

XVAR, VAR Axial location and value of prescribed variable as follows:

IOPT = 1 and LVAR1 = 0, VAR = u_e

IOPT = 1 and LVAR1 = 1, VAR = u_e/u_{e_o}

IOPT = 2, VAR = δ^*

EL Reference length. Needed if input data lengths are nondimensionalized. If lengths are dimensional, put in EL = 1.0.

PT Total pressure, p_t (lb/ft^2), (lb/in^2), or (newton/m^2).

TT Total temperature, T_t (°R) or (°K).

TWONTT Ratio of body surface temperature to total temperature, T_w/T_t.

VISC Constant λ in Sutherlands formula for viscosity.

$$\mu = \lambda \frac{T^{3/2}}{T + T_s}$$

If one of the programmed values is acceptable, put in a value of 0.0. The value used will then be determined by the value of IUNIT on item number 3 as follows:

IUNIT	VISC
1	$2.27(10^{-8})$ lb sec/ft^2 (°R)$^{1/2}$
2	$1.5764(10^{-10})$ lb sec/in^2 (°R)$^{1/2}$
3	$1.4582(10^{-6})$ Newton sec/m^2 (°K)$^{1/2}$

RGAS Gas constant. If one of the programmed values is acceptable, put in a value of 0.0. The value used will be determined by the value of IUNIT as follows:

IUNIT	RGAS
1	1716.0 ft^2/sec^2 °R
2	247104.0 in^2/sec^2 °R
3	286.96 m^2/sec^2 °K

SCON Constant T_s, in Sutherlands viscosity law (see definition for VISC and equation 31). If one of the programmed values is acceptable, put in a value of 0.0. The value used will be determined by the value of IUNIT as follows.

IUNIT	
1	198.6 °R
2	198.6 °R
3	110.333 °K

DFACT Relaxation factor for adding δ^* to body, the factor α in equation (4). Usual value is 0.5. If a value of 0.0 is put in, a value of 0.5 will be used.

XZ Axial location of beginning of boundary-layer calculation.

RLEN Axial location of end of boundary-layer calculation. Usually at least one maximum diameter larger than XBT. For a plume RLEN is automatically extended to match the inviscid grid.

XT Axial location of transition from laminar to turbulent boundary-layer flow.

DXP Axial interval at which velocity profiles are to be printed. If a value of 0.0 is put in, no profiles are printed. In any case, profiles will not be printed more often than the output step size for individual output quantities (see section 11.1).

HLIM Limit value of H_i to indicate separation as discussed in section 5.6. Input of a blank or a value of 0.0 will cause a value of 1.3 to be used. To move the initial value of x_s forward, decrease HLIM. To move x_s downstream, increase HLIM. A value greater than 4.0 will allow the calculation to proceed to a separation singularity if one should occur. The calculation will terminate at that point. See section 7 for a discussion of the use of HLIM in sample calculations.

CFC1 Value of skin-friction coefficient at initial boundary-layer station (see section 10.4).

DELTA1 Value of boundary-layer thickness, δ (compressible), at initial boundary-layer station (see section 10.4).

DELST1 Value of boundary-layer displacement thickness, δ^*, at initial boundary-layer station (see section 10.4).

UE1 Value of boundary-layer-edge velocity u_e at initial boundary-layer station.

DUEDX Value of boundary-layer-edge velocity gradient at initial boundary-layer station.

NR Integer number of values of XRP and RL to be input for body shape. If NSHPBL = 0, this is assumed to be the same as IXY. Maximum value is 200.

XRP,RL Axial and radial coordinates of body shape for boundary-layer calculation. If LSHPBL = 0, these are assumed to be the same as XO and YO, respectively. For two-dimensional configurations, these represent the x and y coordinates of a surface measured from a reference plane.

10.0 PROGRAM OPTIONS

Several optional modes of calculation are available through the input parameters. A description of the options and the corresponding values of the pertinent parameters follows.

10.1 BOUNDARY-LAYER OPTION

To use only the boundary-layer program, put in the three card description, then all values on the fourth input data card, Item 2 in Table II, should be zero. Then the first value on the fifth input data card should be:

LPROG=1 (see Table II, Item 3)

Of the remaining variables shown on item number 3 in Table II, only IUNIT is required. The remaining cards would be those corresponding to item 4 and items 13 to 21 as described in Table II. With this option, the user has the choice of specifying either the free-stream velocity, u_e, or the displacement thickness, δ^*, through the variables NVAR, XVAR, and VAR on items 14 and 15. The boundary-layer calculation can be restarted at any station by inputting the values of the variables at that station as listed in the output. The calculated list of $\delta^* + r_w$ and u_e/u_{e_o} will be written on Logical Unit 10 (data file 4) when the calculation terminates.

Another method is also available for calculating the boundary layer alone. The boundary-layer step of a viscid-inviscid iteration can be executed separately. The appropriate values on the fifth card would be:

LPROG = 0

N1 = 1

N2 = 21

IBL = 0

IUNIT = 1, 2, or 3

This option requires input of all quantities as though the iterative sequence were to be completed. With the values just described, only the boundary layer will be calculated and then the run will be terminated. If it is desired to continue the iteration, simply make N2 less than 21. The free-stream velocity distribution must be provided on Logical Unit 12 for this case. All other optional inputs are the user's choice.

10.2 INVISCID-FLOW OPTION

To use only the inviscid-flow program, put in the three card description, then all values on the fourth card should be zero. Then put in LPROG = -1 on the fifth card (item number 3 in Table II). Of the remaining values on that card, only IUNIT is required and that quantity is required only if PLUMIN is TRUE. After the first five cards only the data for items 4 to 9 or 10 as described in Table II and section 9.2 are required for this option.

10.3 VISCID-INVISCID ITERATION OPTION

To use both the boundary-layer and the inviscid-flow programs iteratively, put in LPROG = 0 and all other quantities as appropriate. Such iterations can be started with only the body shape and free-stream flow quantities known and may be restarted to continue a prematurely terminated iteration. Several options are available to the user for restarting an unfinished iteration. See section 13.2 for an example of restarting. The simplest option is to put in NRSTRT = 1 as the first value on the fourth input data card and to provide the required input data files on Logical Units 11, 12, 13, 14, and 15 (see fig. 16 and Table I). The only other data required for restarting are the three-card description of the case. The calculation then proceeds from where the previous iteration stopped. Another method of restarting would be to omit the restart file and put in NRSTRT = 0. The user can then vary any of the other input quantities, using the data files or punched cards as desired. Note that the calculation terminates when N2 reaches a value of 21. The value of N1 increases continuously throughout the calculation while the value of N2 is reset to 1 each time the x_s-θ_s cycle finds a minimum error without satisfying the convergence criterion.

10.4 BOUNDARY-LAYER INITIAL CONDITIONS

Initial values of boundary-layer quantities can be obtained in several ways. The user can obtain values of the skin-friction coefficient, C_f, and either the boundary-layer thickness, δ, or the displacement thickness, δ^*. These are shown on item 19 in Table II. The appropriate values LSHAPE = 0 and LIC = 1 or 2 are punched on the card corresponding to item 13. For the case when no other source of this information is available, formulas have been included in the program based on the Blasius solution for laminar boundary layers and based on one-seventh power law velocity profiles for turbulent flows. These formulas are only available if u_e is being specified (IOPT = 1). The basic formulas calculate C_f and δ in the transform plane (incompressible, two-dimensional). The formulas are as follows:

Laminar Flow

$$C_{f_i} = \frac{0.664}{\sqrt{\frac{U_e}{\nu_{e_o}} x}} \tag{127}$$

$$\delta_i = \frac{5x}{\sqrt{\frac{U_e}{\nu_{e_o}} x}} \tag{128}$$

Turbulent Flow

$$C_{f_i} = 0.0592 \left(\frac{U_e}{\nu_{e_o}} x\right)^{-0.2} \tag{129}$$

$$\delta_i = 0.37 \ x \left(\frac{U_e}{\nu_{e_o}} x\right)^{-0.2} \tag{130}$$

These formulas provide initial values for boundary layers on flat plates. They are chosen by inputting LSHAPE = 1. For other geometries, the value of the x coordinate is transformed. Thus, LSHAPE = 2 chooses the values for a circular cylinder where

$$x = \frac{r_w^2}{x_a} \tag{131}$$

where x_a is the axial coordinate and LSHAPE = 3 chooses the values for a cone, where

$$x = \frac{1}{3} \left(\frac{r_w^2}{x_a}\right) \tag{132}$$

These formulas have been found to be quite adequate for calculating flows over long bodies. Small initial errors in the calculated boundary layer become negligible in a few boundary-layer thicknesses.

11.0 PROGRAM OUTPUT

11.1 STANDARD OUTPUT

Several options are available for output from the programs. The parameter NPRINT on item number 2 in Table II chooses either all the available output (NPRINT = 1) or only that essential for monitoring the progress of an iterative calculation. The parameter DXP on item 17 controls the printing of boundary-layer velocity profiles. For iterative calculations, the full output from the inviscid-flow program is printed only on the first iteration (N1 = 1). For subsequent iterations, only the short form output is printed. No units are printed in the output since any units are allowed in the input.

The complete program output is presented in the following list. Steps 1-10 are always printed for the first iteration. Of the remaining steps, those denoted by an asterisk (*) are those printed at the end of an x_s-θ_s iteration (N2 index) when NPRINT = 0. For NPRINT = 1 all output (steps 11-18) is printed for every value of N1.

1. Three-line title or description.
2. List of all values of integers on first and second data card.
3. List of Body Geometry input.
4. List of other input values for inviscid flow.
5. List of input indices for boundary-layer calculation.
6. List of Body shape data for boundary layer.
7. List of other boundary-layer input quantities.
8. Computed geometric parameters in normal direction for inviscid flow.

   J - Normal grid index.

   AN - Normal coordinate.

   G - Stretching function derivative (refs. 3 and 5).

   GH - Stretching function derivative at half intervals.
9. Computed geometric parameters in tangential direction.

   I - Tangential grid index.

   S - Arc length along reference surface.

   X - Axial coordinate.

   Y - Radial coordinate.

THET - Angle of reference coordinate surface, θ. For closed bodies, θ is the same as the body angle, θ_B. For open bodies, $\theta = \theta_B$ on the forebody and $\theta = 0$ on the afterbody.

THETB - Body angle, θ_B.

AK - Surface curvature on closed bodies. For open bodies AK is the surface curvature on the forebody and AK = $-(d^2r_w/dx^2)$ on the afterbody.

F - Derivative of the tangential stretch function (refs. 3 and 5).

10. Plume velocity and shape distributions. These lists are printed at the beginning, after the 4th iteration and after the last iteration if the solution converges to the least squares error tolerance.

11. Inviscid relaxation iteration history.

IT - Iteration number.

DPMAX - Maximum ϕ correction, $\max\limits_{ij}\left|\phi_{ij}^{IT} - \phi_{ij}^{IT-1}\right|$

ID,JD - I and J location of DPMAX.

RMAX - Maximum residual, $\max\limits_{ij}\left|R_{ij}\right|$, where R_{ij} is the right-hand side of the difference equation.

IR,JR - I and J location of RMAX.

ISUB,ISUP - Indicates if maximum residual occurred at a subsonic or supersonic point.

RAVG - Average value of the residual.

RF1 - Relaxation factor for subsonic points.

QF3 - Relaxation factor for supersonic points.

NS - Number of supersonic points.

SEC/CY - Time for iteration cycle.

12. List of solution of perturbation potential.

*13. Tabulated values of surface pressure coefficient, C_p, Mach number, and axial velocity on the body along with a rough plot of C_p along the body. This plot is

distorted in the axial direction because it is for equal spacing in the computational space. The asterisks show the level of sonic C_p.

*14. Drag coefficients by trapezoidal integration of the C_p's on the real body. The displacement surface is removed for calculation of the drag.

*15. Coordinates x and y of the sonic line.

16. Boundary-layer reference velocity, u_{e_o}, unit Reynolds number, R_{e_o}/L and viscosity, ν_{e_o}. This is only printed on the first step (N1 = 1).

*17. List of boundary-layer quantities with profiles at intervals governed by DXP. This is always printed on the 4th iteration since that is the last iteration for which the calculation begins at the nose of the body.

AX - Axial distance from the nose, x.

UTAU - Friction velocity, u_τ.

DELTA - Boundary-layer thickness, δ.

DELST - Displacement thickness, δ^*.

THETA - Momentum thickness, θ.

CF - Skin-friction coefficient, C_f.

UE/UZ - Boundary-layer-edge velocity ratio; u_e/u_{e_o}.

DELST+R - Augmented body radius, $\delta^* + r_w$.

DX - Integration step size.

HTR - Transformed shape factor, δ_i^*/θ_i.

*18. Quantities showing status of inner iteration.

XMAX - Location of maximum change in boundary layer δ^* from previous iteration.

DPMAX - Maximum change in δ^*.

RBT - Body radius at nozzle exit.

*19. Rough plot and list of u_{e_V} and u_{e_I}. This is printed at the end of the inner iteration cycle whenever a new comparison is being made between the viscous and inviscid velocities. This is followed by a list of the current results of the iteration.

XSEP = x_s

THET = θ_s (degrees)

DRMS = rms error, s (percent of u_{e_o})

11.2 SPECIAL OUTPUT MESSAGES

Several special messages are contained in the output to call attention to specific conditions that may occur. The messages are listed in this section with instructions about what to do when they are encountered.

(1)---------DIVERGENCE.RMAX EXCEEDS RCHEK,---------

This message is printed by the inviscid-flow program if the relaxation procedure diverges. Check all input to verify that it is correct. If no obvious errors appear, the difficulty is probably either in the choice of parameters for the computational mesh, or the smoothness of the data defining the body shape.

(2) RF1 DECREASED TO ___ BECAUSE 10-CYCLE AVG FOR RMAX INCREASED.

This message refers to the subsonic relaxation factor in the inviscid-flow program. The initial value is 1.4. The value is automatically reduced by 10 percent if: (1) the maximum residual, averaged over 10 cycles, is greater than that for the previous 10 cycles and (2) the last maximum residual occurred at a subsonic point.

(3) QF3 INCREASED TO ___ BECAUSE 10-CYCLE AVE FOR RMAX INCREASED.

This message refers to the supersonic damping factor in the inviscid-flow program. The initial value is 0.1. The value is automatically increased if: (1) the maximum correction, averaged over 10 cycles, is greater than that for the previous 10 cycles, and (2) the last maximum residual is at a supersonic point.

(4) INPUT FROM TAPE13 HAS INCOMPATIBLE DIMENSIONS

This message is printed if the dimensions of the ϕ_{ij} solution read from Logical Unit 13 (data file 2 in figure 3) are not

the same as the values of IMAX and JMAX put on item number 7 in Table II.

(5)****ITERATION FOR BOUNDARY LAYER/INVISCID FLOW EQUILIBRIUM CONVERGED

This message is printed whenever the maximum change in δ^* between iterations is less than the specified percent.

(6) METHOD FOR CALCULATING UTAU IN DERIV DOES NOT CONVERGE

This message refers to the iteration used to solve equation (55) for U_τ when δ^* is prescribed in the boundary-layer calculation. The only known cause of the iteration failing to converge is an error in the input data.

(7) DELTAI HAS BECOME NEGATIVE
STOP INTEGRATION, PRINT PROFILE AT PREVIOUS STEP

This message refers to the transformed boundary-layer thickness, δ_i. The error condition may occur due to the initial integration step size DXZ being too large. Another possible cause might be a too sudden change in the body shape, or in the prescribed u_e or δ^* distribution.

(8) DELTA HAS BECOME NEGATIVE
STOP INTEGRATION, PRINT VALUES AT PREVIOUS STEP

This message is not expected to occur in the finished program. If it does, check the input data carefully.

(9) METHOD FOR CALCULATING K IN ENTRAN DOES NOT CONVERGE

This message refers to the iteration used to solve equation (72) for K when δ^* is prescribed in the entrainment-layer calculation. The only known cause of the iteration failing to converge is an error in the input data.

(10) METHOD FOR CALCULATING INITIAL VALUE OF DELI DOES NOT CONVERGE

When initial values of C_f, δ, or δ^* are known, the calculation must solve an integral equation for the initial value of the transformed thickness, δ_i. This is done by iteration in a similar manner as for u_τ described in message (6). If the iteration does not converge, it is usually due to errors in the input quantities.

(11) INTERMEDIATE RESULTS OF ITERATION

This message is printed at the end of each step of the x_s-θ_s cycle. It is followed by the current value of x_s, XSEP, the current value of θ_s, THET, and the value of the rms error, DRMS.

(12) ***FINAL RESULTS***
BEST SOLUTION WAS ITERATION NO.___

This message is printed whenever the least squared error has been found for the x_s-θ_s cycle discussed in section 2.2.

(13) ****SOLUTION CONVERGED TO LEAST SQUARED ERROR TOLERANCE

This message is printed whenever the rms error is less than 1 percent of u_{e_o} at any stage of the iteration. The inviscid and viscous solutions immediately preceding this message are then the best solutions of the calculation procedure.

(14) SKIN FRICTION HAS BECOME NEGATIVE IN AN INCORRECT MANNER. CHECK ALL INPUT CAREFULLY

This message will be printed if the skin-friction coefficient changes sign. It may indicate that the initial estimate of the separation point location was too far downstream. It has usually been observed to occur when strong shocks are present, or when too few relaxation steps, MIT were used initially.

(15) ATTACHED BOUNDARY LAYER SOLUTION TERMINATED AFTER ___ ITERATIONS

This message will be printed if the viscous-inviscid interaction converges (Message 5) and no separation occurred or the separation point for the next iteration would have been downstream of the end of the body.

12.0 PROGRAM OPERATING PROCEDURE

In this section, the construction of card decks for operation of the computer programs is described. First, a general description of the operations required is given. Then the specific Job Control cards needed for operation on an IBM 370 computer are listed. The same card decks should be applicable at any 370 installation with minor modifications.

12.1 GENERAL JOB CONTROL SEQUENCE

The following list is the general Job Control procedure that would be required to run the programs for a complete viscid-inviscid interaction calculation. The reader is referred to figure 16 and Table I.

1. Create partitioned data sets for restart files (files 1-5 in figure 16).
2. Define units 2,3,8,9, and 10. These unit numbers are needed for output.
3. Define units 11,12,13,14, and 15 if NRSTRT = 1 in the input data. These unit numbers correspond to the input files. They contain data created in a previous run.

For starting an initial calculation, the partitioned data sets would be created in a separate operation. Then, since no data would be on file, only units 2,3,8,9, and 10 need to be defined. For restarting an iterative calculation, all data files would exist, so units 11 to 15 must also be defined.

To execute the boundary-layer program alone, unit 10 must be defined in order to output the $\delta^* + r_w$ and u_e/u_{e_o} list. Unit 12 must be defined when LVAR1 = 2, and unit 15 must be defined when LDSTAR = 1.

To execute the inviscid program alone, units 2 and 8 must be defined. Unit 13 is also required when LREADP = 1, and unit 14 is required when IXY = 0.

12.2 JOB CONTROL EXAMPLES

In this section, specific examples of Job Control cards used for the operations discussed previously are presented. In the examples, the computer program is referred to as "ITER" with the source code names "SITER" and the load module or binary version named "BITER". The account ID used in the examples is WYL.XM.K01. Logical units 5 and 6 are the standard input/output file numbers. It is not necessary to specifically define these unit numbers in the JCL deck.

12.2.1 Creating Partitioned Data Sets

Partitioned data sets for use as input/output disk files must be created before the normal program operation can proceed. The following procedure is suggested:

Use IBM Utility Program IEFBR14.

Use default values for DCB (DSORG=PO,RECFM=VS).

On 3330 disk, use SPACE in tracks as follows (refer to figure 16 and Table I for explanation of file numbers):

```
VELBOD (File 3)         SPACE = (TRK,(2,1,10))
RESTRT (File 5)         SPACE = (TRK,(10,2,10))
PHI    (File 2)         SPACE = (TRK,(20,4,10))
XOFILE (File 1)         SPACE = (TRK,(4,1,10))
DSFILE (File 4)         SPACE = (TRK,(6,1,10))
```

Example of creating a partitioned data set called VELBOD:

```
//EXEC PGM=IEFBR14
//A DD DSN=WYL.XM.K01.VELBOD,VOL=volume,
//      UNIT=3330,DISP=(,CATLG),
//      SPACE=(TRK,(2,1,10))
```

12.2.2 Starting an Iteration Sequence

To start an iteration sequence, unit numbers 2, 3, 8, 9, and 10 must be defined. The specific sequence of cards used to perform the calculations presented in section 13.1 is as follows:

```
//EXEC FORTGO,PROG=ITER,VOL=volume
//      LIB='WYL.XM.K01.BITER'
//GO.FT02F001 DD DSN=WYL.XM.K01.VELBOD(RUN1),
//      DISP=OLD
//GO.FT03F001 DD DSN=WYL.XM.K01.RESTRT(RUN1),
//      DISP=OLD
//GO.FT08F001 DD DSN=WYL.XM.K01.PHI(RUN1),
//      DISP=OLD
//GO.FT09F001 DD DSN=WYL.XM.K01.XOFILE(RUN1),
//      DISP=OLD
//GO.FT10F001 DD DSN=WYL.XM.K01,DSFILE(RUN1),
//      DISP=OLD
//GO.SYSIN DD *
        { Input data cards
/*
```

12.2.3 Restarting an Iteration Sequence

The specific cards used to perform a restart of the calculation started in the previous section are:

```
// EXEC FORTGO,PROG=ITER,VOL=volume,
//       LIB='WYL.XM.K01.BITER'
//GO.FT02F001 DD DSN=WYL.XM.K01.VELBOD(RUN2),
//       DISP=OLD
//GO.FT03F001 DD DSN=WYL.XM.K01.RESTRT(RUN2),
//       DISP=OLD
//GO.FT08F001 DD DSN=WYL.XM.K01.PHI(RUN2),
//       DISP=OLD
//GO.FT09F001 DD DSN=WYL.XM.K01.XOFILE(RUN2),
//       DISP=OLD
//GO.FT10F001 DD DSN=WYL.XM.K01.DSFILE(RUN2),
//       DISP=OLD
//GO.FT11F001 DD DSN=WYL.XM.K01.RESTRT(RUN1),
//       DISP=OLD,LABEL=(,,,IN)
//GO.FT12F001 DD DSN=WYL.XM.K01.VELBOD(RUN1),
//       DISP=OLD,LABEL=(,,,IN)
//GO.FT13F001 DD DSN=WYL.XM.K01.PHI(RUN1),
//       DISP=OLD,LABEL=(,,,IN)
//GO.FT14F001 DD DSN-WYL.XM.K01.XOFILE(RUN1),
//       DISP=OLD,LABEL=(,,,IN)
//GO.FT15F001 DD DSN=WYL.XM.K01.DSFILE(RUN1),
//       DISP=OLD,LABEL=(,,,IN)
//GO.SYSIN DD *
        { Input data cards
/*
```

These cards were used with the example discussed in section 13.2. The input data cards required for restarting are summarized in Table III.

12.2.4 Executing the Boundary-Layer Program Alone

The specific cards used to perform the calculations discussed in section 13.3 are listed in this section. In the example shown here, all input is assumed to be from cards, but the output list of $\delta^* + r_w$ and u_e/u_{e_o} is to be saved on unit 10. Unit 12 would be required for input if LVAR1 = 2, and unit 15 would be required if LDSTAR = 1. The cards used in the example in section 13.3 are:

```
// EXEC FORTGO,PROG=ITER,VOL=volume
//        LIB='WYL.XM.K01.BITER'
//GO.FT10F001 DD DSN=WYL.XM.K01.DSFILE(RUN1),
//        DISP=OLD
//GO.SYSIN DD *
        { Input data cards
/*
```

12.2.5 Executing the Inviscid Program Alone

The cards used to perform the calculations discussed in section 13.4 are listed in this section. In this example, the velocity potential, ϕ, is input from unit 13, and the new solution for ϕ is output on unit 8. The calculated velocity on the body is output on unit 2. Input from unit 13 corresponds to LREADP = 1 in the card input data. In addition, unit 14 would be required for input of the body shape if IXY = 0 in the card input data. The specific cards used in the example are:

```
// EXEC FORTGO,PROG=ITER,VOL=volume,
//        LIB='WYL.XM.K01.BITER'
//GO.FT02F001 DD DSN=WYL.XM.K01.VELBOD(RUN2),
//        DISP=OLD
//GO.FT08F001 DD DSN=WYL.XM.K01.PHI(RUN2),
//        DISP=OLD
//GO.FT13F001 DD DSN=WYL.XM.K01.PHI(RUN1),
//        DISP=OLD,LABEL=(,,,IN)
//GO.SYSIN DD *
        { Input data cards
/*
```

13.0 NUMERICAL EXAMPLES

In this section, several example calculations are presented to aid in program checkout. An example is presented of a complete viscid-inviscid interaction. An example is also presented of the use of the boundary-layer program alone for a two-dimensional geometry. That example also demonstrates the two options for boundary conditions, having u_e specified in the beginning of the calculation, and δ^* specified in the second part. Input data for another sample case are also presented to demonstrate the use of the program to calculate the inviscid flow alone.

13.1 AXISYMMETRIC INTERACTION

A list of the punched card input data for a sample calculation on the boattailed body shown in figure 8a and b is presented in figure 17. The case being calculated is for a free-stream Mach number of 0.8. The body corresponds to the ogive-cylinder body with a circular-arc boattail described in reference 20. The JCL card deck for this case has been presented in section 12.2.2. The running time for the complete calculation is about 3.6 minutes on the IBM 370/165.

Selected output for the sample case is shown in figure 18. The solution converged to the least squared error tolerance in 25 iterations.

The complete list of output for this case, with NPRINT = 0, consisted of a total of approximately 2500 lines. Output steps 1-7 as listed in section 11.1 have been omitted from this presentation since they simply verify the input data. The output pages shown are those corresponding to steps 8-19 of the set described in section 11.1 for NPRINT = 0 on the first iteration and then a few samples of the rough plots of u_{e_V} and u_{e_I} at intermediate steps, including that at iteration 25 (fig. 18(f)). Finally, figure 18 concludes with the inviscid solution and boundary-layer and plume solutions corresponding to the final result.

13.2 EXAMPLE OF RESTARTING AN INTERACTION CALCULATION

The punched card input data for restarting the interaction calculation of section 13.1 if that calculation should undergo premature termination at an intermediate iteration is presented in figure 19. The JCL card deck for this calculation was presented in section 12.2.3. Note that the iterative calculations cannot be restarted at any arbitrary iteration using the restart file, unit 11. That file and the other output files contain only the data that were output just prior to the termination.

13.3 TWO-DIMENSIONAL BOUNDARY LAYER

A list of the punched card input data for a sample calculation on the two-dimensional configuration shown in figure 20 is presented in figure 21. Note that two sets of input are presented for this case, giving an example of the options of prescribed u_e and prescribed δ^*. The data for u_e and δ^* were obtained from the experimental results of reference 18 which indicate separation occurring in an adverse pressure gradient region downstream of a shock wave. The output for the complete boundary-layer calculation are presented in figure 22. No external data files were used for input for this case. The JCL card deck for this case was presented in section 12.2.4.

13.4 AXISYMMETRIC INVISCID FLOW

The punched card input data for a sample calculation of the inviscid flow alone are presented in figure 23. The output for this case is shown in figure 24.

REFERENCES

1. Presz, W. M., Jr. and Pitkin, E. T.: Analytical Model of Axisymmetric Afterbody Flow Separation. Journal of Aircraft, Vol. 13, No. 7, July 1976, pp. 500-505.

2. Cosner, R. R. and Bower, W. W.: A Patched Solution of the Transonic Flow Fields About an Axisymmetric Boattail. AIAA Paper No. 77-227, presented at Fifteenth Aerospace Sciences Meeting, Los Angeles, CA, Jan. 24-26, 1977.

3. Keller, J. D. and South, J. C., Jr.: RAXBOD: A FORTRAN Program for Inviscid Transonic Flow Over Axisymmetric Bodies. NASA TM X-72831, Feb. 1976.

4. Reubush, D. E. and Putnam, L. E.: An Experimental and Analytical Investigation of the Effect on Isolated Boattail Drag of Varying Reynolds Number up to 130×10^6. NASA TN D-8210, May 1976.

5. South, J. C., Jr. and Jameson, A.: Relaxation Solutions for Inviscid Axisymmetric Transonic Flow Over Blunt or Pointed Bodies. Proceedings of the AIAA Computational Fluid Dynamics Conference, Palm Springs, CA, July 19-20, 1973.

6. Henson, J. R. and Robertson, J. E.: Methods of Approximating Jet Boundaries for Highly Underexpanded Supersonic Nozzles. AEDC-TDR-62-7, May 1962.

7. Kuhn, G. D.: Calculation of Compressible, Nonadiabatic Boundary Layers in Laminar, Transitional and Turbulent Flow by the Method of Integral Relations. NASA CR-1797, Nov. 1971.

8. Probstein, R. F. and Elliott, D.: The Transverse Curvature Effect in Compressible Axially Symmetric Laminar Boundary-Layer Flow. J. Aero. Sci., Vol. 23, 1956, p. 208.

9. Stewartson, K.: Correlated Incompressible and Compressible Boundary Layers. Proc. of the Royal Soc., A, Vol. 200, 1949, pp. 85-100.

10. Kuhn, G. D. and Nielsen, J. N.: An Analytical Method for Calculating Turbulent Separated Flow Due to Adverse Pressure Gradients. Project SQUID Tech. Rept. NEAR-1-PU, Oct. 1971.

11. Coles, D.: The Law of the Wake in the Turbulent Boundary Layer. J. Fluid Mech., Vol. 1, pt. 2, 1956, pp. 191-226.

12. Nash, J. F. and Hicks, J. G.: An Integral Method Including the Effect of Upstream History on the Turbulent Shear Stress. Proceedings of the 1968 AFOSR-IFP-Stanford Conference on Computation of Turbulent Boundary Layers. Stanford University, CA, p. 41.

13. Stewartson, K.: On Goldstein's Theory of Laminar Separation. Quarterly Journal of Mechanics and Applied Mathematics, Vol. XI, Pt. 4, 1958.

14. Cebeci, T., Mosinskis, G., and Smith, A.M.O.: Calculation of Separation Points in Incompressible Turbulent Flows. Jour. of Aircraft, Vol. 9, No. 9, 1972, pp. 618-624.

15. Gerhart, P. and Bober, L.: Comparison of Several Methods for Predicting Separation in a Compressible Turbulent Boundary Layer. NASA TM X-3102, 1974.

16. Newman, B. G.: Some Contributions to the Study of the Turbulent Boundary Layer Near Separation. Australian Dept. of Supply, Rept. ACA-53, March 1951.

17. Simpson, R. L.: Characteristics of a Separating Incompressible Turbulent Boundary Layer. Paper No. 14 in Flow Separation, AGARD CP-168, May 1975.

18. Alber, I. E., Bacon, J. W., Masson, B. S., and Collins, D.J.: An Experimental Investigation of Turbulent Transonic Viscous-Inviscid Interactions. AIAA Journal, Vol. 11, No. 5, 1973, pp. 620-627.

19. Nielsen, J. N., Stahara, S. S., and Woolley, J. P.: A Study of Ingestion and Dispersion of Engine Exhaust Products in Trailing Vortex Systems. NASA CR-114,721, November 1973.

20. Reubush, D. E.: Experimental Study of the Effectiveness of Cylindrical Plume Simulators for Predicting Jet-On Boattail Drag at Mach Numbers up to 1.3. NASA TN D-7795, Nov. 1974.

21. Abeyounis, W. K.: Boundary Layer Separation on Isolated Boattail Nozzles. M.S. Thesis, School of Engineering and Applied Science, The George Washington University, May 1977.

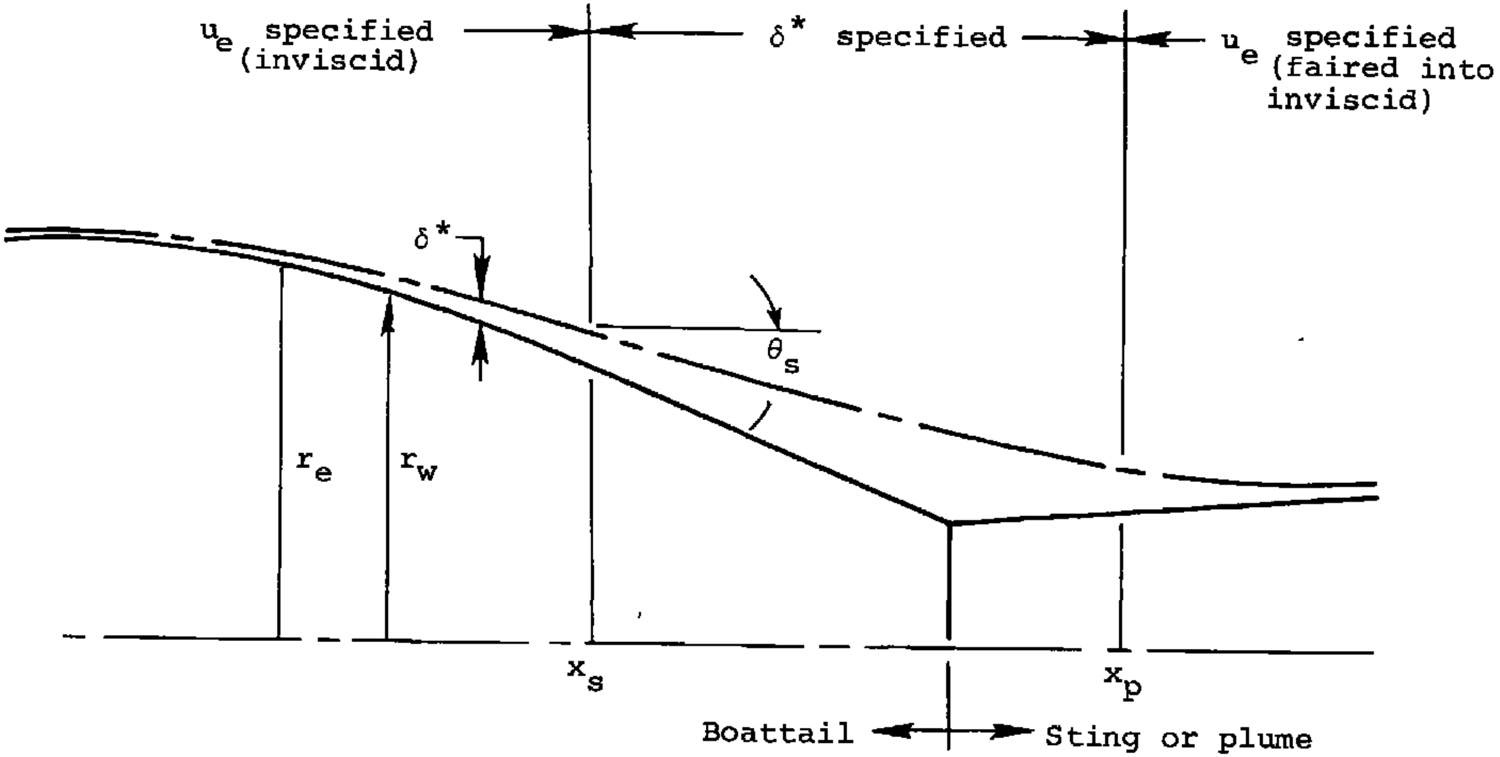

Figure 1.- Effective body shape for separated flow.

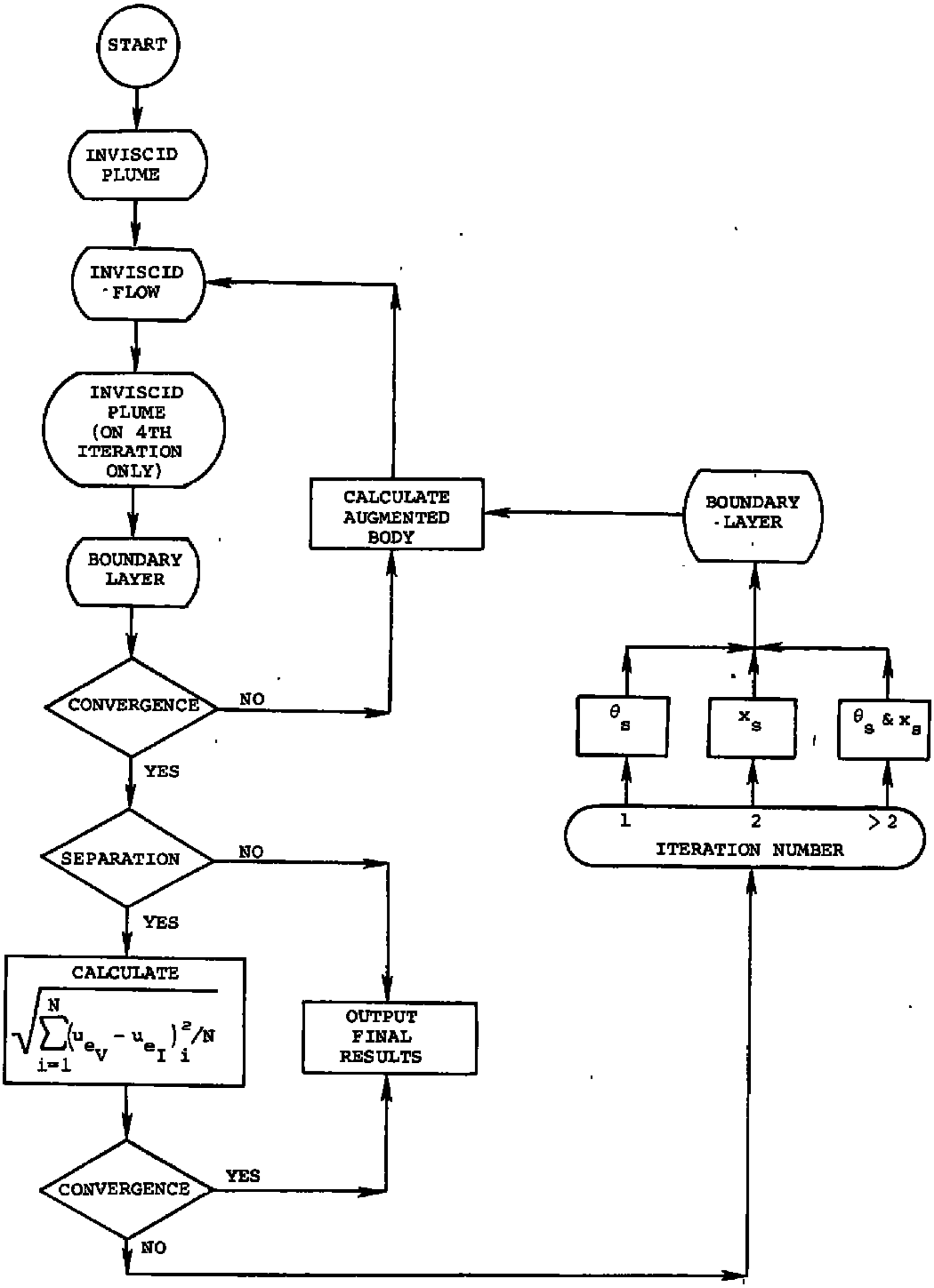

Figure 2.- Schematic of viscous-inviscid interaction iteration.

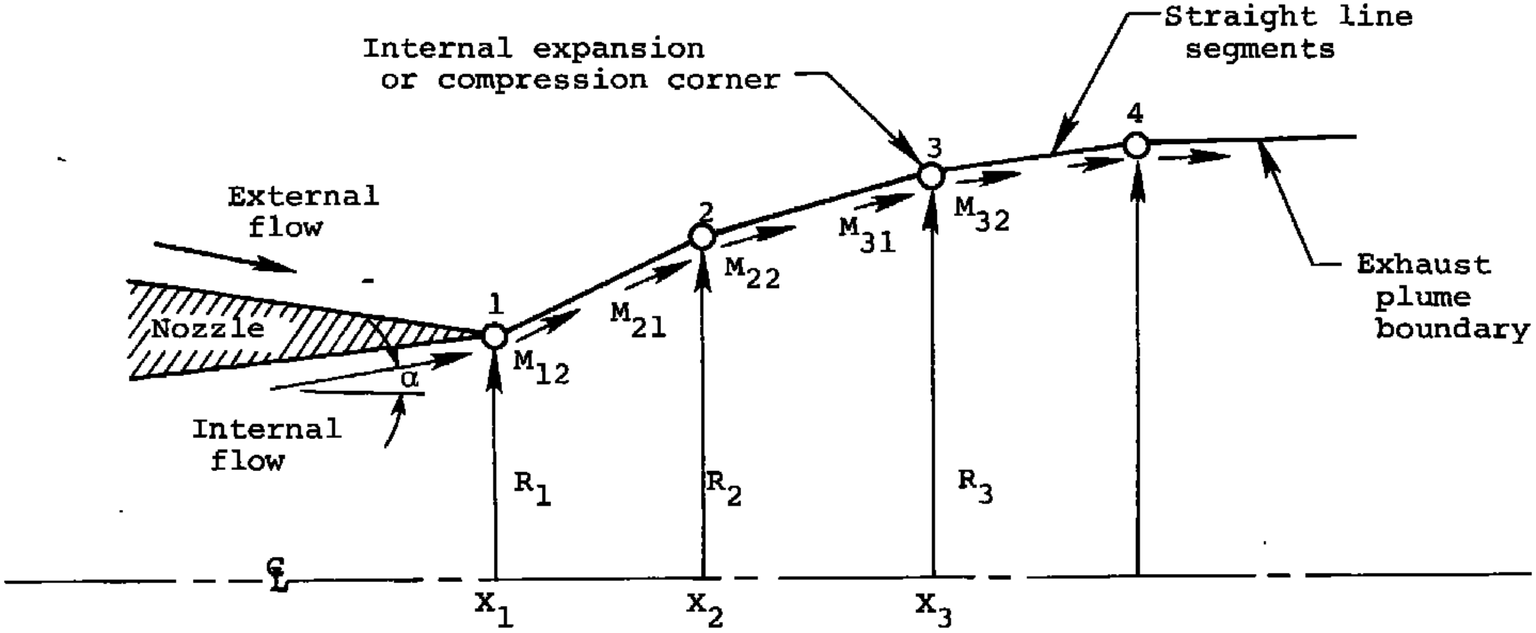

Figure 3.- Illustration of exhaust plume construction.

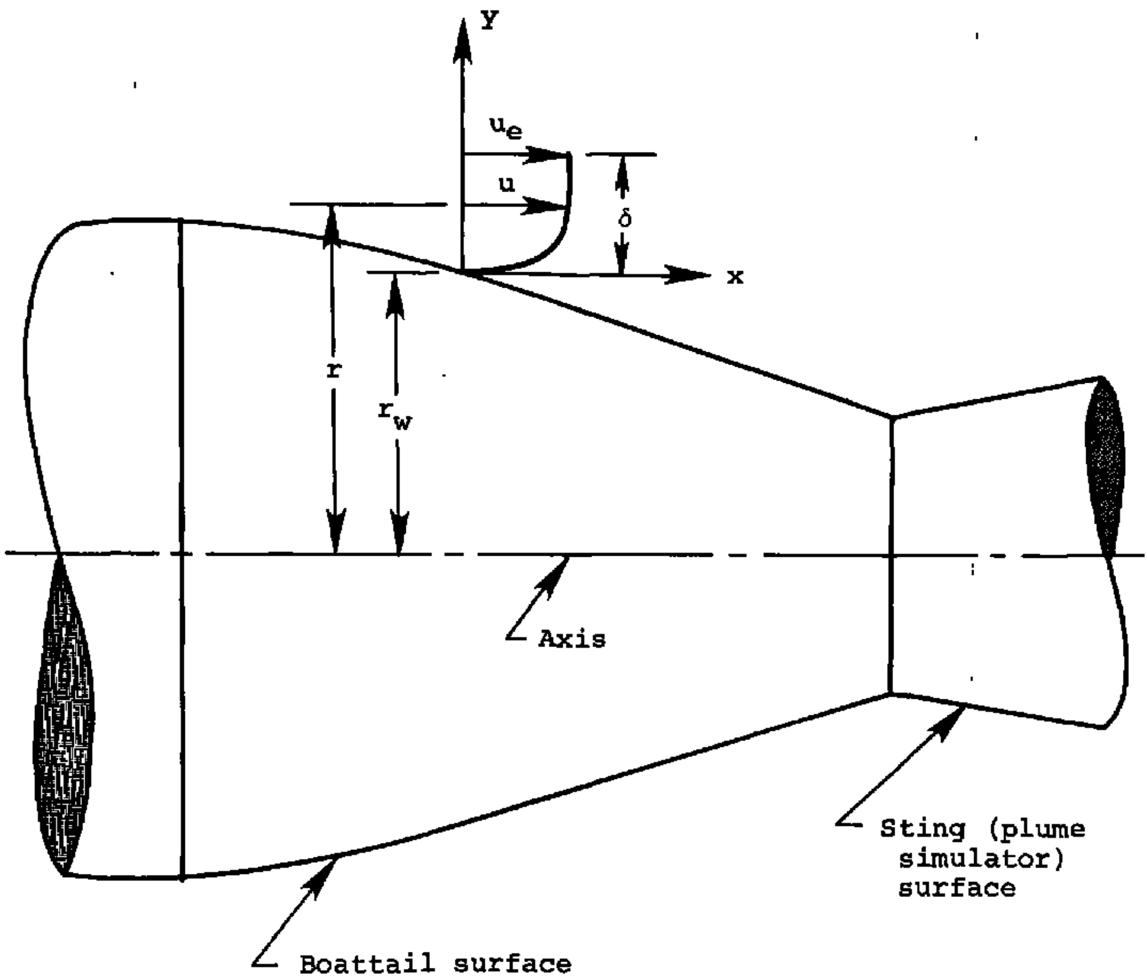

Figure 4.- Boundary layer coordinates and notation.

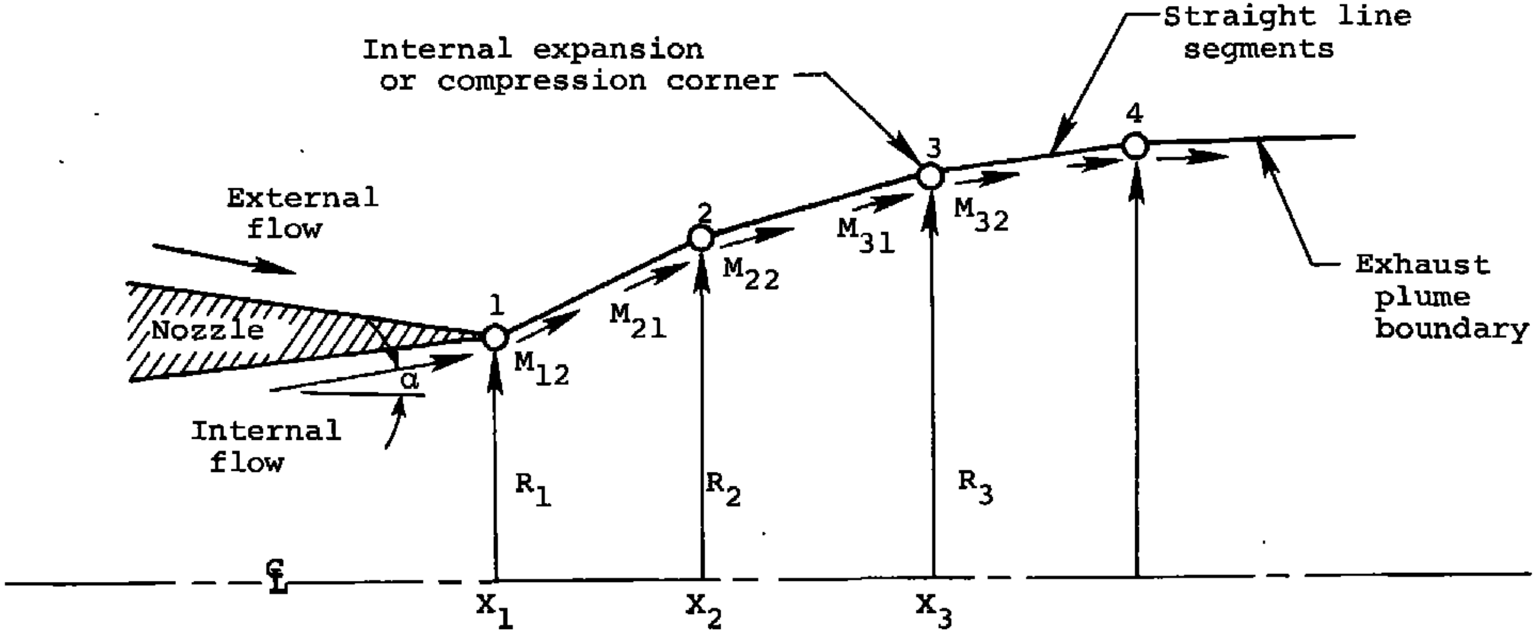

Figure 3.- Illustration of exhaust plume construction.

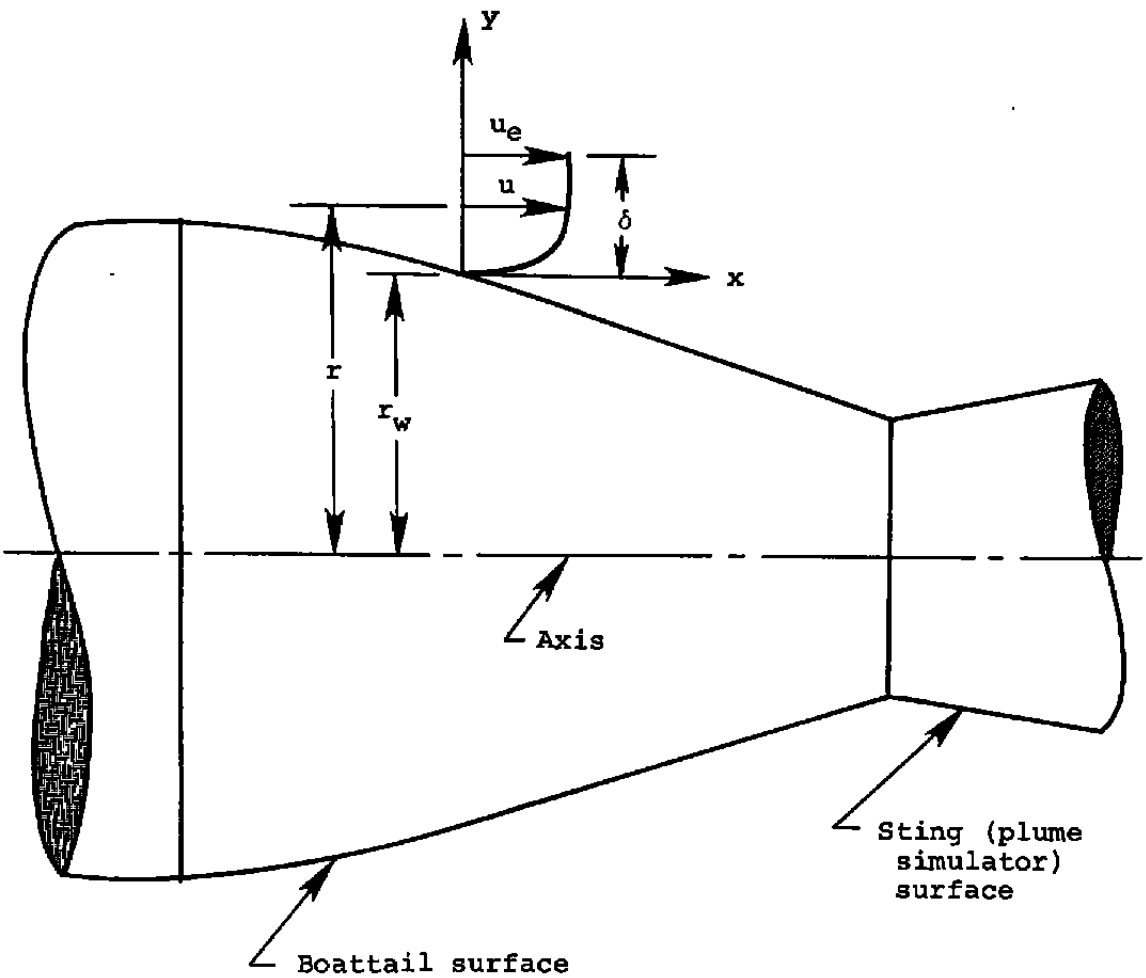

Figure 4.- Boundary layer coordinates and notation.

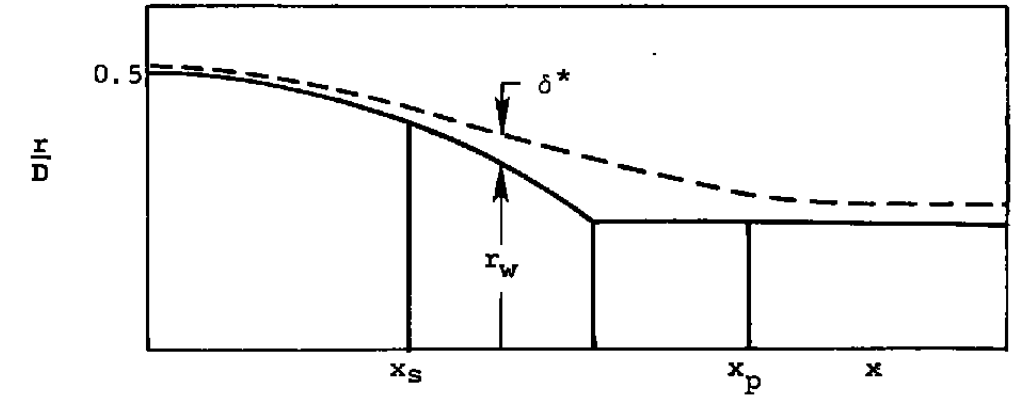

(a) Body shape.

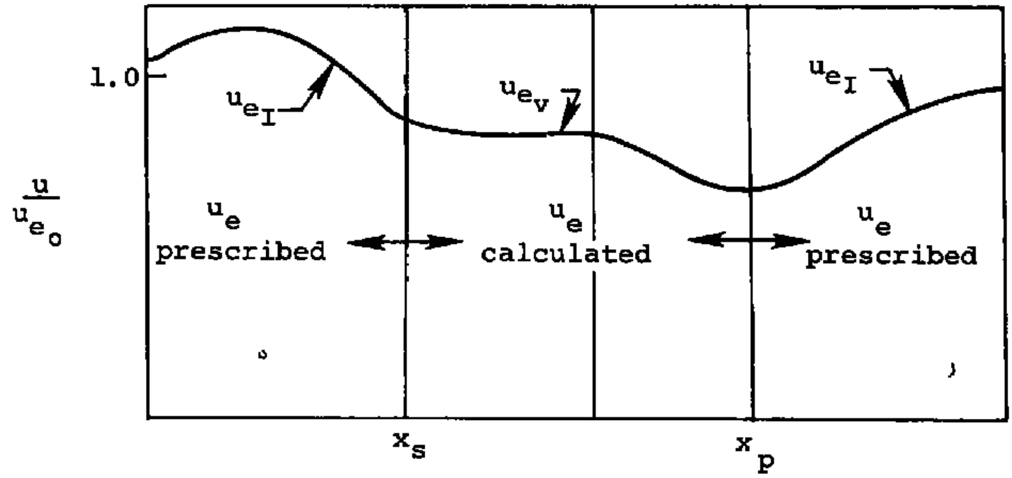

(b) Velocity, u_e

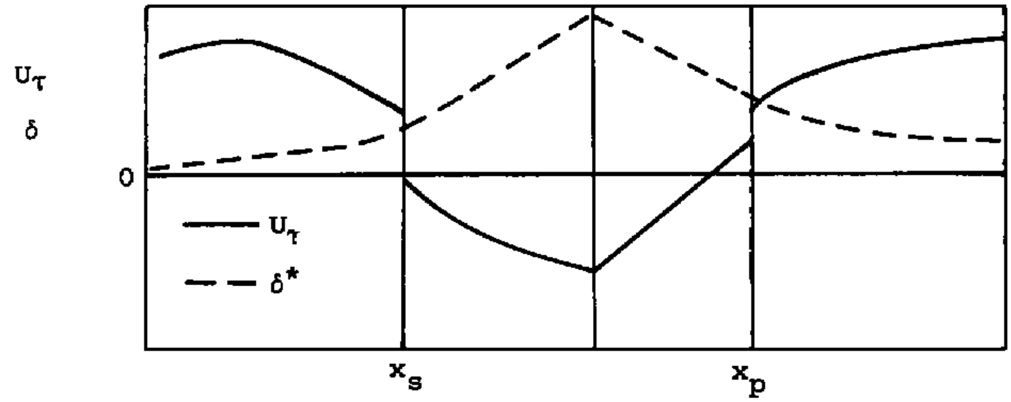

(c) Friction velocity and displacement thickness.

Figure 5.- Typical variation of boundary layer quantities for separated boattail flow.

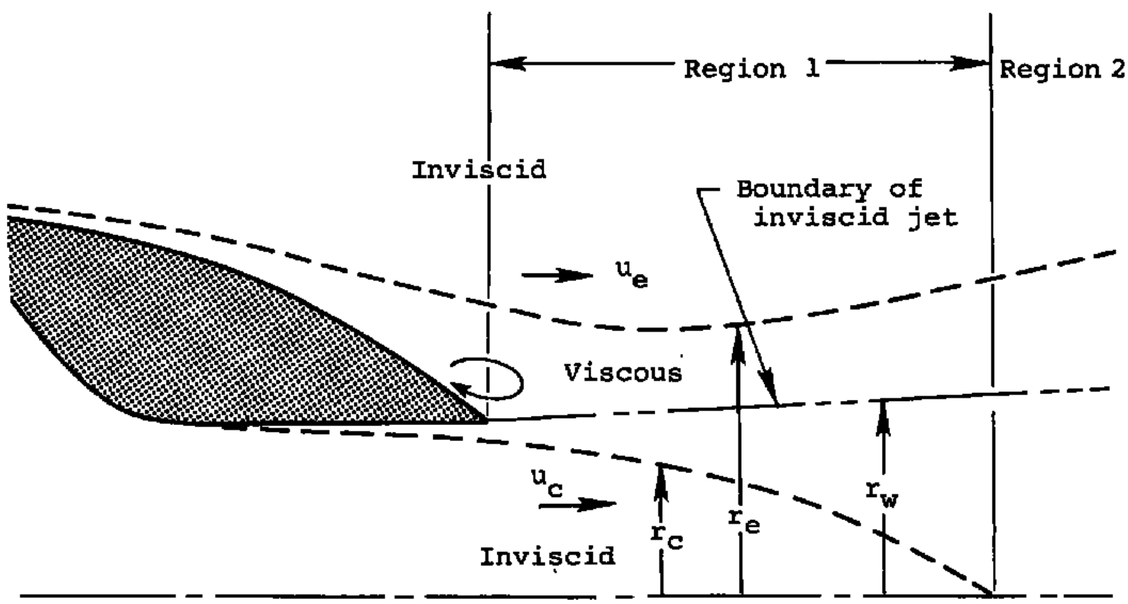

Figure 6.- Schematic of exhaust plume-separated flow entrainment model.

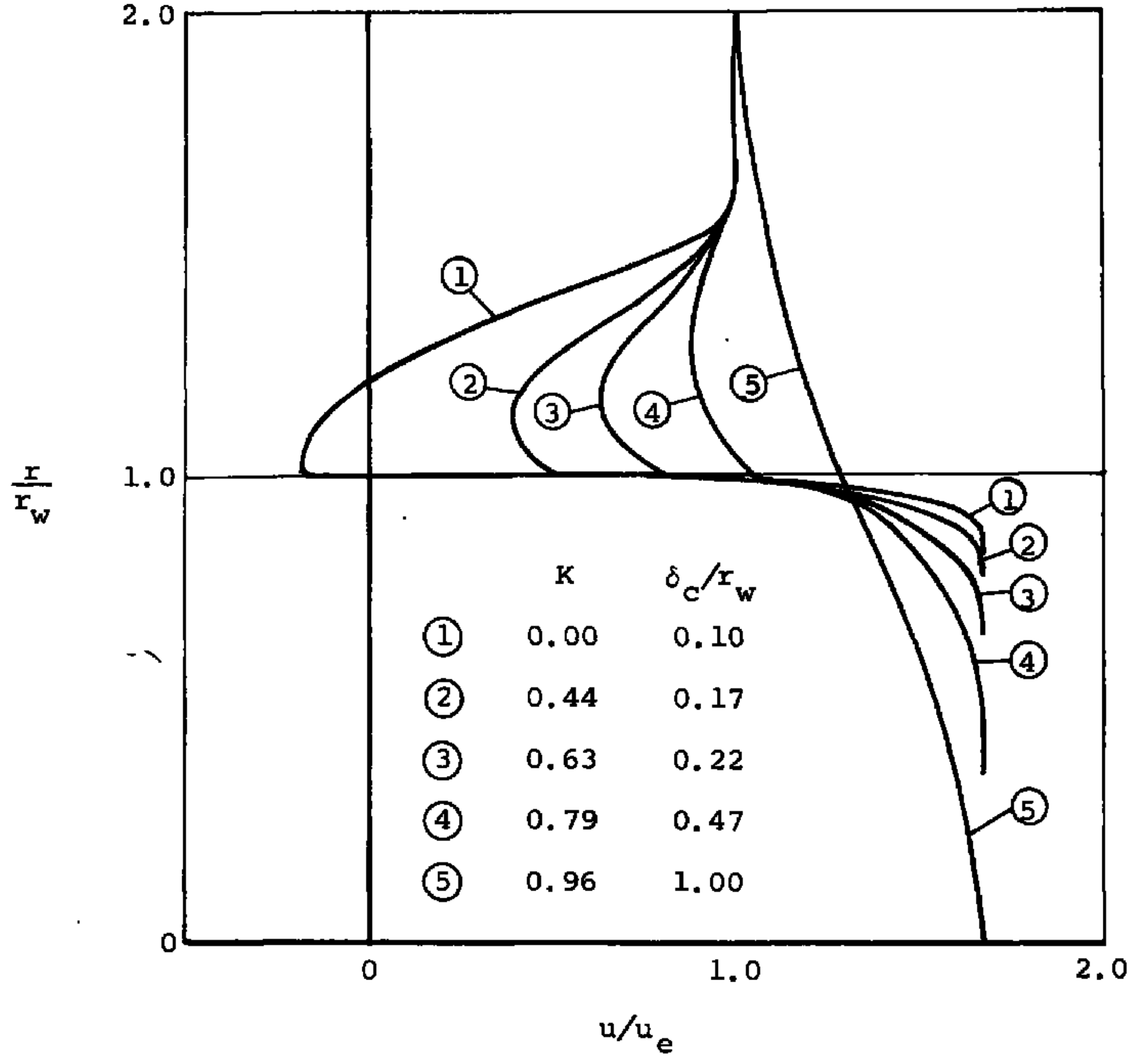

Figure 7.- Typical velocity profiles in the entrainment region.

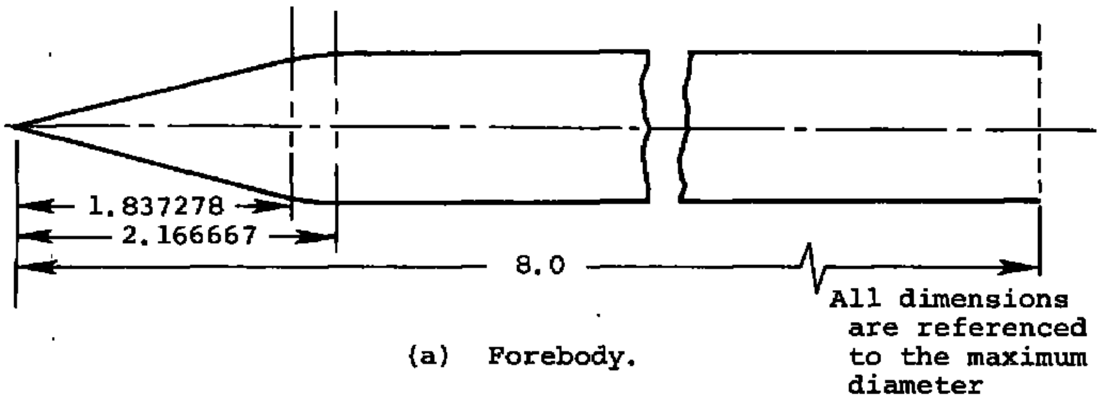

(a) Forebody.

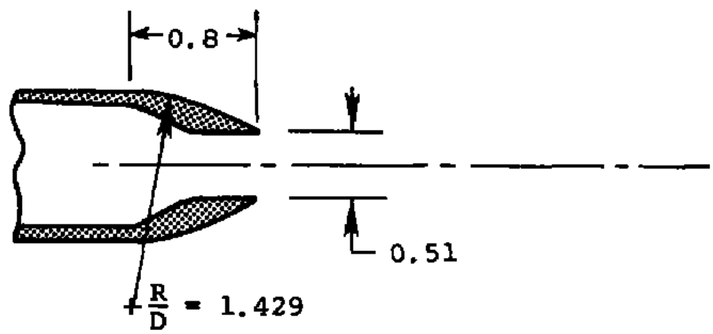

(b) Boattail configuration 1.

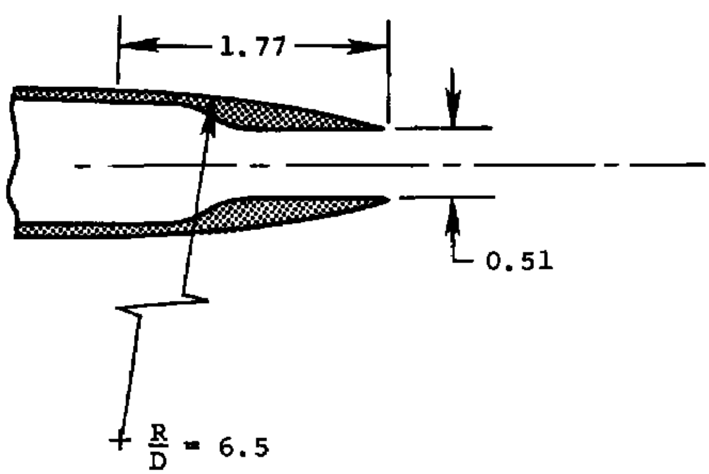

(c) Boattail configuration 2.

Figure 8.- Body with circular arc boattail (ref. 20).

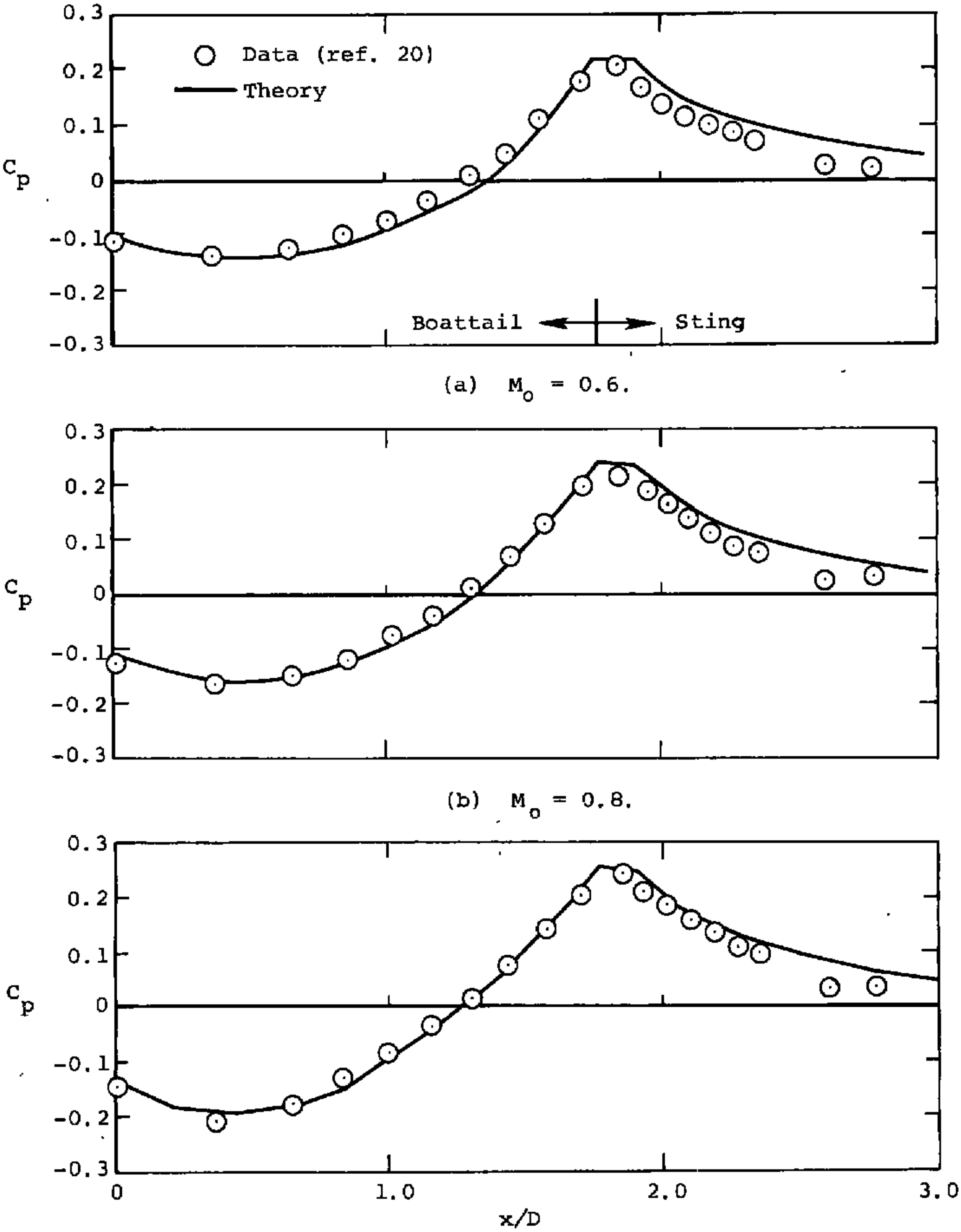

(c) $M_o = 0.9$.

Figure 9.- Comparison between calculated and measured pressure coefficient distributions on unseparated boattail-sting configuration.

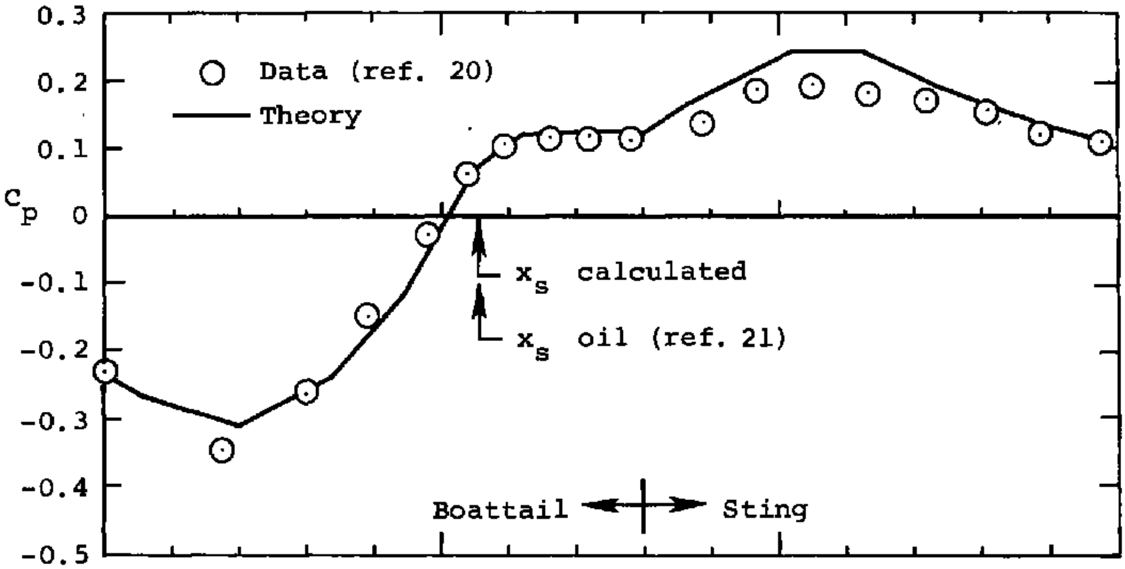

(a) $M_o = 0.6$.

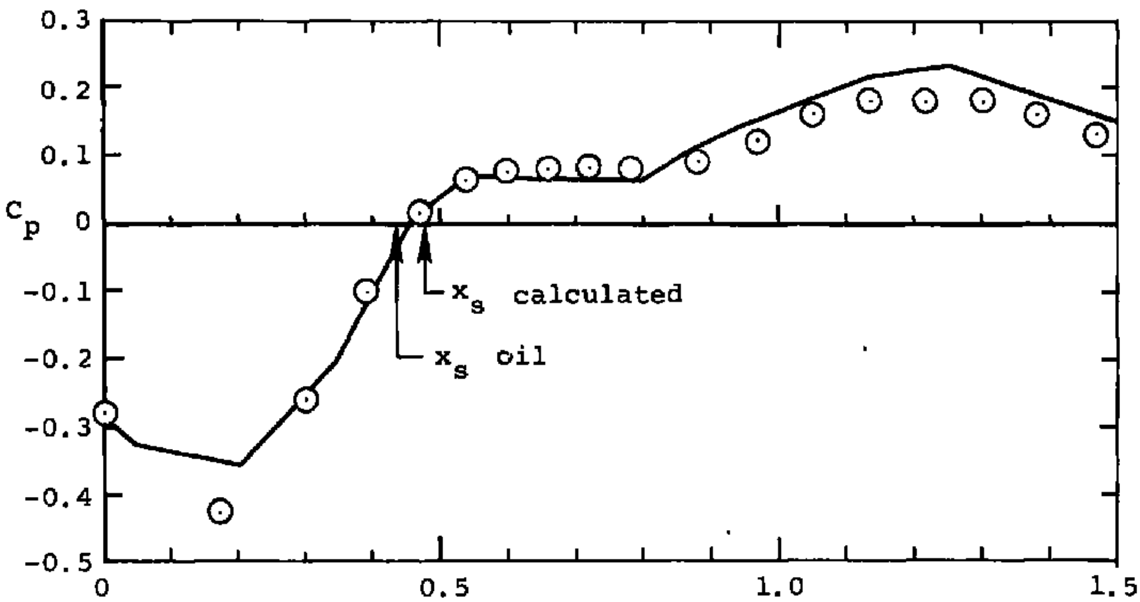

(b) $M_o = 0.8$.

Figure 10.- Comparison between calculated and measured pressure coefficient distributions on a boattail-sting configuration with separation.

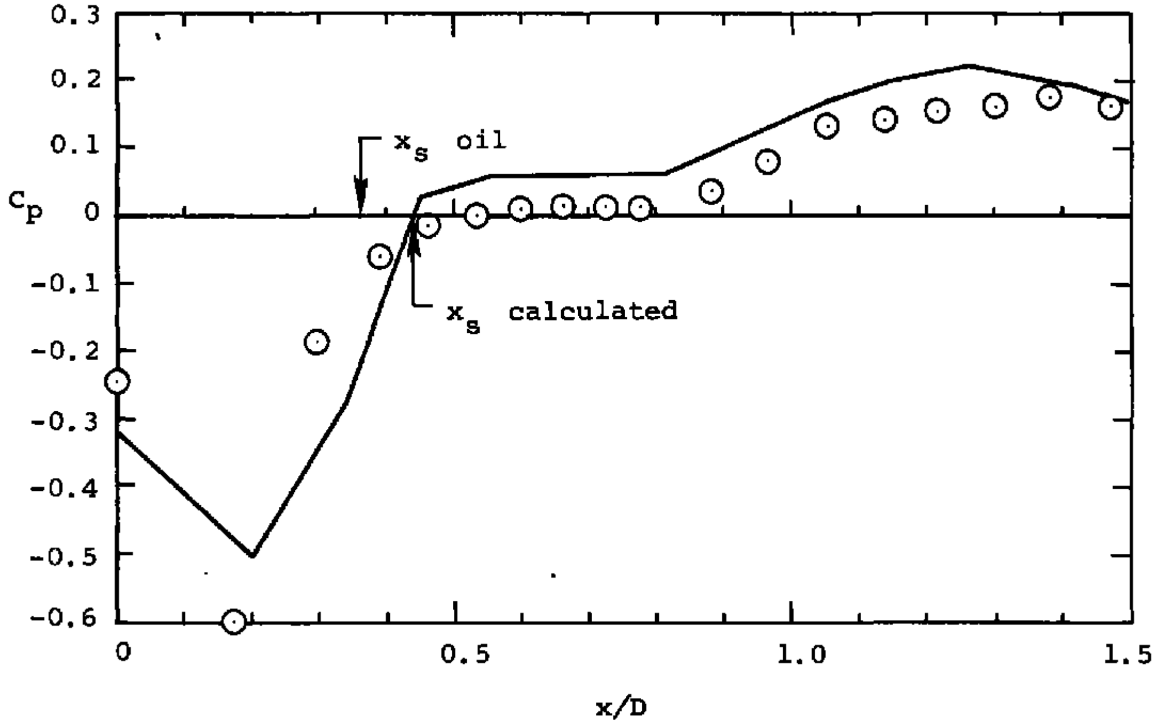

(c) $M_o = 0.9$.

Figure 10.- Concluded.

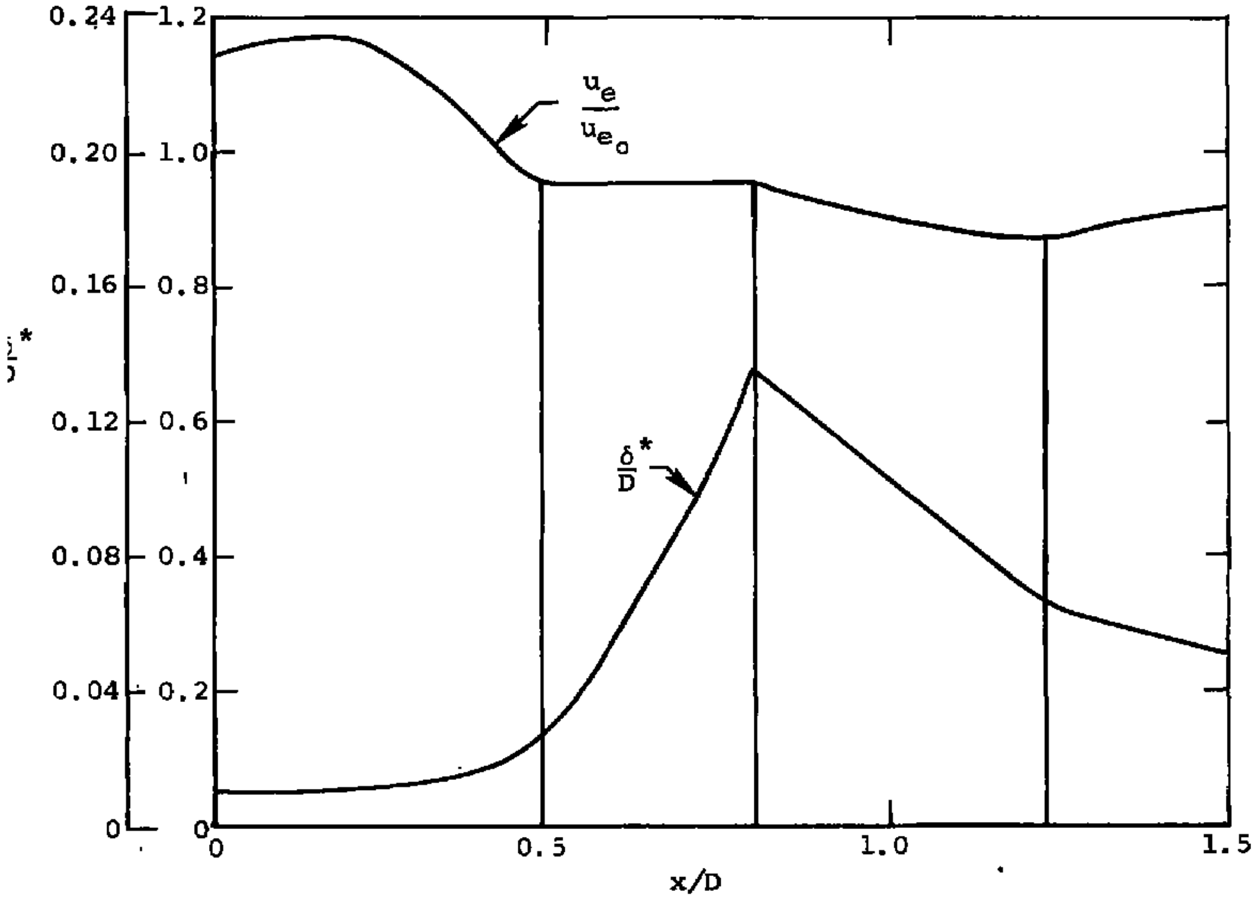

(a) Free-stream velocity and displacement thickness.

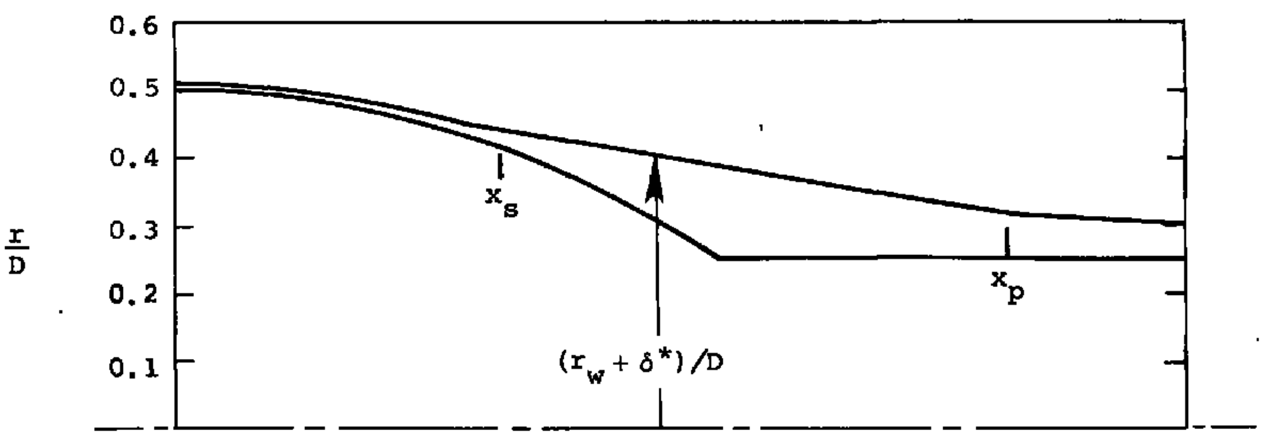

(b) Effective body shape.

Figure 11.- Calculated boundary layer quanties on configuration 1; M_∞ = 0.8.

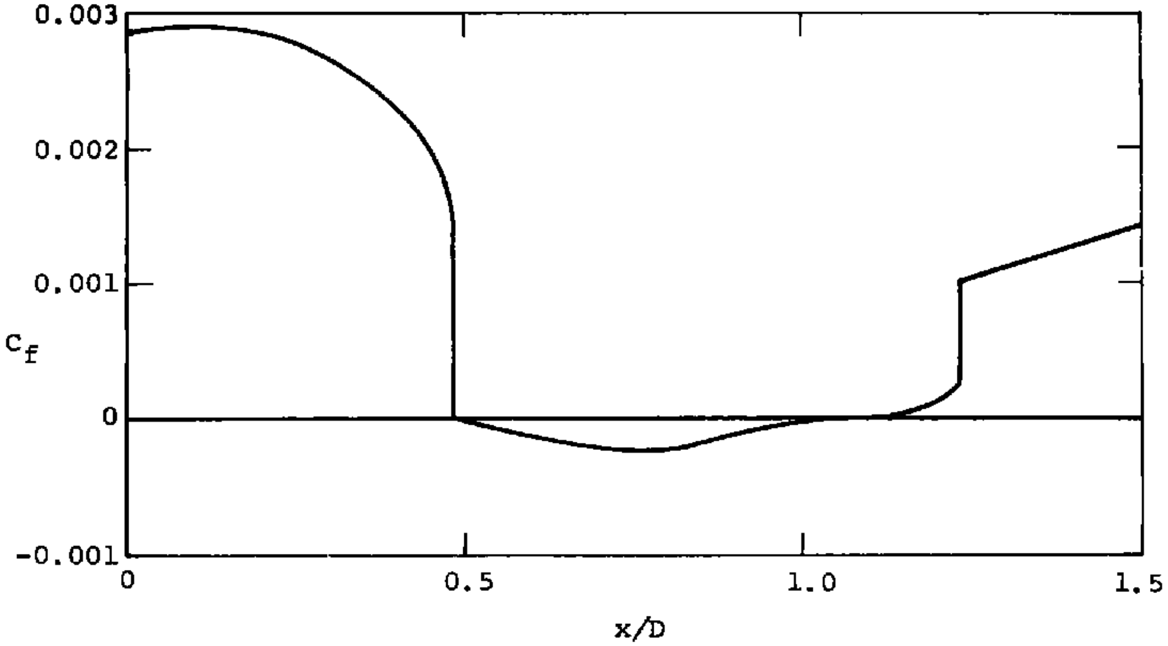

(c) Skin-friction coefficient.

Figure 11.- Concluded.

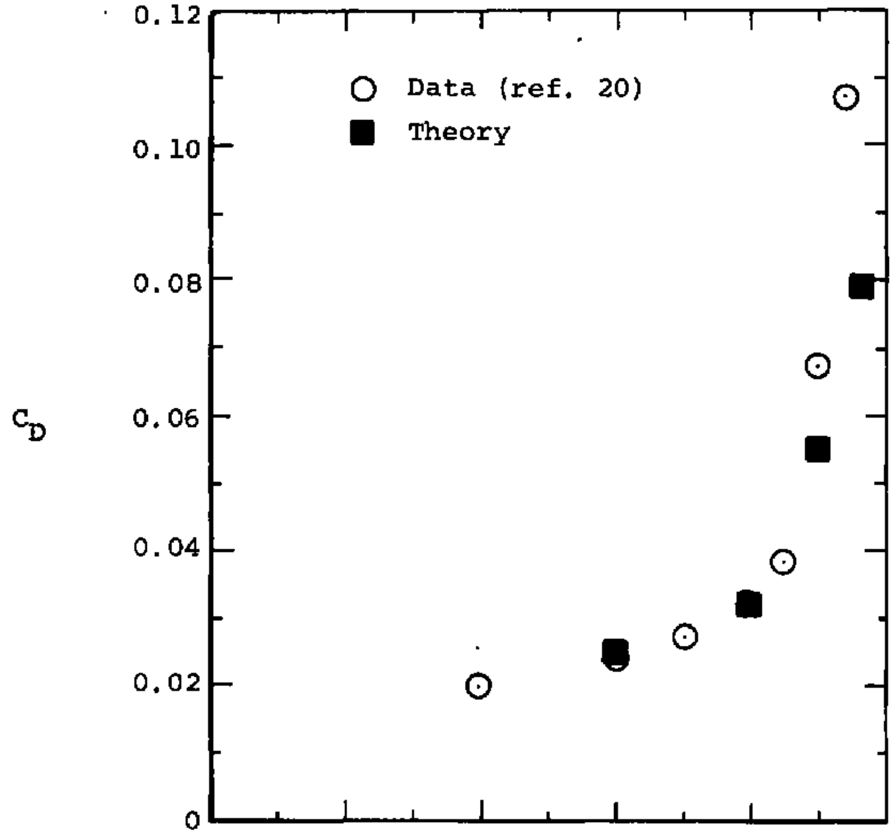

(a) Configuration 1.

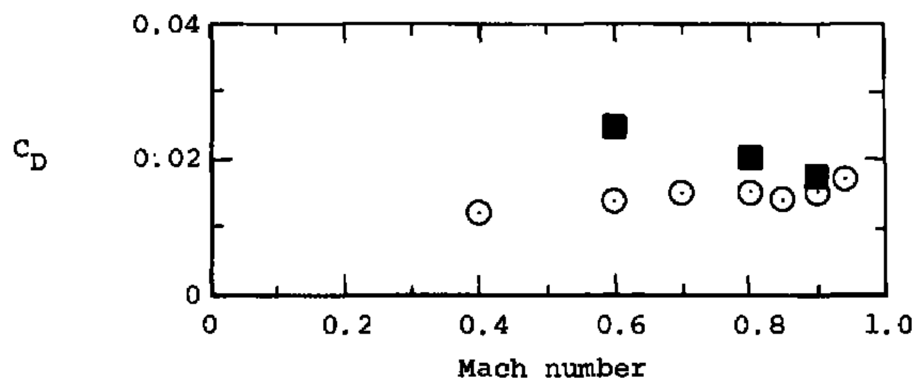

(b) Configuration 2.

Figure 12.- Comparison between the theory and experimental data for integrated boattail drag coefficient on boattails with solid plume simulators.

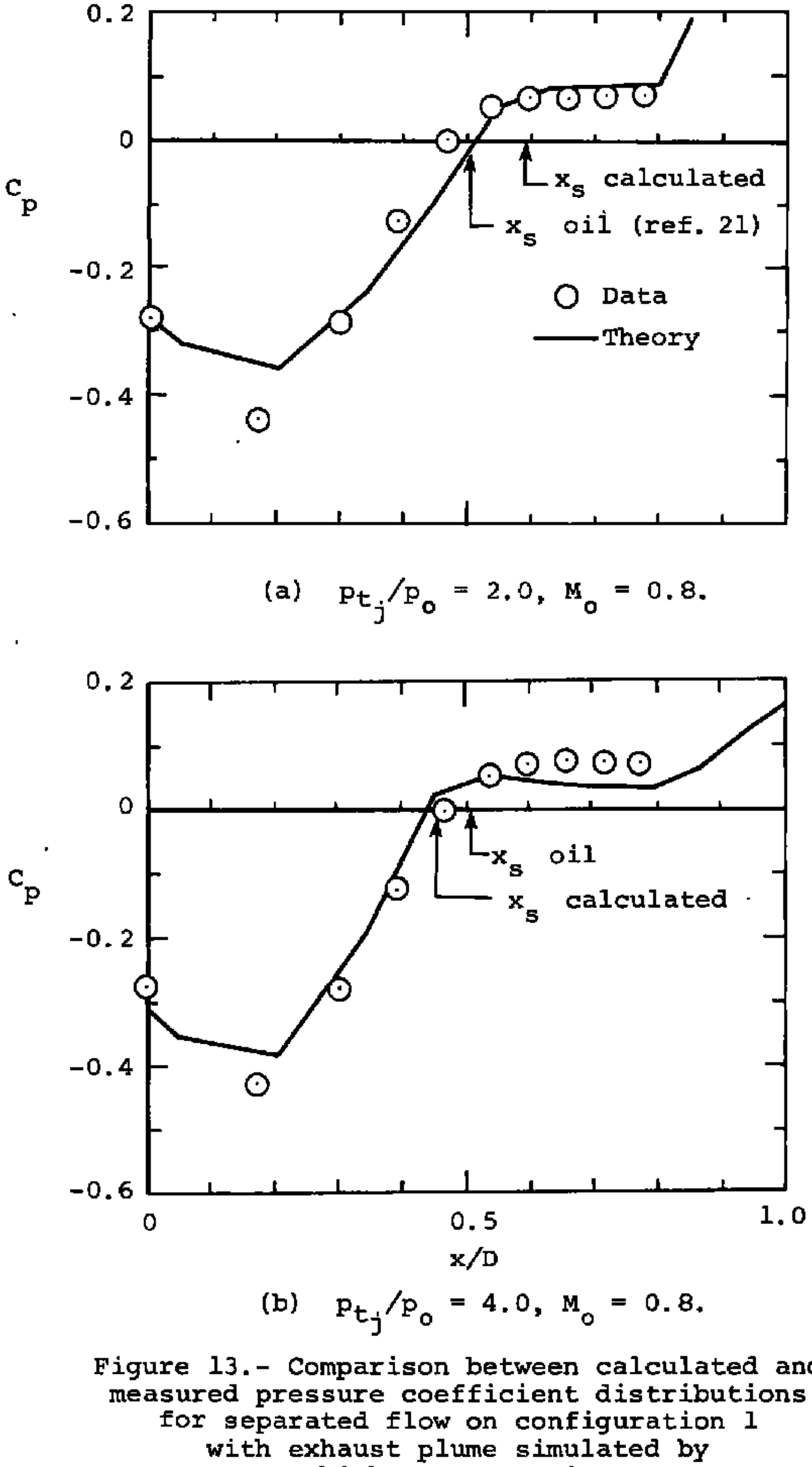

Figure 13.- Comparison between calculated and measured pressure coefficient distributions for separated flow on configuration 1 with exhaust plume simulated by high pressure air.

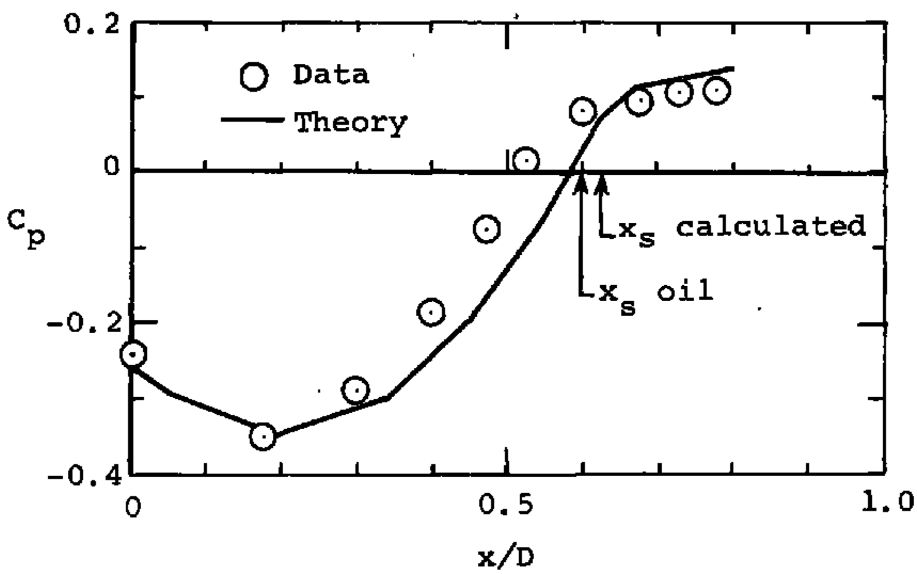

(c) $p_{t_j}/p_o = 2.0$, $M_o = 0.6$.

Figure 13.- Concluded.

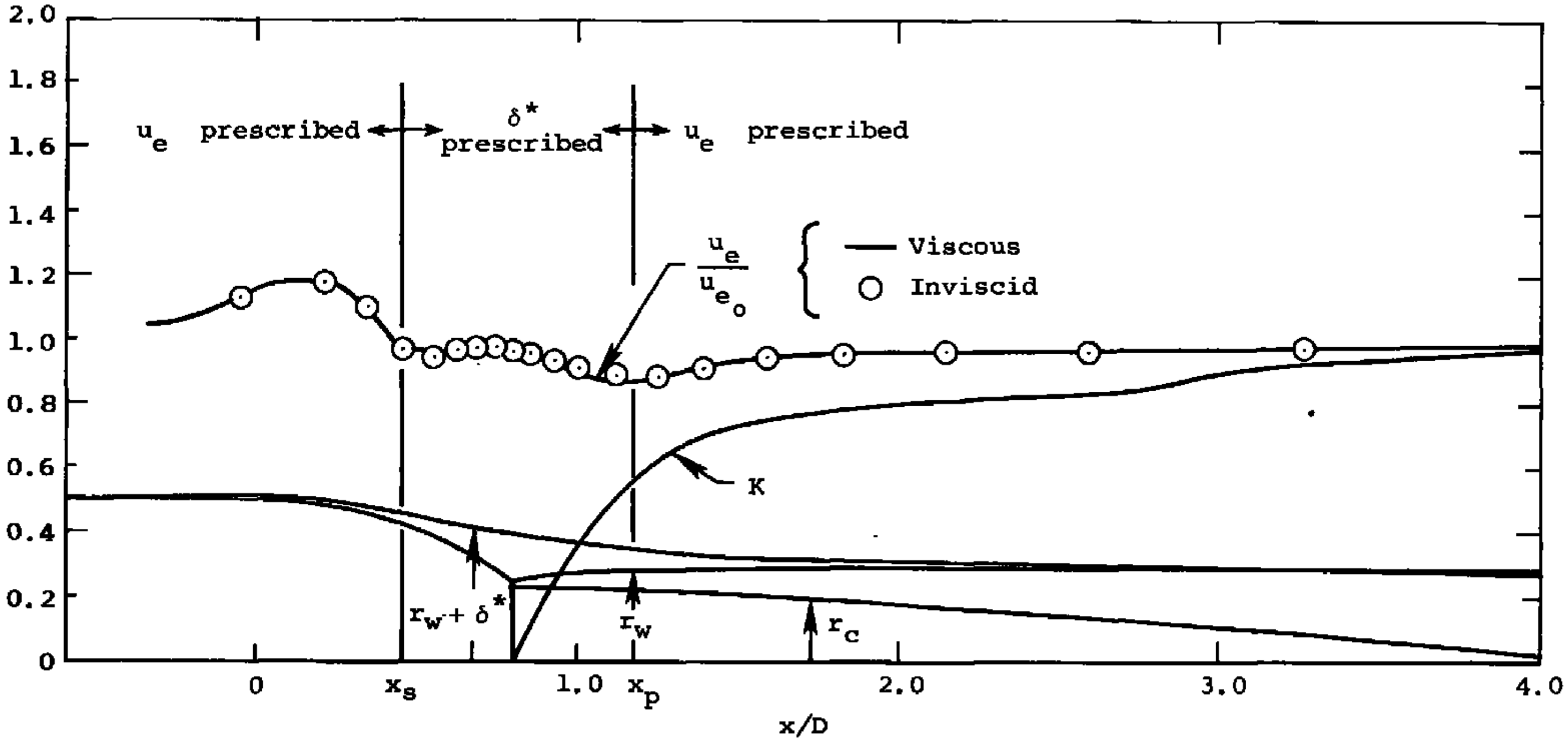

(a) $p_{t_j}/p_o = 4.0$.

Figure 14.- Calculated entrainment quantities.

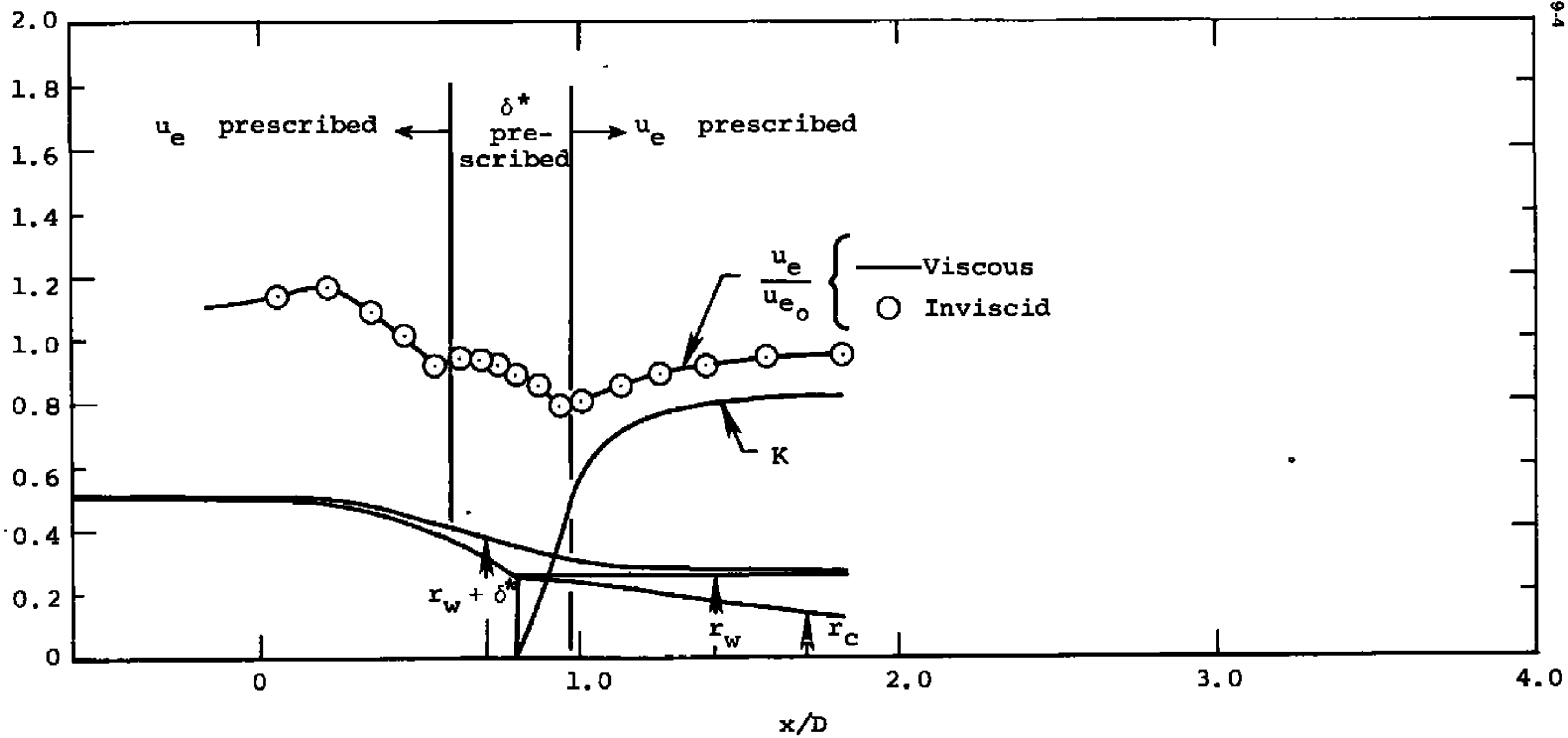

(b) $p_{t_j}/p_o = 2.0$.

Figure 14.- Concluded.

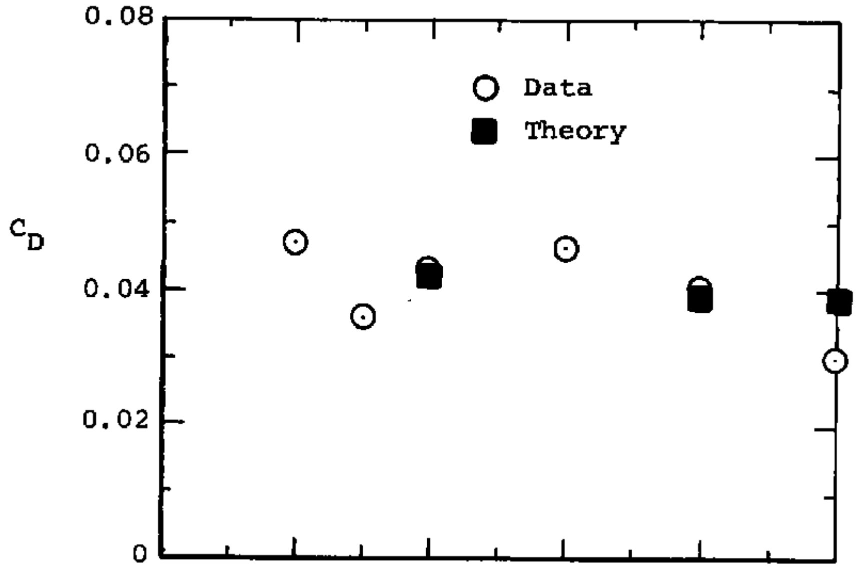

(a) $M_o = 0.8$.

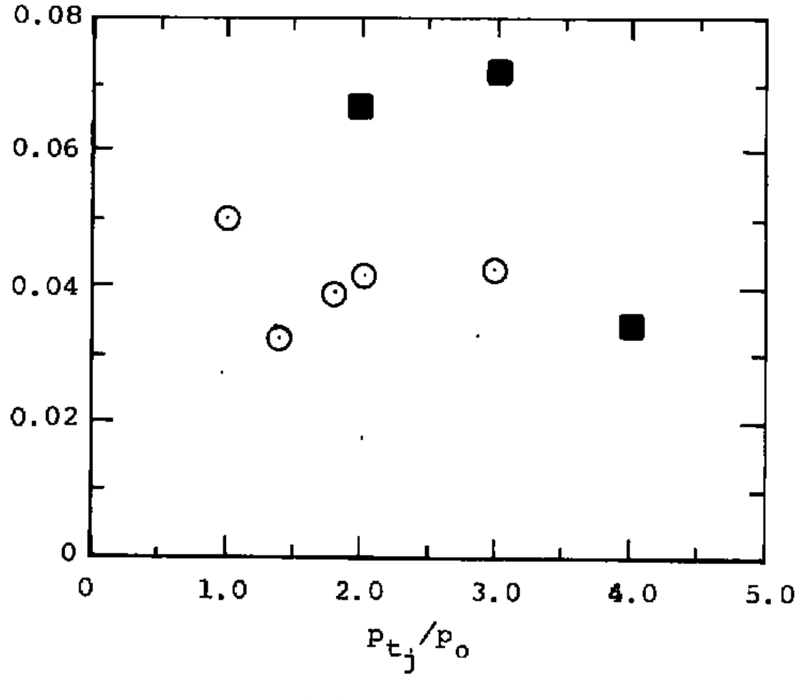

(b) $M_o = 0.6$.

Figure 15.- Comparison of experimental and calculated boattail drag on configuration 1 with plume simulated with high pressure air.

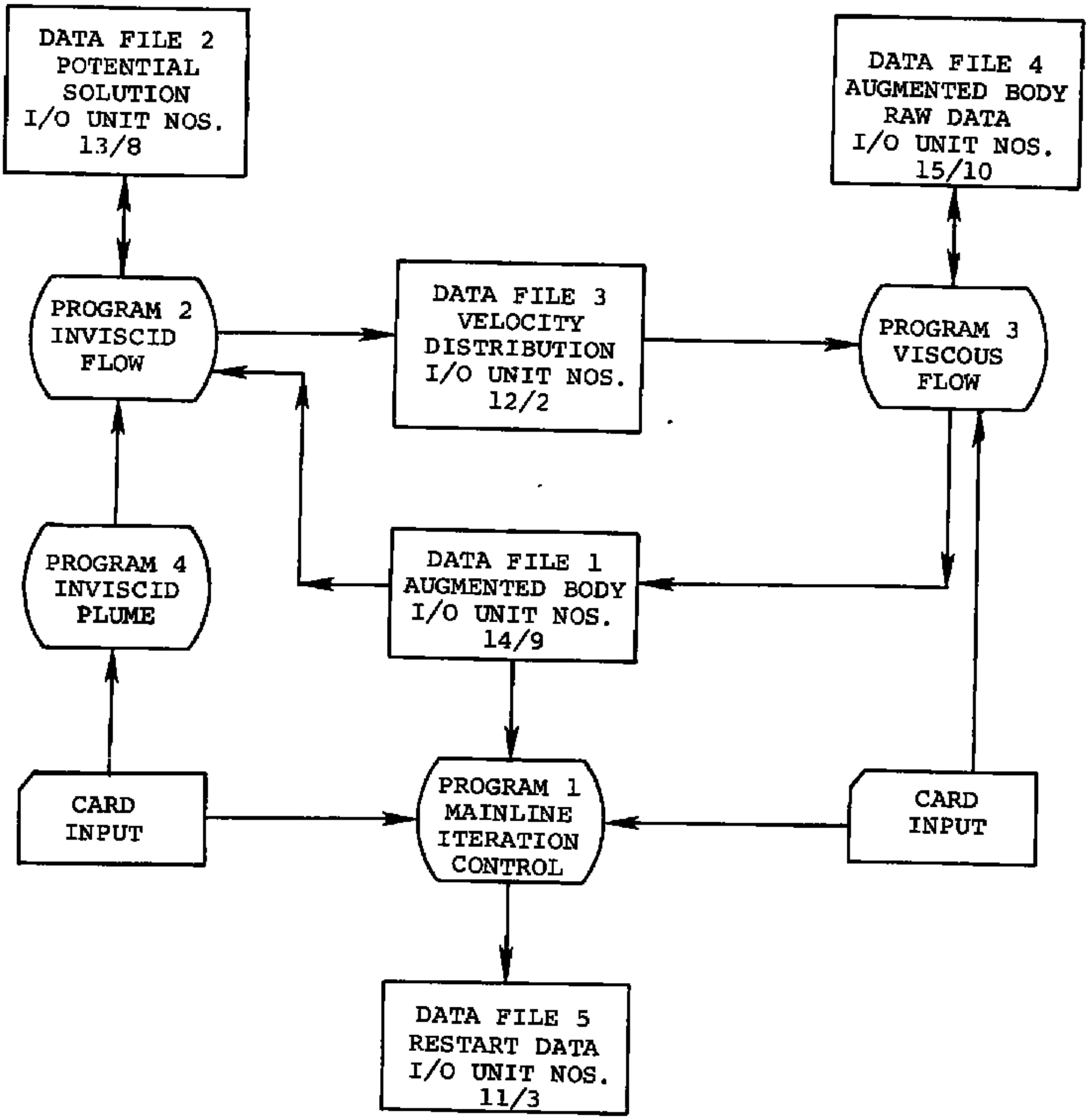

Figure 16.- General relationship of programs and data files.

```
NASA DATA COMPARISON - CONFIGURATION 1
JET SIMULATED WITH HIGH PRESSURE AIR
BOATTAIL L/D = 0.8      DE/D = 0.51
    0     0     0  700       0
    0     1     1     1     1     0
   1.4      0.8
   98
   0.0      0.0
   0.1      0.025013
   0.2      0.050026
   0.3      0.075038
   0.4      0.100051
   0.5      0.125064
   0.6      0.150077
   0.7      0.175090
   0.8      0.200102
   0.9      0.225115
   1.0      0.250128
   1.1      0.275141
   1.2      0.300154
   1.3      0.325166
   1.4      0.350179
   1.5      0.375192
   1.6      0.400205
   1.7      0.425218
   1.8      0.450230
   1.9      0.473630
   2.0      0.489760
   2.1      0.498366
   2.2      0.500000
   2.3      0.500000
   2.5      0.500000
   3.0      0.500000
   3.5      0.500000
   4.0      0.500000
   5.0      0.500000
   6.0      0.500000
   7.0      0.500000
   7.5      0.500000
   8.0      0.500000
   8.025    0.499781
   8.05     0.499125
   8.075    0.498030
   8.1      0.496496
   8.125    0.494521
   8.15     0.492104
   8.175    0.489241
   8.2      0.485931
   8.225    0.482171
```

(a) First 49 cards.

Figure 17.- Input data for viscous-inviscid interaction calculation.

8.25	0.477956
8.275	0.473282
8.3	0.468146
8.325	0.462542
8.35	0.456463
8.375	0.449905
8.4	0.442859
8.425	0.435319
8.45	0.427277
8.475	0.418722
8.5	0.409646
8.525	0.400037
8.55	0.389885
8.575	0.379176
8.6	0.367897
8.625	0.356032
8.65	0.343565
8.675	0.330479
8.7	0.316753
8.725	0.302368
8.75	0.287298
8.775	0.271518
8.8	0.255000
8.81	0.255000
8.82	0.255000
8.83	0.255000
8.84	0.255000
8.85	0.255000
8.86	0.255000
8.87	0.255000
8.88	0.255000
8.89	0.255000
8.9	0.255000
8.92	0.255000
8.94	0.255000
8.96	0.255000
8.98	0.255000
9.0	0.255000
9.025	0.255000
9.05	0.255000
9.075	0.255000
9.1	0.255000
9.15	0.255000
9.2	0.255000
9.3	0.255000
9.4	0.255000
9.5	0.255000
9.7	0.255000
9.9	0.255000

(b) Next 49 cards.

Figure 17.- Continued.

```
10.1        0.255000
10.3        0.255000
10.5        0.255000
10.8        0.255000
11.2        0.255000
11.6        0.255000
12.0        0.255000
 61    31    0     0     0
0.0         0.0        0.0        0.0         8.8    1.0     8.0
  T
 1.4         4.0        1.0        0.0       523.8    1.0     0.0125
  F
  1     1     2     3     1     0     0
0.5         2134.1     576.9      0.97
0.15         10.0      0.166667   0.0
```

(c) Remaining 15 cards.

Figure 17.- Concluded.

------ NORMAL COORD. STRETCH FOR ALF= 1.300 ------

J	AN	G	GH
1	0.3490E-58	0.0	0.7725E-04
2	0.1617E 03	0.1545E-03	0.4607E-03
3	0.6339E 02	0.7668E-03	0.1365E-02
4	0.3608E 02	0.1964E-02	0.2900E-02
5	0.2391E 02	0.3836E-02	0.5148E-02
6	0.1720E 02	0.6460E-02	0.8182E-02
7	0.1303E 02	0.9905E-02	0.1207E-01
8	0.1022E 02	0.1424E-01	0.1687E-01
9	0.8215E 01	0.1951E-01	0.2265E-01
10	0.6729E 01	0.2579E-01	0.2947E-01
11	0.5588E 01	0.3314E-01	0.3738E-01
12	0.4690E 01	0.4161E-01	0.4644E-01
13	0.3968E 01	0.5126E-01	0.5670E-01
14	0.3377E 01	0.6215E-01	0.6824E-01
15	0.2886E 01	0.7433E-01	0.9110E-01
16	0.2474E 01	0.8737E-01	0.9535E-01
17	0.2123E 01	0.1028E 00	0.1110E 00
18	0.1822E 01	0.1193E 00	0.1282E 00
19	0.1561E 01	0.1372E 00	0.1470E 00
20	0.1334E 01	0.1568E 00	0.1674E 00
21	0.1135E 01	0.1780E 00	0.1895E 00
22	0.9585E 00	0.2010E 00	0.2134E 00
23	0.8020E 00	0.2258E 00	0.2391E 00
24	0.6623E 00	0.2524E 00	0.2667E 00
25	0.5371E 00	0.2810E 00	0.2962E 00
26	0.4245E 00	0.3116E 00	0.3280E 00
27	0.3227E 00	0.3443E 00	0.3617E 00
28	0.2304E 00	0.3792E 00	0.3977E 00
29	0.1465E 00	0.4163E 00	0.4362E 00
30	0.7000E-01	0.4558E 00	0.4767E 00
31	0.1198E-06	0.4976E 00	0.5198E 00

(a) Computed geometric parameters in normal direction for inviscid flow.

Figure 18.- Selected output for viscid-inviscid interation calculation.

I	S	X	Y	THET	THETB	AK	F
1	0.0	0.0	0.0	0.9000E 02	0.9000E 02	0.2747E-04	0.2381E 00
2	0.7030E-01	0.6820E-01	0.1706E-01	0.1404E 02	0.1404E 02	0.3216E-04	0.2250E 00
3	0.1434E 00	0.1382E 00	0.3456E-01	0.1404E 02	0.1404E 02	0.4410E-04	0.2264E 00
4	0.2181E 00	0.2116E 00	0.5293E-01	0.1404E 02	0.1404E 02	0.1595E-03	0.2174E 00
5	0.2992E 00	0.2903E 00	0.7260E-01	0.1404E 02	0.1404E 02	0.1723E-03	0.1977E 00
6	0.3873E 00	0.3757E 00	0.9358E-01	0.1404E 02	0.1404E 02	0.1889E-05	0.1809E 00
7	0.4840E 00	0.4696E 00	0.1175E 00	0.1404E 02	0.1404E 02	0.9037E-05	0.1642E 00
8	0.5908E 00	0.5722E 00	0.1434E 00	0.1404E 02	0.1404E 02	0.2906E-04	0.1484E 00
9	0.7091E 00	0.6879E 00	0.1721E 00	0.1404E 02	0.1404E 02	0.1578E-03	0.1340E 00
10	0.8400E 00	0.8149E 00	0.2038E 00	0.1404E 02	0.1404E 02	0.1533E-03	0.1211E 00
11	0.9846E 00	0.9552E 00	0.2389E 00	0.1404E 02	0.1404E 02	0.9358E-05	0.1099E 00
12	0.1144E 01	0.1110E 01	0.2775E 00	0.1404E 02	0.1404E 02	0.7055E-04	0.1000E 00
13	0.1318E 01	0.1279E 01	0.3198E 00	0.1404E 02	0.1404E 02	0.9078E-04	0.9156E-01
14	0.1508E 01	0.1463E 01	0.3659E 00	0.1404E 02	0.1404E 02	0.1108E-03	0.8426E-01
15	0.1714E 01	0.1662E 01	0.4158E 00	0.1404E 02	0.1404E 02	0.1400E-02	0.7800E-01
16	0.1935E 01	0.1878E 01	0.4689E 00	0.1251E 02	0.1251E 02	0.6692E 00	0.7265E-01
17	0.2172E 01	0.2112E 01	0.4989E 00	0.2243E 01	0.2243E 01	0.7612E 00	0.6809E-01
18	0.2425E 01	0.2365E 01	0.5000E 00	0.0	-0.3978E-02	-0.4900E-02	0.6422E-01
19	0.2691E 01	0.2631E 01	0.5000E 00	0.0	0.2473E-02	0.8255E-03	0.6096E-01
20	0.2971E 01	0.2911E 01	0.5000E 00	0.0	-0.3711E-02	-0.5435E-04	0.5823E-01
21	0.3263E 01	0.3203E 01	0.5000E 00	0.0	0.1437E-03	-0.1585E-03	0.5599E-01
22	0.3566E 01	0.3506E 01	0.5000E 00	0.0	0.6285E-03	0.9587E-04	0.5419E-01
23	0.3878E 01	0.3818E 01	0.5000E 00	0.0	-0.2230E-03	-0.5328E-06	0.5279E-01
24	0.4197E 01	0.4137E 01	0.5000E 00	0.0	0.4268E-03	-0.3248E-04	0.5178E-01
25	0.4521E 01	0.4461E 01	0.5000E 00	0.0	0.4920E-03	0.2546E-04	0.5114E-01
26	0.4848E 01	0.4788E 01	0.5000E 00	0.0	-0.5324E-03	0.8391E-04	0.5087E-01
27	0.5175E 01	0.5115E 01	0.5000E 00	0.0	-0.2378E-02	0.5825E-04	0.5098E-01
28	0.5501E 01	0.5441E 01	0.5000E 00	0.0	-0.1788E-02	-0.1216E-03	0.5148E-01
29	0.5822E 01	0.5762E 01	0.5000E 00	0.0	0.2081E-02	-0.2990E-03	0.5242E-01
30	0.6136E 01	0.6076E 01	0.5000E 00	0.0	0.8595E-02	-0.2757E-03	0.5387E-01
31	0.6440E 01	0.6380E 01	0.5001E 00	0.0	0.8029E-02	0.3416E-03	0.5579E-01
32	0.6732E 01	0.6672E 01	0.5001E 00	0.0	-0.2662E-02	0.9352E-03	0.5840E-01
33	0.7010E 01	0.6950E 01	0.5000E 00	0.0	-0.2203E-01	0.1499E-02	0.6179E-01
34	0.7271E 01	0.7211E 01	0.4999E 00	0.0	-0.1939E-01	-0.2769E-02	0.6614E-01
35	0.7513E 01	0.7454E 01	0.4999E 00	0.0	0.5385E-01	-0.7781E-02	0.7172E-01
36	0.7735E 01	0.7676E 01	0.5003E 00	0.0	0.8941E-01	0.6040E-02	0.7858E-01
37	0.7936E 01	0.7876E 01	0.5004E 00	0.0	-0.7667E-01	0.2291E-01	0.8812E-01
38	0.8114E 01	0.8054E 01	0.4990E 00	0.0	-0.2162E 01	0.6643E 00	0.1001E 00
39	0.8269E 01	0.8209E 01	0.4847E 00	0.0	-0.8398E 01	0.7227E 00	0.1159E 00
40	0.8401E 01	0.8341E 01	0.4586E 00	0.0	-0.1383E 02	0.7626E 00	0.1368E 00
41	0.8513E 01	0.8453E 01	0.4263E 00	0.0	-0.1848E 02	0.8251E 00	0.1642E 00
42	0.8605E 01	0.8545E 01	0.3918E 00	0.0	-0.2244E 02	0.8863E 00	0.1992E 00
43	0.8681E 01	0.8621E 01	0.3578E 00	0.0	-0.2579E 02	0.9650E 00	0.2404E 00
44	0.8745E 01	0.8686E 01	0.3248E 00	0.0	-0.2971E 02	0.9442E 00	0.2792E 00
45	0.8803E 01	0.8743E 01	0.2916E 00	0.0	-0.3106E 02	-0.1939E 01	0.2977E 00

(b) Computed tangential geometric parameters.

Figure 18.- Continued.

46	0.8860E 01	0.8800E 01	0.2550E 00	0.0	-0.1086E 02	-0.6596E 02	0.2790E 00
47	0.8924E 01	0.8864E 01	0.2550E 00	0.0	0.1355E-03	-0.1205E-01	0.2471E 00
48	0.8998E 01	0.8938E 01	0.2550E 00	0.0	-0.2549E-05	-0.2950E-05	0.2096E 00
49	0.9084E 01	0.9024E 01	0.2550E 00	0.0	-0.1286E-07	-0.2236E-07	0.1786E 00
50	0.9186E 01	0.9126E 01	0.2550E 00	0.0	-0.5914E-10	0.1232E-09	0.1501E 00
51	0.9308E 01	0.9249E 01	0.2550E 00	0.0	-0.4399E-11	0.6637E-11	0.1240E 00
52	0.9457E 01	0.9397E 01	0.2550E 00	0.0	0.2231E-11	0.1034E-11	0.1004E 00
53	0.9644E 01	0.9584E 01	0.2550E 00	0.0	0.4848E-13	-0.1016E-12	0.7937E-01
54	0.9884E 01	0.9824E 01	0.2550E 00	0.0	-0.5845E-13	0.1246E-13	0.6076E-01
55	0.1020E 02	0.1014E 02	0.2550E 00	0.0	0.4784E-14	0.3016E-14	0.4464E-01
56	0.1065E 02	0.1059E 02	0.2550E 00	0.0	0.1875E-15	0.1476E-15	0.3109E-01
57	0.1132E 02	0.1126E 02	0.2550E 00	0.0	0.4834E-16	0.1178E-16	0.1984E-01
58	0.1244E 02	0.1238E 02	0.2550E 00	0.0	0.0	0.0	0.1116E-01
59	0.1468E 02	0.1462E 02	0.2550E 00	0.0	0.0	0.0	0.4961E-02
60	0.2140E 02	0.2134E 02	0.2550E 00	0.0	0.0	0.0	0.1240E-02
61	0.1000E 31	0.1000E 31	0.2550E 00	0.0	0.0	0.0	0.1000E-29

UZ = 8.86764E 02
REZ = 3.82561E 06
NUZ = 2.31797E-04

(b) Concluded.

Figure 18.- Continued.

PLUME VELOCITY

NUT = 55

X	U
8.8000E 00	1.4179E 03
8.8160E 00	1.4179E 03
8.8320E 00	1.4084E 03
8.8480E 00	1.3995E 03
8.8640E 00	1.3909E 03
8.8824E 00	1.3850E 03
8.9009E 00	1.3817E 03
8.9194E 00	1.3787E 03
8.9378E 00	1.3760E 03
8.9594E 00	1.3752E 03
8.9809E 00	1.3788E 03
9.0024E 00	1.3827E 03
9.0240E 00	1.3867E 03
9.0494E 00	1.3924E 03
9.0749E 00	1.3964E 03
9.1003E 00	1.4005E 03
9.1258E 00	1.4048E 03
9.1563E 00	1.4106E 03
9.1869E 00	1.4115E 03
9.2174E 00	1.4127E 03
9.2480E 00	1.4141E 03
9.2853E 00	1.4166E 03
9.3226E 00	1.4173E 03
9.3600E 00	1.4182E 03
9.3973E 00	1.4192E 03
9.4440E 00	1.4211E 03
9.4906E 00	1.4218E 03
9.5373E 00	1.4227E 03
9.5840E 00	1.4237E 03
9.6440E 00	1.4254E 03
9.7040E 00	1.4258E 03
9.7640E 00	1.4264E 03
9.8240E 00	1.4271E 03
9.9040E 00	1.4283E 03
9.9840E 00	1.4287E 03
1.0064E 01	1.4292E 03
1.0144E 01	1.4298E 03
1.0256E 01	1.4308E 03
1.0368E 01	1.4310E 03
1.0480E 01	1.4313E 03
1.0592E 01	1.4318E 03
1.0760E 01	1.4326E 03
1.0928E 01	1.4321E 03
1.1096E 01	1.4323E 03
1.1264E 01	1.4324E 03
1.1544E 01	1.4327E 03
1.1824E 01	1.4326E 03
1.2104E 01	1.4329E 03
1.2384E 01	1.4330E 03
1.2944E 01	1.4333E 03
1.3504E 01	1.4333E 03
1.4064E 01	1.4333E 03
1.4624E 01	1.4333E 03
1.4304E 01	1.4332E 03
1.7584E 01	1.4333E 03

PLUME SHAPE

JP = 56

X	R
8.8000E 00	2.5510E-01
8.8160E 00	2.5827E-01
8.8320E 00	2.6109E-01
8.8480E 00	2.6350E-01
8.8640E 00	2.6556E-01
8.8824E 00	2.6758E-01
8.9009E 00	2.6933E-01
8.9194E 00	2.7083E-01
8.9378E 00	2.7213E-01
8.9594E 00	2.7343E-01
8.9809E 00	2.7462E-01
9.0024E 00	2.7572E-01
9.0240E 00	2.7673E-01
9.0494E 00	2.7786E-01
9.0749E 00	2.7889E-01
9.1003E 00	2.7986E-01
9.1258E 00	2.8076E-01
9.1563E 00	2.8180E-01
9.1869E 00	2.8268E-01
9.2174E 00	2.8345E-01
9.2480E 00	2.8413E-01
9.2853E 00	2.8487E-01
9.3226E 00	2.8549E-01
9.3600E 00	2.8601E-01
9.3973E 00	2.8647E-01
9.4440E 00	2.8697E-01
9.4906E 00	2.8739E-01
9.5373E 00	2.8774E-01
9.5840E 00	2.8804E-01
9.6440E 00	2.8840E-01
9.7040E 00	2.8867E-01
9.7640E 00	2.8839E-01
9.8240E 00	2.8909E-01
9.9040E 00	2.8932E-01
9.9840E 00	2.8949E-01
1.0064E 01	2.8963E-01
1.0144E 01	2.8975E-01
1.0256E 01	2.8991E-01
1.0368E 01	2.9002E-01
1.0480E 01	2.9011E-01
1.0592E 01	2.9019E-01
1.0760E 01	2.9030E-01
1.0928E 01	2.9033E-01
1.1096E 01	2.9035E-01
1.1264E 01	2.9037E-01
1.1544E 01	2.9041E-01
1.1824E 01	2.9042E-01
1.2104E 01	2.9045E-01
1.2384E 01	2.9046E-01
1.2944E 01	2.9051E-01
1.3504E 01	2.9051E-01
1.4064E 01	2.9051E-01
1.4624E 01	2.9051E-01
1.6304E 01	2.9051E-01
1.7984E 01	2.9051E-01
1.9663E 01	2.9051E-01

(c) Calculated inviscid plume velocity and shape after four iterations.

Figure 18.- Continued.

ITERATION NO. 4

AX	UTAU	DELTA	DELST	THETA	CF	UE/UZ	DELST+R	DX	HTR
1.50000E-01	2.33722E 01	8.12110E-04	2.99359E-04	1.17398E-04	2.48232E-03	0.76755	3.78189E-02	1.250E 29	2.3664
1.89778E-01	2.55566E 01	8.44613E-04	2.98955E-04	1.21524E-04	2.75536E-03	0.79457	4.55170E-02	7.695E-03	2.2599
2.11557E-01	2.97197E 01	9.50981E-04	3.00651E-04	1.33346E-04	3.46842E-03	0.82138	5.32174E-02	7.695E-03	2.0364
2.50871E-01	3.31723E 01	1.32066E-03	3.49580E-04	1.71777E-04	4.16471E-03	0.83546	6.30994E-02	9.829E-03	1.7842
2.99136E-01	3.52674E 01	1.81454E-03	4.11406E-04	2.13936E-04	4.54002E-03	0.84948	7.29945E-02	9.829E-03	1.6139
3.32904E-01	3.54707E 01	2.34252E-03	4.94322E-04	2.63096E-04	4.49364E-03	0.85800	8.37624E-02	1.068E-02	1.5249
3.75622E-01	3.54577E 01	2.80815E-03	5.71088E-04	3.07384E-04	4.39370E-03	0.86650	9.45243E-02	1.068E-02	1.4737
4.22519E-01	3.51695E 01	3.27641E-03	6.54452E-04	3.54614E-04	4.25620E-03	0.87274	1.06338E-01	1.172E-02	1.4410
4.69416E-01	3.50368E 01	3.71552E-03	7.29910E-04	3.97470E-04	4.15884E-03	0.87897	1.18144E-01	1.172E-02	1.4150
5.21212E-01	3.48334E 01	4.18222E-03	8.11525E-04	4.43672E-04	4.05851E-03	0.88411	1.31181E-01	1.295E-02	1.3942
5.73008E-01	3.47334E 01	4.63265E-03	8.87229E-04	4.86727E-04	3.98432E-03	0.88923	1.44213E-01	1.295E-02	1.3758
6.30354E-01	3.46102E 01	5.11783E-03	9.69349E-04	5.33218E-04	3.90954E-03	0.89404	1.58639E-01	1.434E-02	1.3597
6.87702E-01	3.45476E 01	5.58996E-03	1.04707E-03	5.77312E-04	3.84983E-03	0.89883	1.73061E-01	1.434E-02	1.3453
7.51181E-01	3.44856E 01	6.10030E-03	1.13089E-03	6.24772E-04	3.79037E-03	0.90373	1.89022E-01	1.587E-02	1.3320
8.14662E-01	3.44616E 01	6.59389E-03	1.21136E-03	6.70268E-04	3.74031E-03	0.90862	2.04981E-01	1.587E-02	1.3201
8.84776E-01	3.44644E 01	7.13670E-03	1.29713E-03	7.18645E-04	3.69230E-03	0.91402	2.22604E-01	1.753E-02	1.3084
9.54890E-01	3.44892E 01	7.66259E-03	1.38028E-03	7.65373E-04	3.64987E-03	0.91941	2.40225E-01	1.753E-02	1.2981
1.03205E 00	3.45736E 01	8.22651E-03	1.46708E-03	8.13957E-04	3.61203E-03	0.92579	2.59611E-01	1.929E-02	1.2873
1.10921E 00	3.46655E 01	8.77690E-03	1.55206E-03	8.61208E-04	3.57649E-03	0.93216	2.78997E-01	1.929E-02	1.2779
1.19373E 00	3.48792E 01	9.35990E-03	1.63672E-03	9.07886E-04	3.55074E-03	0.94039	3.00222E-01	2.113E-02	1.2670
1.27826E 00	3.50805E 01	9.92495E-03	1.72096E-03	9.53774E-04	3.52304E-03	0.94859	3.21449E-01	2.113E-02	1.2581
1.37035E 00	3.55529E 01	1.05087E-02	1.79453E-03	9.92829E-04	3.51757E-03	0.96071	3.44558E-01	2.303E-02	1.2452
1.46246E 00	3.59728E 01	1.10627E-02	1.87131E-03	1.03257E-03	3.50290E-03	0.97277	3.67673E-01	2.303E-02	1.2357
1.56725E 00	3.73569E 01	1.15888E-02	1.89072E-03	1.03716E-03	3.56584E-03	0.99795	3.92654E-01	2.495E-02	1.2113
1.66205E 00	3.85255E 01	1.20366E-02	1.93213E-03	1.05097E-03	3.58643E-03	1.02290	4.17657E-01	2.495E-02	1.1974
1.76974E 00	4.31532E 01	1.24262E-02	1.79148E-03	9.46336E-04	3.85213E-03	1.09468	4.44452E-01	2.692E-02	1.1356
1.87743E 00	4.69889E 01	1.26458E-02	1.77124E-03	9.02030E-04	3.95402E-03	1.16430	4.70121E-01	2.692E-02	1.1104
1.99481E 00	4.59360E 01	1.27623E-02	2.03574E-03	1.03135E-03	3.67774E-03	1.17771	4.90959E-01	2.935E-02	1.1677
2.11220E 00	4.53606E 01	1.35572E-02	2.30412E-03	1.15815E-03	3.49154E-03	1.19102	5.00869E-01	2.935E-02	1.1861
2.23829E 00	3.91642E 01	1.49761E-02	3.02712E-03	1.53585E-03	2.91888E-03	1.13462	5.03027E-01	3.152E-02	1.2855
2.36438E 00	3.41821E 01	1.73931E-02	3.86262E-03	1.97059E-03	2.51095E-03	1.07674	5.03863E-01	3.152E-02	1.3532
2.49766E 00	3.14853E 01	2.00676E-02	4.28871E-03	2.22781E-03	2.51425E-03	1.05699	5.04289E-01	3.332E-02	1.3257
2.63094E 00	3.25153E 01	2.27232E-02	4.76754E-03	2.50880E-03	2.47592E-03	1.03709	5.04768E-01	3.332E-02	1.3128
2.77090E 00	3.26185E 01	2.52495E-02	5.06888E-03	2.70412E-03	2.52791E-03	1.03053	5.05069E-01	3.499E-02	1.2793
2.91086E 00	3.24675E 01	2.78481E-02	5.40366E-03	2.90941E-03	2.54126E-03	1.02395	5.05404E-01	3.499E-02	1.2587
3.05689E 00	3.24796E 01	3.03379E-02	5.70605E-03	3.09563E-03	2.56159E-03	1.02070	5.05706E-01	3.651E-02	1.2376
3.20292E 00	3.23860E 01	3.27380E-02	6.02343E-03	3.28633E-03	2.56535E-03	1.01744	5.06023E-01	3.651E-02	1.2227
3.35431E 00	3.22932E 01	3.51542E-02	6.34535E-03	3.47829E-03	2.56527E-03	1.01488	5.06345E-01	3.785E-02	1.2096
3.50569E 00	3.21587E 01	3.75140E-02	6.67404E-03	3.67254E-03	2.55854E-03	1.01232	5.06674E-01	3.785E-02	1.1994
3.66159E 00	3.21024E 01	3.98895E-02	6.98608E-03	3.85704E-03	2.55656E-03	1.01110	5.06986E-01	3.898E-02	1.1886
3.81750E 00	3.20196E 01	4.22145E-02	7.30225E-03	4.04273E-03	2.55035E-03	1.00988	5.07302E-01	3.898E-02	1.1798
3.97698E 00	3.19579E 01	4.45498E-02	7.61566E-03	4.22631E-03	2.54462E-03	1.00916	5.07616E-01	3.987E-02	1.1714
4.13647E 00	3.18823E 01	4.68461E-02	7.93097E-03	4.41031E-03	2.53667E-03	1.00844	5.07931E-01	3.987E-02	1.1643
4.29351E 00	3.17982E 01	4.91466E-02	8.25184E-03	4.59711E-03	2.52735E-03	1.00773	5.08252E-01	4.051E-02	1.15[illegible]

(d) Boundary-layer after four iterations.

Figure 18.- Continued.

4.46055E 00	3.17089E 01	5.14199E-02	8.57225E-03	4.78394E-03	2.51718E-03	1.00702	5.08573E-01	4.051E-02	1.1524
4.62403E 00	3.16349E 01	5.36889E-02	9.89015E-03	4.96801E-03	2.50799E-03	1.00657	5.08890E-01	4.087E-02	1.1470
4.78752E 00	3.15579E 01	5.59742E-02	9.20700E-03	5.15189E-03	2.49833E-03	1.00612	5.09207E-01	4.087E-02	1.1422
4.95126E 00	3.15022E 01	5.81621E-02	9.51535E-03	5.33069E-03	2.49007E-03	1.00596	5.09515E-01	4.094E-02	1.1372
5.11501E 00	3.14403E 01	6.03685E-02	9.82352E-03	5.50914E-03	2.48149E-03	1.00580	5.09824E-01	4.094E-02	1.1328
5.27779E 00	3.13986E 01	6.25421E-02	1.01208E-02	5.68109E-03	2.47427E-03	1.00592	5.10121E-01	4.070E-02	1.1283
5.44059E 00	3.13552E 01	6.46958E-02	1.04177E-02	5.85267E-03	2.46681E-03	1.00603	5.10418E-01	4.070E-02	1.1241
5.60111E 00	3.13110E 01	6.68024E-02	1.07102E-02	6.02153E-03	2.45927E-03	1.00614	5.10710E-01	4.013E-02	1.1203
5.76165E 00	3.12664E 01	6.88932E-02	1.10019E-02	6.18988E-03	2.45170E-03	1.00624	5.11002E-01	4.013E-02	1.1168
5.91867E 00	3.12308E 01	7.09243E-02	1.12825E-02	6.35158E-03	2.44492E-03	1.00646	5.11283E-01	3.925E-02	1.1134
6.07368E 00	3.11950E 01	7.29412E-02	1.15623E-02	6.51278E-03	2.43813E-03	1.00668	5.11562E-01	3.925E-02	1.1101
6.22788E 00	3.11720E 01	7.48845E-02	1.18267E-02	6.66481E-03	2.43244E-03	1.00706	5.11827E-01	3.805E-02	1.1069
6.38009E 00	3.11406E 01	7.68143E-02	1.20903E-02	6.81631E-03	2.42672E-03	1.00744	5.12090E-01	3.805E-02	1.1038
6.52623E 00	3.11455E 01	7.86572E-02	1.23320E-02	6.95472E-03	2.42267E-03	1.00810	5.12332E-01	3.654E-02	1.1005
6.67238E 00	3.11416E 01	8.04859E-02	1.25730E-02	7.09261E-03	2.41851E-03	1.00875	5.12573E-01	3.654E-02	1.0974
6.81126E 00	3.12104E 01	8.22186E-02	1.27591E-02	7.19732E-03	2.41988E-03	1.01047	5.12759E-01	3.472E-02	1.0928
6.95015E 00	3.12756E 01	8.39300E-02	1.29461E-02	7.30187E-03	2.42069E-03	1.01218	5.12946E-01	3.472E-02	1.0885
7.08067E 00	3.14241E 01	8.55338E-02	1.30686E-02	7.36692E-03	2.42759E-03	1.01515	5.13069E-01	3.263E-02	1.0825
7.21119E 00	3.15665E 01	8.71105E-02	1.31933E-02	7.43245E-03	2.43351E-03	1.01812	5.13193E-01	3.263E-02	1.0768
7.33236E 00	3.17860E 01	8.85734E-02	1.32560E-02	7.45918E-03	2.44484E-03	1.02226	5.13256E-01	3.029E-02	1.0697
7.45352E 00	3.19980E 01	9.00070E-02	1.33225E-02	7.48708E-03	2.45493E-03	1.02640	5.13322E-01	3.029E-02	1.0630
7.56450E 00	3.24814E 01	9.14006E-02	1.32133E-02	7.40307E-03	2.48365E-03	1.03472	5.13213E-01	2.774E-02	1.0501
7.67548E 00	3.29479E 01	9.27621E-02	1.31200E-02	7.32549E-03	2.50944E-03	1.04301	5.13120E-01	2.774E-02	1.0381
7.77563E 00	3.40920E 01	9.44088E-02	1.26455E-02	6.99374E-03	2.57829E-03	1.06200	5.12645E-01	2.504E-02	1.0104
7.87578E 00	3.51911E 01	9.61257E-02	1.22420E-02	6.69406E-03	2.63820E-03	1.08083	5.12242E-01	2.504E-02	0.9849
7.96469E 00	3.73129E 01	9.91520E-02	1.13989E-02	6.06749E-03	2.75098E-03	1.11650	5.11399E-01	2.223E-02	0.9354
8.05359E 00	3.93225E 01	1.02084E-01	1.07564E-02	5.52741E-03	2.84160E-03	1.15161	5.09724E-01	2.223E-02	0.8887
8.13112E 00	3.95440E 01	1.04533E-01	1.09047E-02	5.58002E-03	2.83764E-03	1.15779	5.04834E-01	1.939E-02	0.8861
8.20866E 00	3.97343E 01	1.06775E-01	1.11470E-02	5.68015E-03	2.82929E-03	1.16397	4.95775E-01	1.938E-02	0.8831
8.27503E 00	3.71675E 01	1.04317E-01	1.25702E-02	6.68407E-03	2.68315E-03	1.12474	4.85846E-01	1.659E-02	0.9470
8.34140E 00	3.44723E 01	1.04577E-01	1.44581E-02	7.91667E-03	2.51016E-03	1.08401	4.73013E-01	1.659E-02	1.0096
8.39716E 00	3.15736E 01	1.06212E-01	1.69063E-02	9.43149E-03	2.30723E-03	1.04246	4.60565E-01	1.394E-02	1.0771
8.45292E 00	2.85331E 01	1.10010E-01	2.02242E-02	1.13608E-02	2.07359E-03	0.99937	4.46500E-01	1.394E-02	1.1515
8.49910E 00	2.56509E 01	1.15064E-01	2.42374E-02	1.35461E-02	1.83453E-03	0.95989	4.34208E-01	1.155E-02	1.2293
8.54529E 00	2.25796E 01	1.22392E-01	2.98527E-02	1.63763E-02	1.56284E-03	0.91982	4.21650E-01	1.155E-02	1.3247
8.58337E 00	2.28330E 01	1.26880E-01	3.06594E-02	1.69008E-02	1.58533E-03	0.92316	4.06059E-01	9.520E-03	1.3088
8.58337E 00	0.0	5.45527E-02	3.06594E-02	6.96424E-03	0.0	0.92316	4.06058E-01	9.520E-03	4.0939
8.62241E 00	-1.69767E 00	6.02329E-02	3.50257E-02	7.37382E-03	-8.88462E-06	0.91748	4.01780E-01	4.760E-03	4.3543
8.62145E 00	-2.72218E 00	6.58273E-02	3.93940E-02	7.77784E-03	-2.30088E-05	0.91449	3.97110E-01	4.760E-03	4.6891
8.65349E 00	-4.31888E 00	7.62267E-02	4.75100E-02	8.42734E-03	-5.57226E-05	0.91109	3.89650E-01	8.010E-03	5.3586
8.68553E 00	-5.24587E 00	8.73331E-02	5.73398E-02	9.13989E-03	-8.63999E-05	0.90991	3.82038E-01	8.010E-03	6.0079
8.71416E 00	-5.97823E 00	9.74651E-02	6.64550E-02	9.75541E-03	-1.12200E-04	0.90994	3.75060E-01	7.158E-03	6.6144
8.74279E 00	-6.52781E 00	1.08495E-01	7.68384E-02	1.04835E-02	-1.34047E-04	0.91037	3.68480E-01	7.158E-03	7.2100
8.77138E 00	-6.89115E 00	1.19655E-01	8.79177E-02	1.12487E-02	-1.49076E-04	0.91020	3.61719E-01	7.147E-03	7.7028
8.79997E 00	-7.02704E 00	1.30874E-01	9.96709E-02	1.24793E-02	-1.55279E-04	0.90925	3.54689E-01	7.147E-03	7.9946

(d) Concluded.

Figure 18.- Continued.

ITERATION NO. 8

COMPARISON OF VISCOUS AND INVISCID VELOCITIES IN SEPARATED REGION

+ = BOUNDARY LAYER
O = INVISCID SOLUTION

X	UEBL	UEINV	0.3 UE/UZ 1.0
8.545	0.93526	0.93526	O
8.621	0.94065	0.96393	+ O
8.686	0.93673	0.94599	+O
8.743	0.93753	0.93474	O
8.800	0.92655	0.90539	O +
8.864	0.87486	0.84899	O +
8.938	0.84958	0.78708	O +
9.024	0.85976	0.80207	O +
9.126	0.87179	0.87179	O

RESULTS OF ITERATION

XSEP = 8.5834
THET = -10.7665
DRMS = 3.6858

ITERATION NO. 9

COMPARISON OF VISCOUS AND INVISCID VELOCITIES IN SEPARATED REGION

+ = BOUNDARY LAYER
O = INVISCID SOLUTION

X	UEBL	UEINV	0.3 UE/UZ 1.0
8.545	0.93514	0.93514	O
8.621	0.94208	0.96738	+ O
8.686	0.93778	0.94548	+O
8.743	0.93839	0.93216	O
8.800	0.92731	0.90085	O +
8.864	0.87386	0.84152	O +
8.928	0.85058	0.78716	O +
9.024	0.86112	0.80522	O +
9.126	0.87358	0.87358	O

RESULTS OF ITERATION

XSEP = 8.5834
THET = -10.5165
DRMS = 3.8265

(e) Comparison of viscous and inviscid calculations after eight and nine iterations.

Figure 18.- Continued.

```
ITERATION NO. 16

COMPARISON OF VISCOUS AND INVISCID VELOCITIES IN SEPARATED REGION

        + = BOUNDARY LAYER
        O = INVISCID SOLUTION

   X        UEBL       UEINV   0.3                        UE/UZ                        1.0
 8.453   0.98914    0.98514                                                           O
 8.545   0.95302    0.95183                                                          O
 8.621   0.94601    0.95359                                                          O
 8.686   0.94805    0.95366                                                          O
 8.743   0.94923    0.93704                                                         O+
 8.800   0.94820    0.91070                                                       O  +
 8.864   0.90478    0.87447                                                     O +
 8.938   0.86563    0.82679                                                  O +
 9.024   0.86101    0.83286                                                  O +
 9.126   0.87325    0.87325                                                    O

 RESULTS OF ITERATION

  XSEP   =    8.5307
  THET   =  -10.7932
  DRMS   =    2.4658

ITERATION NO. 25

COMPARISON OF VISCOUS AND INVISCID VELOCITIES IN SEPARATED REGION

        + = BOUNDARY LAYER
        O = INVISCID SOLUTION

   X        UEBL       UEINV   0.3                        UE/UZ                        1.0
 8.341   1.07127    1.07127                                                             O
 8.453   0.97377    0.97336                                                          O
 8.545   0.96454    0.94500                                                          O+
 8.621   0.96964    0.97057                                                          O
 8.686   0.97305    0.98364                                                          +O
 8.743   0.97383    0.98522                                                          +O
 8.800   0.97361    0.97512                                                          +O
 8.864   0.95968    0.94256                                                         O+
 8.938   0.92769    0.92213                                                       O
 9.024   0.89913    0.91389                                                      +O
 9.126   0.88098    0.89018                                                     +O
 9.248   0.89078    0.89063                                                      O
 9.397   0.91337    0.91338                                                       O

 RESULTS OF ITERATION

  XSEP   =    8.4518
  THET   =  -10.8333
  DRMS   =    1.0675


COMPUTING TIME= 215.9 SECONDS
```

(f) Comparison of viscous and inviscid calculations after 16 and 25 iterations.

Figure 18.- Continued.

ITERATION NO. 25

PLOT OF CP AT EQUAL XI-INCREMENTS

I	XB	YB	FM	QS	CP
1	0.0	0.0	0.0	0.0	1.1704
2	0.068	0.017	0.838	1.041	-0.0831
3	0.138	0.035	0.591	0.758	0.4547
4	0.212	0.053	0.646	0.824	0.3180
5	0.290	0.073	0.671	0.853	0.2849
6	0.376	0.095	0.686	0.870	0.2520
7	0.469	0.118	0.697	0.883	0.2278
8	0.573	0.144	0.706	0.894	0.2078
9	0.688	0.172	0.714	0.903	0.1892
10	0.815	0.205	0.723	0.913	0.1703
11	0.955	0.240	0.732	0.924	0.1495
12	1.109	0.279	0.744	0.937	0.1248
13	1.278	0.321	0.758	0.953	0.0928
14	1.462	0.368	0.780	0.977	0.0452
15	1.662	0.418	0.825	1.028	-0.0553
16	1.877	0.469	0.959	1.170	-0.3478
17	2.112	0.500	0.984	1.196	-0.4013
18	2.364	0.504	0.874	1.080	-0.1629
19	2.621	0.505	0.837	1.041	-0.0826
20	2.911	0.505	0.824	1.027	-0.0542
21	3.203	0.506	0.819	1.021	-0.0412
22	3.506	0.507	0.815	1.017	-0.0321
23	3.817	0.507	0.812	1.014	-0.0271
24	4.136	0.508	0.810	1.011	-0.0230
25	4.461	0.509	0.809	1.010	-0.0208
26	4.787	0.509	0.809	1.010	-0.0200
27	5.115	0.510	0.809	1.010	-0.0200
28	5.441	0.510	0.809	1.010	-0.0208
29	5.762	0.511	0.810	1.011	-0.0220
30	6.076	0.512	0.811	1.012	-0.0239
31	6.380	0.512	0.812	1.013	-0.0268
32	6.672	0.513	0.814	1.016	-0.0319
33	6.950	0.513	0.819	1.021	-0.0412
34	7.211	0.513	0.825	1.027	-0.0547
35	7.454	0.513	0.834	1.037	-0.0748
36	7.675	0.513	0.850	1.055	-0.1117
37	7.876	0.512	0.893	1.101	-0.2051
38	8.054	0.510	0.963	1.172	-0.3559
39	9.209	0.496	0.974	1.175	-0.3796
40	8.341	0.474	0.884	1.071	-0.1861

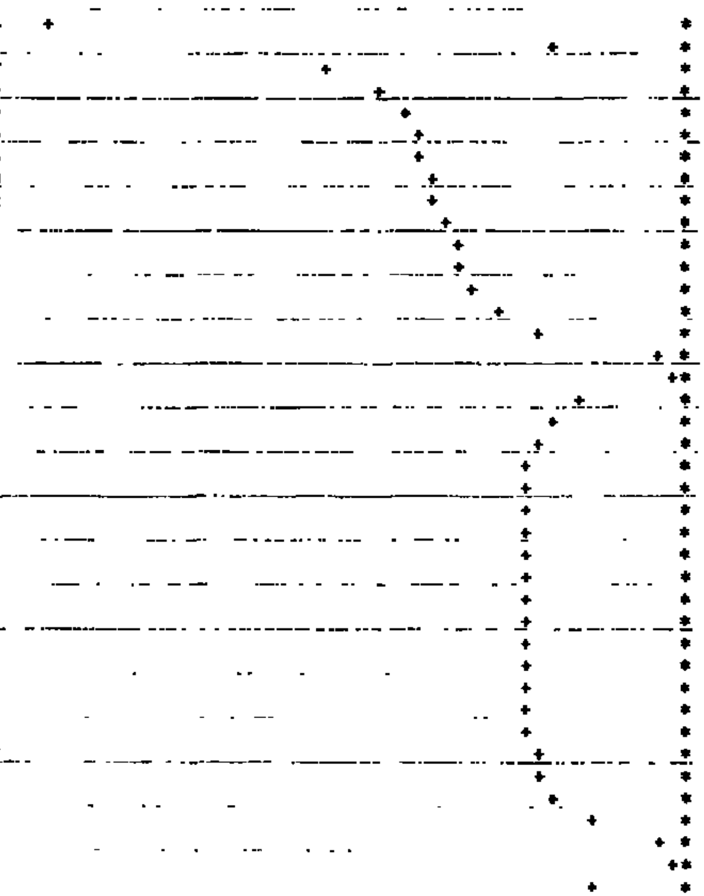

(g) Final plot of inviscid solution.

Figure 18.- Continued.

41	8.453	0.450	0.789	0.973	0.0239
42	8.546	0.437	0.776	0.945	0.0521
43	8.621	0.427	0.781	0.971	0.0428
44	8.686	0.418	0.784	0.984	0.0363
45	8.743	0.411	0.784	0.985	0.0351
46	8.800	0.402	0.783	0.975	0.0367
47	8.864	0.394	0.773	0.943	0.0596
48	8.938	0.384	0.744	0.922	0.1248
49	9.024	0.372	0.718	0.914	0.1814
50	9.126	0.358	0.702	0.890	0.2174
51	9.248	0.342	0.706	0.891	0.2080
52	9.397	0.332	0.724	0.913	0.1679
53	9.584	0.324	0.744	0.937	0.1242
54	9.824	0.317	0.761	0.956	0.0860
55	10.144	0.310	0.775	0.972	0.0561
56	10.592	0.302	0.785	0.983	0.0341
57	11.264	0.291	0.793	0.992	0.0163
58	12.384	0.269	0.793	0.992	0.0153
59	14.624	0.240	0.796	0.996	0.0083
60	21.343	0.240	0.800	1.000	0.0010
61	********	0.240	0.800	1.000	0.0

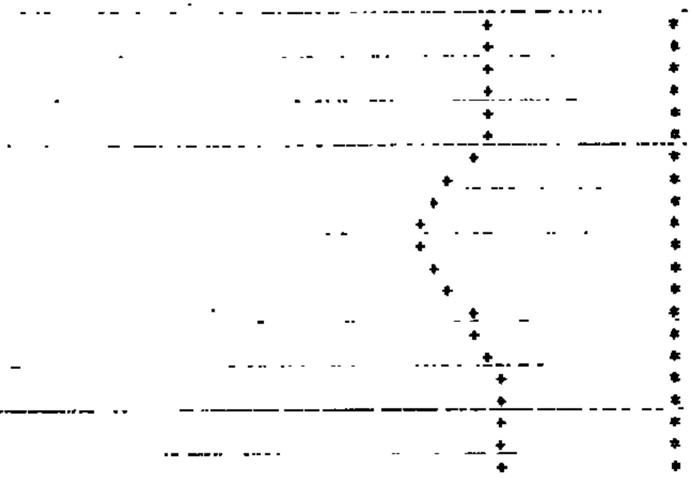

TOTAL BODY DRAG COEFFICIENT= 0.03189

AFTERBODY DRAG COEFFICIENT= 0.03967

(g) Concluded.

Figure 18.- Continued.

ITERATION NO. 25

AX	UTAU	DELTA	DELST	THETA	CF	UE/UZ	DELST*R	DX	HTR
8.00914E 00	3.91546E 01	1.02245E-01	1.12257E-02	5.80113E-03	2.79906E-03	1.15480	5.11146E-01	2.223E-02	0.9081
8.02135E 00	3.96610E 01	1.03300E-01	1.10752E-02	5.67115E-03	2.82070E-03	1.16365	5.10689E-01	5.555E-03	0.8966
8.05358E 00	4.01587E 01	1.04464E-01	1.09416E-02	5.54926E-03	2.84076E-03	1.17245	5.09910E-01	5.555E-03	0.8852
8.13111E 00	4.00892E 01	1.05264E-01	1.12013E-02	5.69001E-03	2.82317E-03	1.17382	5.05132E-01	1.938E-02	0.8901
8.20865E 00	3.99904E 01	1.06902E-01	1.15599E-02	5.88058E-03	2.80156E-03	1.17518	4.96190E-01	1.938E-02	0.8942
8.27501E 00	3.66348E 01	1.03729E-01	1.33734E-02	7.15085E-03	2.61171E-03	1.12283	4.86653E-01	1.659E-02	0.9748
8.34138E 00	3.30697E 01	1.04101E-01	1.59314E-02	8.77878E-03	2.37790E-03	1.07127	4.74489E-01	1.659E-02	1.0566
8.39715E 00	2.96769E 01	1.06712E-01	1.91035E-02	1.06506E-02	2.12867E-03	1.02279	4.62764E-01	1.394E-02	1.1377
8.45293E 00	2.60677E 01	1.11899E-01	2.36257E-02	1.21135E-02	1.83646E-03	0.97336	4.49901E-01	1.394E-02	1.2333
8.45177E 00	0.0	4.24177E-02	2.34964E-02	5.25742E-03	0.0	0.97438	4.50168E-01	1.394E-02	4.0000
8.45234E 00	-1.14449E-01	4.26364E-02	2.36276E-02	5.28432E-03	-3.53424E-08	0.97407	4.50103E-01	1.447E-04	4.0022
8.45293E 00	-2.73031E-01	4.28066E-02	2.37617E-02	5.29573E-03	-2.08717E-07	0.97377	4.50037E-01	1.447E-04	4.0176
8.49910E 00	-4.51343E 00	5.66293E-02	3.43410E-02	6.02680E-03	-5.61956E-05	0.96448	4.44314E-01	1.154E-02	5.2751
8.54529E 00	-6.94120E 00	7.13699E-02	4.63711E-02	6.52384E-03	-1.32885E-04	0.96454	4.38172E-01	1.154E-02	6.8209
8.58336E 00	-8.17123E 00	8.43926E-02	5.74075E-02	6.93779E-03	-1.83294E-04	0.96658	4.32812E-01	9.521E-03	8.1649
8.62145E 00	-9.16538E 00	9.89143E-02	7.04032E-02	7.30141E-03	-2.28984E-04	0.96964	4.28122E-01	9.521E-03	9.8242
8.65347E 00	-9.59041E 00	1.11220E-01	8.17484E-02	7.78156E-03	-2.49819E-04	0.97119	4.23494E-01	8.008E-03	10.9271
8.68551E 00	-9.96322E 00	1.24609E-01	9.48239E-02	8.28063E-03	-2.68468E-04	0.97305	4.19531E-01	8.008E-03	12.1859
8.71414E 00	-1.01062E 01	1.36480E-01	1.06960E-01	8.89622E-03	-2.75839E-04	0.97365	4.15574E-01	7.159E-03	12.9805
8.74279E 00	-1.00945E 01	1.48725E-01	1.20051E-01	9.77574E-03	-2.75092E-04	0.97383	4.11696E-01	7.159E-03	13.3537
8.77137E 00	-1.01389E 01	1.60925E-01	1.34352E-01	1.05960E-02	-2.77301E-04	0.97417	4.09158E-01	7.147E-03	13.9341
8.79997E 00	-1.00524E 01	1.72157E-01	1.48655E-01	1.16629E-02	-2.72942E-04	0.97361	4.03677E-01	7.147E-03	14.0456

AX	DK	RC	DELST	UE/UZ	UC/UZ	RW	DELST+R	RD
8.80797E 00	8.72780E-05	2.44131E-01	1.46329E-01	0.97112	1.56950	2.56631E-01	4.02959E-01	2.55000E-01
8.83597E 00	5.60873E-02	2.48248E-01	1.38094E-01	0.97118	1.56980	2.61687E-01	3.99781E-01	2.54203E-01
8.86398E 00	1.12712E-01	2.50936E-01	1.29860E-01	0.95968	1.55700	2.65558E-01	3.95417E-01	2.54636E-01
8.90390E 00	1.71440E-01	2.53233E-01	1.21310E-01	0.94406	1.55199	2.69325E-01	3.90634E-01	2.53598E-01
8.93783E 00	2.27433E-01	2.54593E-01	1.13175E-01	0.92769	1.54839	2.72132E-01	3.85307E-01	2.52422E-01
8.98090E 00	2.83222E-01	2.55516E-01	1.05026E-01	0.91234	1.55287	2.74621E-01	3.79647E-01	2.50212E-01
9.02390E 00	3.37110E-01	2.56049E-01	9.70934E-02	0.89913	1.56234	2.76732E-01	3.73825E-01	2.47565E-01
9.07484E 00	3.97761E-01	2.56336E-01	8.80947E-02	0.88771	1.57357	2.78895E-01	3.66989E-01	2.44917E-01
9.12580E 00	4.55556E-01	2.56270E-01	7.94509E-02	0.88098	1.58345	2.80763E-01	3.60214E-01	2.42933E-01
9.17161E 00	5.07110E-01	2.55871E-01	7.16978E-02	0.87923	1.59067	2.82239E-01	3.53936E-01	2.41769E-01
9.20979E 00	5.64014E-01	2.54891E-01	6.32061E-02	0.88501	1.59236	2.83260E-01	3.46466E-01	2.42010E-01
9.24798E 00	5.97423E-01	2.53849E-01	5.81230E-02	0.89078	1.59442	2.84132E-01	3.42254E-01	2.42200E-01
9.32264E 00	6.43473E-01	2.51408E-01	5.09957E-02	0.90208	1.59810	2.85488E-01	3.36484E-01	2.42628E-01
9.39731E 00	6.77311E-01	2.48447E-01	4.56034E-02	0.91337	1.60037	2.86470E-01	3.32074E-01	2.43289E-01
9.49064E 00	7.07239E-01	2.44429E-01	4.05657E-02	0.92495	1.60334	2.87187E-01	3.27953E-01	2.43933E-01
9.58797E 00	7.31613E-01	2.39876E-01	3.63032E-02	0.93653	1.60553	2.88044E-01	3.24347E-01	2.44798E-01
9.70397E 00	7.53637E-01	2.34113E-01	3.21835E-02	0.94643	1.60788	2.88670E-01	3.20854E-01	2.45600E-01
9.82397E 00	7.72159E-01	2.27824E-01	2.84834E-02	0.95624	1.60937	2.89088E-01	3.17571E-01	2.46704E-01
9.98397E 00	7.90199E-01	2.15871E-01	2.45159E-02	0.96398	1.61111	2.89489E-01	3.14005E-01	2.47785E-01

(h) Final viscous solution.

Figure 18.- Continued.

1.01440E 01	8.05512E-01	2.11370E-01	2.08527E-02	0.97162	1.61240	2.89753E-01	3.10606E-01	2.49187E-01
1.03683E 01	8.21948E-01	2.00125E-01	1.64286E-02	0.97719	1.61258	2.90020E-01	3.06449E-01	2.50811E-01
1.05920E 01	8.35694E-01	1.88368E-01	1.22658E-02	0.98277	1.61466	2.90185E-01	3.02451E-01	2.52753E-01
1.08279E 01	8.51912E-01	1.71002E-01	6.58318E-03	0.98724	1.61501	2.90325E-01	2.96909E-01	2.55533E-01
1.12639E 01	8.64779E-01	1.52427E-01	1.17062E-03	0.99171	1.61534	2.90371E-01	2.91542E-01	2.58627E-01
1.18039E 01	8.81097E-01	1.25065E-01	-7.26258E-03	0.99189	1.61557	2.90418E-01	2.83156E-01	2.62601E-01
1.23139E 01	9.22980E-01	8.81230E-02	-2.11589E-02	0.99208	1.61594	2.90461E-01	2.69302E-01	2.67433E-01
1.35039E 01	9.59355E-01	2.22456E-02	-4.32254E-02	0.99396	1.61632	2.90506E-01	2.47280E-01	2.75617E-01
1.46234E 01	9.65550E-01	0.0	-5.01219E-02	0.99467	1.61632	2.90506E-01	2.40384E-01	2.77994E-01
1.79835E 01	9.65550E-01	0.0	-5.01219E-02	0.99467	1.61632	2.90506E-01	2.40384E-01	2.77994E-01
2.13433E 01	9.65550E-01	0.0	-5.01219E-02	0.99467	1.61632	2.90506E-01	2.40384E-01	2.77994E-01

STATUS OF ITERATION

XMAX = 9.1258
DPMAX = 0.5501E-03
RBT = 0.2550E 00

****ITERATION FOR BOUNDARY LAYER/INVISCID FLOW EQUILIBRIUM CONVERGED
*********SOLUTION CONVERGED TO LEAST SQUARED ERROR TOLERANCE

(h) Concluded.

Figure 18.- Continued.

PLUME VELOCITY

NUI = 55

X	U
8.8000E 00	1.4565E 03
8.8160E 00	1.4565E 03
8.8320E 00	1.4520E 03
8.8480E 00	1.4479E 03
8.8640E 00	1.4443E 03
8.8824E 00	1.4437E 03
8.9009E 00	1.4379E 03
8.9194E 00	1.4325E 03
8.9378E 00	1.4274E 03
8.9594E 00	1.4245E 03
8.9809E 00	1.4198E 03
9.0024E 00	1.4154E 03
9.0240E 00	1.4112E 03
9.0494E 00	1.4082E 03
9.0749E 00	1.4051E 03
9.1003E 00	1.4023E 03
9.1258E 00	1.3996E 03
9.1563E 00	1.3977E 03
9.1869E 00	1.3976E 03
9.2174E 00	1.3975E 03
9.2480E 00	1.3975E 03
9.2853E 00	1.3980E 03
9.3226E 00	1.3998E 03
9.3600E 00	1.4016E 03
9.3973E 00	1.4034E 03
9.4440E 00	1.4056E 03
9.4906E 00	1.4075E 03
9.5373E 00	1.4094E 03
9.5840E 00	1.4114E 03
9.6440E 00	1.4139E 03
9.7040E 00	1.4154E 03
9.7640E 00	1.4169E 03
9.8240E 00	1.4186E 03
9.9040E 00	1.4209E 03
9.9840E 00	1.4217E 03
1.0064E 01	1.4229E 03
1.0144E 01	1.4241E 03
1.0256E 01	1.4260E 03
1.0368E 01	1.4264E 03
1.0480E 01	1.4272E 03
1.0592E 01	1.4281E 03

PLUME SHAPE

JP = 56

X	R
8.8000E 00	2.5500E-01
8.8160E 00	2.5879E-01
8.8320E 00	2.6214E-01
8.8480E 00	2.6512E-01
8.8640E 00	2.6777E-01
8.8824E 00	2.7049E-01
8.9009E 00	2.7285E-01
8.9194E 00	2.7488E-01
8.9378E 00	2.7663E-01
8.9594E 00	2.7838E-01
8.9809E 00	2.7985E-01
9.0024E 00	2.8107E-01
9.0240E 00	2.8209E-01
9.0494E 00	2.8305E-01
9.0749E 00	2.8382E-01
9.1003E 00	2.8444E-01
9.1258E 00	2.8492E-01
9.1563E 00	2.8537E-01
9.1869E 00	2.8575E-01
9.2174E 00	2.8606E-01
9.2480E 00	2.8632E-01
9.2853E 00	2.8659E-01
9.3226E 00	2.8686E-01
9.3600E 00	2.8711E-01
9.3973E 00	2.8737E-01
9.4440E 00	2.8768E-01
9.4906E 00	2.8798E-01
9.5373E 00	2.8826E-01
9.5840E 00	2.8855E-01
9.6440E 00	2.8891E-01
9.7040E 00	2.8922E-01
9.7640E 00	2.8951E-01
9.8240E 00	2.8978E-01
9.9040E 00	2.9013E-01
9.9840E 00	2.9041E-01
1.0064E 01	2.9065E-01
1.0144E 01	2.9086E-01
1.0256E 01	2.9115E-01
1.0368E 01	2.9135E-01
1.0480E 01	2.9151E-01
1.0592E 01	2.9166E-01
1.0760E 01	2.9189E-01

(i) Final inviscid plume solution.

Figure 18.- Continued.

1.0760E 01	1.4296E 03	1.0928E 01	2.9201E-01
1.0928E 01	1.4298E 03	1.1096E 01	2.9213E-01
1.1096E 01	1.4306E 03	1.1264E 01	2.9225E-01
1.1264E 01	1.4314E 03	1.1544E 01	2.9245E-01
1.1544E 01	1.4328E 03	1.1824E 01	2.9245E-01
1.1824E 01	1.4328E 03	1.2104E 01	2.9245E-01
1.2104E 01	1.4328E 03	1.2384E 01	2.9245E-01
1.2384E 01	1.4328E 03	1.2944E 01	2.9245E-01
1.2944E 01	1.4328E 03	1.3504E 01	2.9245E-01
1.3504E 01	1.4328E 03	1.4064E 01	2.9245E-01
1.4064E 01	1.4328E 03	1.4624E 01	2.9245E-01
1.4624E 01	1.4328E 03	1.6304E 01	2.9245E-01
1.6304E 01	1.4328E 03	1.7984E 01	2.9245E-01
1.7984E 01	1.4328E 03	1.9663E 01	2.9245E-01

(i) Concluded.

Figure 18.- Concluded.

```
NASA CONFIGURATION 1
(BLANK CARD)
RESTARTING ITERATION SCHEME AFTER    ITERATIONS FOR RUN
   1    0    0  600    0
```

Figure 19.- Input data for restart.

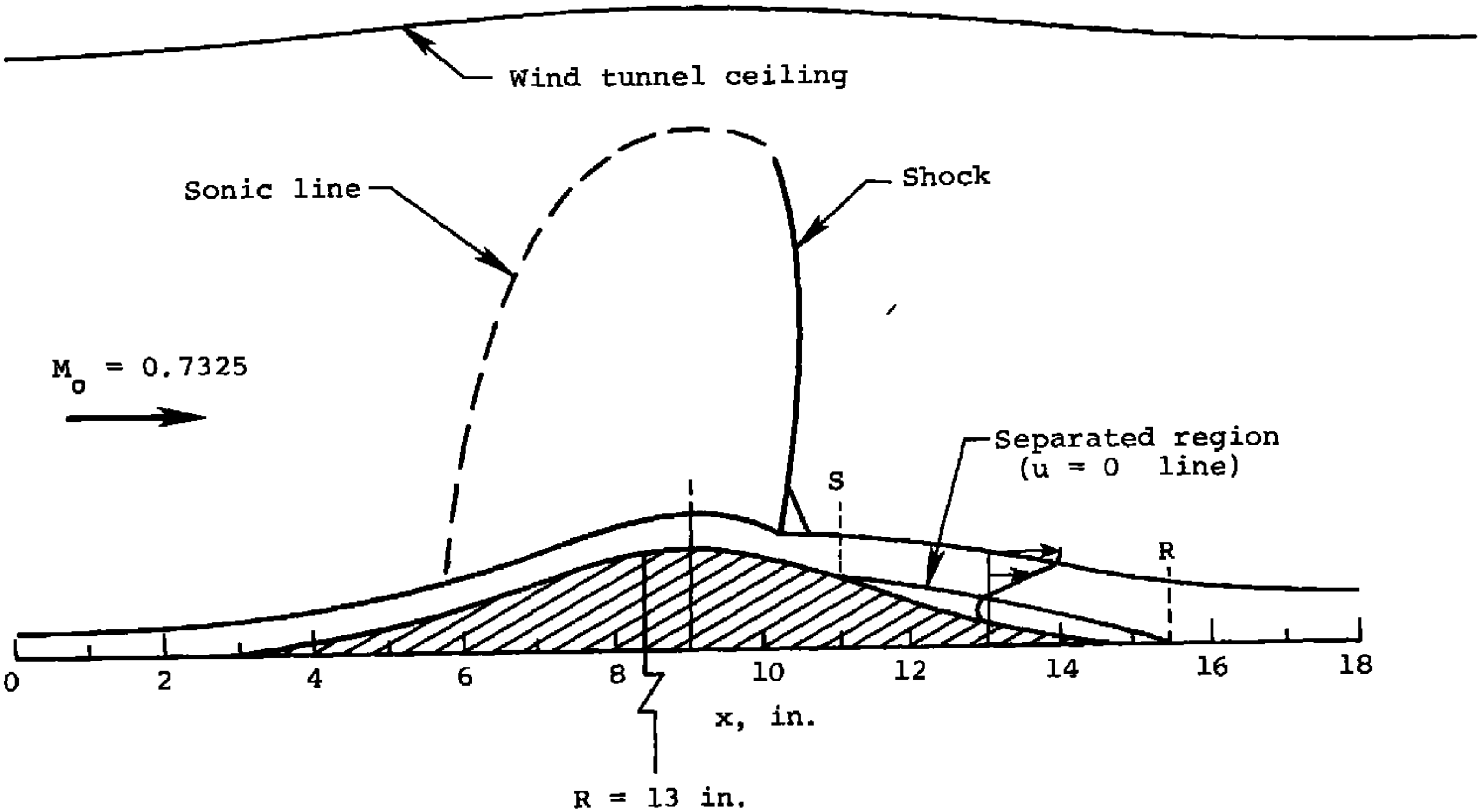

Figure 20.- Two-dimensional configuration for boundary-layer calculation.

```
           ALBER TEST CASE
  TWO-DIMENSIONAL BOUNDARY LAYER CALCULATION
  SPECIFYING VELOCITY DISTRIBUTION FROM X=0
 0    0    0    0    0
 1    0    0    0    2    0
 1.4       .7325
 1    0    0    0    2    0    0
22
 0.0      9750.
 1.0      9480.
 2.0      9400.
 3.0      8500.
 4.0      8650.
 5.0      9750.
 6.0     11650.
 7.0     12980.
 8.0     14200.
 9.0     15480.
10.0     16100.
10.25    14800.
10.75    13400.
11.0     12600.
11.50    12100.
12.0     11150.
13.0     10900.
14.0     10800.
15.0     10300.
16.0      9900.
17.0      9800.
18.0     10200.
 1.0      15.0    585.0       .99      0.0      0.0      0.0      0.0
 0.0      15.0     -5.0     0.0       0.0      0.0      0.0
.00233   .065
19
 0.0       0.0
 1.0       0.0
 2.0       0.0
 3.0       0.0
 4.0       0.25
 5.0       0.50
 6.0       0.70
 7.0       0.85
 8.0       0.98
 9.0       1.0
10.0       0.98
11.0       0.85
12.0       0.70
13.0       0.50
14.0       0.25
15.0       0.0
16.0       0.0
17.0       0.0
18.0       0.0
```

(a) Input for case with u_e specified.

Figure 21.- Input data for two-dimensional boundary-layer calculation.

```
          ALBER TEST CASE
 TWO-DIMENSIONAL BOUNDARY LAYER CALCULATION
 SPECIFYING DELST DISTRIBUTION FROM X=10.75
 0    0    0    0    0
 1    0    0    0    2    0
 1.4       .7325
 2    0    0    0    2    0    0
13
10.0     .03
10.25    .05
10.75    .07
11.0     .083
11.5     .112
12.0     .148
13.0     .314
14.0     .435
14.5     .460
15.0     .440
16.0     .306
17.0     .230
18.0     .190
 1.0     15.0     585.0     .99     0.0     0.0     0.0     0.0
10.75    18.0      -5.0     0.0     0.0     0.0     0.0
.00077
13400.   -2820.
19
 0.0      0.0
 1.0      0.0
 2.0      0.0
 3.0      0.0
 4.0      0.25
 5.0      0.50
 6.0      0.70
 7.0      0.85
 8.0      0.98
 9.0      1.0
10.0      0.98
11.0      0.85
12.0      0.70
13.0      0.50
14.0      0.25
15.0      0.0
16.0      0.0
17.0      0.0
18.0      0.0
```

(b) Input data for case with δ^* specified.

Figure 21.- Concluded.

```
UZ    = 9.90272E 03
REZ   = 3.02426E 05
NUZ   = 3.27443E-02
```

AX	UTAU	DELTA	DELST	THETA	CF	UE/UZ	DELST*R	DX	HTR
0.0	3.32242E 02	3.90140E-01	6.52716E-02	3.68389E-02	2.33000E-03	0.98458	6.52716E-02	0.0	1.1853
5.00000E-01	3.21310E 02	3.99803E-01	6.93925E-02	3.91283E-02	2.24705E-03	0.97097	6.93925E-02	1.250E-01	1.2071
1.00000E 00	3.10535E 02	4.10471E-01	7.37869E-02	4.15399E-02	2.16527E-03	0.95731	7.37869E-02	1.250E-01	1.2288
1.50000E 00	3.08182E 02	4.20119E-01	7.55540E-02	4.25883E-02	2.15244E-03	0.95328	7.55540E-02	1.250E-01	1.2293
2.00000E 00	3.05816E 02	4.29808E-01	7.73537E-02	4.36547E-02	2.13935E-03	0.94923	7.73537E-02	1.250E-01	1.2300
2.50000E 00	2.67468E 02	4.51458E-01	9.40342E-02	5.19691E-02	1.82001E-03	0.90409	9.40342E-02	1.250E-01	1.3310
3.00000E 00	2.25982E 02	4.85408E-01	1.18051E-01	6.25757E-02	1.45358E-03	0.85835	1.18051E-01	1.250E-01	1.4640
3.50000E 00	2.38377E 02	4.91889E-01	1.12308E-01	6.08659E-02	1.58704E-03	0.86593	2.37308E-01	1.250E-01	1.4072
4.00000E 00	2.49094E 02	4.98767E-01	1.07677E-01	5.93432E-02	1.70071E-03	0.87350	3.57677E-01	1.250E-01	1.3613
4.50000E 00	3.00004E 02	4.87966E-01	8.40418E-02	4.81035E-02	2.15565E-03	0.92949	4.59042E-01	1.250E-01	1.2059
5.00000E 00	3.43194E 02	4.89869E-01	6.94349E-02	3.98973E-02	2.48613E-03	0.98458	5.69435E-01	1.250E-01	1.0984
5.50000E 00	4.12184E 02	5.12687E-01	5.25996E-02	2.88568E-02	2.90462E-03	1.08214	6.52600E-01	1.250E-01	0.9467
6.00000E 00	4.72248E 02	5.79759E-01	4.32235E-02	2.11969E-02	3.15095E-03	1.17644	7.43223E-01	1.250E-01	0.8087
6.50000E 00	5.10831E 02	6.99677E-01	3.95237E-02	1.65049E-02	3.23355E-03	1.24456	8.14524E-01	1.250E-01	0.6903
7.00000E 00	5.46276E 02	4.73384E-01	3.81249E-02	1.73663E-02	3.26948E-03	1.31075	8.88125E-01	1.250E-01	0.8184
7.50000E 00	5.84737E 02	5.41189E-01	3.61652E-02	1.45727E-02	3.34613E-03	1.37327	9.51165E-01	1.250E-01	0.7332
8.00000E 00	6.15961E 02	7.38021E-01	3.61176E-02	1.10344E-02	3.33669E-03	1.43395	1.01612E 00	1.250E-01	0.5954
8.50000E 00	6.63138E 02	3.24366E-01	3.25074E-02	1.35469E-02	3.45291E-03	1.49974	1.02251E 00	1.250E-01	0.8748
9.00000E 00	7.08463E 02	3.51955E-01	3.19577E-02	1.22138E-02	3.54016E-03	1.56321	1.03196E 00	1.250E-01	0.8211
9.50000E 00	7.28881E 02	3.56577E-01	3.25226E-02	1.20838E-02	3.55447E-03	1.59481	1.02252E 00	1.250E-01	0.8153
1.00000E 01	7.49256E 02	3.60902E-01	3.31672E-02	1.19900E-02	3.56767E-03	1.62581	1.01317E 00	1.250E-01	0.8107
1.05000E 01	5.69590E 02	1.97071E-01	3.51045E-02	1.62790E-02	2.89740E-03	1.42514	9.50104E-01	1.250E-01	1.1481
1.10000E 01	4.02644E 02	2.01348E-01	5.12561E-02	2.38486E-02	1.90670E-03	1.27238	9.01256E-01	1.250E-01	1.4164
1.15000E 01	3.53120E 02	2.17810E-01	6.01654E-02	2.76050E-02	1.61324E-03	1.22188	8.35165E-01	1.250E-01	1.5065
1.20000E 01	2.34226E 02	2.56490E-01	8.96149E-02	3.67189E-02	8.57211E-04	1.12595	7.89615E-01	1.250E-01	1.8657
1.25000E 01	2.49992E 02	2.71578E-01	8.92057E-02	3.83132E-02	1.00182E-03	1.11336	6.89206E-01	1.250E-01	1.7627
1.30000E 01	2.57452E 02	2.87398E-01	9.05402E-02	4.00555E-02	1.09042E-03	1.10071	5.90540E-01	1.250E-01	1.7029
1.35000E 01	2.71775E 02	3.00251E-01	8.91909E-02	4.08723E-02	1.22784E-03	1.09566	4.64191E-01	1.250E-01	1.6243
1.40000E 01	2.81560E 02	3.13199E-01	8.87628E-02	4.17275E-02	1.33169E-03	1.09061	3.38763E-01	1.250E-01	1.5686
1.45000E 01	2.62903E 02	3.34089E-01	9.73644E-02	4.54369E-02	1.22371E-03	1.06547	2.22564E-01	1.250E-01	1.6110
1.50000E 01	2.43585E 02	3.57543E-01	1.07992E-01	4.96323E-02	1.10873E-03	1.04012	1.07992E-01	1.250E-01	1.6616

(a) Output from case with u_e specified.

Figure 22.- Output from two-dimensional boundary-layer calculation.

UZ = 9.90272E 03
REZ = 3.02428E 05
NUZ = 3.27443E-02

AX	UTAU	DELTA	DELST	THETA	CF	UE/UZ	DELST*R	DX	HTR
1.07500E 01	2.75853E 02	1.78872E-01	7.00000E-02	2.49773E-02	7.71981E-04	1.35316	9.52500E-01	0.0	1.9901
1.08750E 01	2.40572E 02	1.88664E-01	7.64999E-02	2.64890E-02	6.40700E-04	1.33210	9.42750E-01	3.125E-02	2.0924
1.10000E 01	2.21972E 02	1.98821E-01	8.29999E-02	2.79512E-02	5.37044E-04	1.31357	9.33000E-01	3.125E-02	2.1881
1.15000E 01	1.46280E 02	2.45658E-01	1.12000E-01	3.39078E-02	2.60983E-04	1.25296	8.87000E-01	1.250E-01	2.5641
1.20000E 01	9.16353E 01	3.04655E-01	1.48000E-01	4.03923E-02	1.12095E-04	1.20558	8.48000E-01	1.250E-01	2.9561
1.25000E 01	-8.26830E 00	4.23961E-01	2.31000E-01	4.79995E-02	-9.75678E-07	1.17132	8.31000E-01	1.250E-01	4.0823
1.30000E 01	-5.42523E 01	5.44706E-01	3.14000E-01	5.36157E-02	-4.33315E-05	1.15562	8.14000E-01	1.250E-01	5.1393
1.35000E 01	-6.56214E 01	6.38968E-01	3.74500E-01	5.95115E-02	-6.51881E-05	1.14165	7.49500E-01	1.250E-01	5.6144
1.40000E 01	-7.71282E 01	7.29138E-01	4.35000E-01	6.35875E-02	-9.13034E-05	1.13480	6.85000E-01	1.250E-01	6.2043
1.45000E 01	-7.18564E 01	7.76348E-01	4.60000E-01	6.92785E-02	-8.11766E-05	1.12291	5.85000E-01	1.250E-01	6.0171
1.50000E 01	-4.45844E 01	7.73524E-01	4.40000E-01	7.83358E-02	-3.26269E-05	1.10182	4.40000E-01	1.250E-01	4.9922
1.55000E 01	2.00228E 01	7.15603E-01	3.73000E-01	8.69426E-02	6.88464E-06	1.08002	3.73000E-01	1.250E-01	3.7074
1.60000E 01	8.27965E 01	6.58124E-01	3.06000E-01	9.05431E-02	1.20372E-04	1.06939	3.06000E-01	1.250E-01	2.8259
1.65000E 01	1.25859E 02	6.34677E-01	2.68000E-01	9.15319E-02	2.80038E-04	1.06617	2.68000E-01	1.250E-01	2.3887
1.70000E 01	1.72894E 02	6.12617E-01	2.30000E-01	8.94216E-02	5.21237E-04	1.07271	2.30000E-01	1.250E-01	2.0342
1.75000E 01	2.02841E 02	6.08530E-01	2.10000E-01	8.76884E-02	7.08257E-04	1.07886	2.10000E-01	1.250E-01	1.8524
1.80000E 01	2.34176E 02	6.03411E-01	1.90000E-01	8.43694E-02	9.19959E-04	1.09125	1.90000E-01	1.250E-01	1.6961

(b) Output from case with δ^* specified.

Figure 22.- Concluded.

```
NASA DATA COMPARISON -  CONFIGURATION 1
JET SIMULATED WITH A SOLID STING
BOATTAIL L/D = 0.8
    0     0     0   700     0
   -1     0     0     1     1     0
   1.4        0.9
   98
   0.0        0.0
   0.1        0.025013
   0.2        0.050026
   0.3        0.075038
   0.4        0.100051
   0.5        0.125064
   0.6        0.150077
   0.7        0.175090
   0.8        0.200102
   0.9        0.225115
   1.0        0.250128
   1.1        0.275141
   1.2        0.300154
   1.3        0.325166
   1.4        0.350179
   1.5        0.375192
   1.6        0.400205
   1.7        0.425218
   1.8        0.450230
   1.9        0.473630
   2.0        0.489760
   2.1        0.498366
   2.2        0.500000
   2.3        0.500000
   2.5        0.500000
   3.0        0.500000
   3.5        0.500000
   4.0        0.500000
   5.0        0.500000
   6.0        0.500000
   7.0        0.500000
   7.5        0.500000
   8.0        0.500000
   8.025      0.499781
   8.05       0.499125
   8.075      0.498030
   8.1        0.496496
   8.125      0.494521
   8.15       0.492104
   8.175      0.489241
   8.2        0.485931
   8.225      0.482171
   8.25       0.477956
```

(a) First 50 cards.

Figure 23.- Input data for inviscid calculation.

8.275	0.473282
8.3	0.468146
8.325	0.462542
8.35	0.456463
8.375	0.449905
8.4	0.442859
8.425	0.435319
8.45	0.427277
8.475	0.418722
8.5	0.409646
8.525	0.400037
8.55	0.389885
8.575	0.379176
8.6	0.367897
8.625	0.356032
8.65	0.343565
8.675	0.330479
8.7	0.316753
8.725	0.302368
8.75	0.287298
8.775	0.271518
8.8	0.255000
8.81	0.255000
8.82	0.255000
8.83	0.255000
8.84	0.255000
8.85	0.255000
8.86	0.255000
8.87	0.255000
8.88	0.255000
8.89	0.255000
8.9	0.255000
8.92	0.255000
8.94	0.255000
8.96	0.255000
8.98	0.255000
9.0	0.255000
9.025	0.255000
9.05	0.255000
9.075	0.255000
9.1	0.255000
9.15	0.255000
9.2	0.255000
9.3	0.255000
9.4	0.255000
9.5	0.255000
9.7	0.255000
9.9	0.255000
10.1	0.255000
10.3	0.255000

(b) Next 50 cards.

Figure 23.- Continued.

```
10.5       0.255000
10.8       0.255000
11.2       0.255000
11.6       0.255000
12.0       0.255000
 61   31     0    0     0
0.0        0.0         0.0        0.0         8.8      1.0        8.0
  F
```

(c) Remaining 7 cards.

Figure 23.- Concluded.

------ NORMAL COORD. STRETCH FOR ALF= 1.300 ------

J	AN	G	GH
1	0.2510E 00	0.0	0.7725E-04
2	0.1617E 03	0.1545E-03	0.4607E-03
3	0.6339E 02	0.7668E-03	0.1365E-02
4	0.3608E 02	0.1964E-02	0.2900E-02
5	0.2391E 02	0.3836E-02	0.5148E-02
6	0.1720E 02	0.6460E-02	0.8183E-02
7	0.1303E 02	0.9905E-02	0.1207E-01
8	0.1022E 02	0.1424E-01	0.1687E-01
9	0.8215E 01	0.1951E-01	0.2265E-01
10	0.6729E 01	0.2579E-01	0.2947E-01
11	0.5588E 01	0.3314E-01	0.3738E-01
12	0.4690E 01	0.4161E-01	0.4644E-01
13	0.3968E 01	0.5126E-01	0.5670E-01
14	0.3377E 01	0.6215E-01	0.6824E-01
15	0.2886E 01	0.7433E-01	0.8110E-01
16	0.2474E 01	0.8787E-01	0.9535E-01
17	0.2123E 01	0.1028E 00	0.1110E 00
18	0.1822E 01	0.1193E 00	0.1282E 00
19	0.1561E 01	0.1372E 00	0.1470E 00
20	0.1334E 01	0.1568E 00	0.1674E 00
21	0.1135E 01	0.1780E 00	0.1895E 00
22	0.9585E 00	0.2010E 00	0.2134E 00
23	0.8020E 00	0.2258E 00	0.2391E 00
24	0.6623E 00	0.2524E 00	0.2667E 00
25	0.5371E 00	0.2810E 00	0.2963E 00
26	0.4245E 00	0.3116E 00	0.3280E 00
27	0.3227E 00	0.3443E 00	0.3617E 00
28	0.2304E 00	0.3792E 00	0.3977E 00
29	0.1465E 00	0.4163E 00	0.4360E 00
30	0.7000E-01	0.4558E 00	0.4767E 00
31	0.1198E-06	0.4976E 00	0.5198E 00

(a) Normal coordinates.

Figure 24.- Output for inviscid calculation.

I	S	X	Y	THET	THETB	AK	F
1	0.0	0.0	0.0	0.9000E 02	0.9000E 02	0.2743E-04	0.2381E 00
2	0.7030E-01	0.6820E-01	0.1706E-01	0.1404E 02	0.1404E 02	0.3316E-04	0.2350E 00
3	0.1424E 00	0.1382E 00	0.3456E-01	0.1404E 02	0.1404E 02	0.4410E-04	0.2264E 00
4	0.2181E 00	0.2116E 00	0.5293E-01	0.1404E 02	0.1404E 02	0.1595E-03	0.2134E 00
5	0.2992E 00	0.2903E 00	0.7260E-01	0.1404E 02	0.1404E 02	0.1723E-03	0.1977E 00
6	0.3873E 00	0.3757E 00	0.9398E-01	0.1404E 02	0.1404E 02	0.1889E-05	0.1809E 00
7	0.4840E 00	0.4696E 00	0.1175E 00	0.1404E 02	0.1404E 02	0.8037E-05	0.1642E 00
8	0.5908E 00	0.5732E 00	0.1434E 00	0.1404E 02	0.1404E 02	0.2906E-04	0.1484E 00
9	0.7091E 00	0.6879E 00	0.1721E 00	0.1404E 02	0.1404E 02	0.1578E-03	0.1340E 00
10	0.8400E 00	0.8149E 00	0.2038E 00	0.1404E 02	0.1404E 02	0.1533E-03	0.1211E 00
11	0.9846E 00	0.9552E 00	0.2389E 00	0.1404E 02	0.1404E 02	0.9358E-05	0.1099E 00
12	0.1144E 01	0.1110E 01	0.2775E 00	0.1404E 02	0.1404E 02	0.3056E-04	0.1000E 00
13	0.1318E 01	0.1279E 01	0.3198E 00	0.1404E 02	0.1404E 02	0.9078E-04	0.9156E-01
14	0.1508E 01	0.1463E 01	0.3659E 00	0.1404E 02	0.1404E 02	0.1108E-03	0.8426E-01
15	0.1714E 01	0.1662E 01	0.4158E 00	0.1404E 02	0.1404E 02	0.1400E-02	0.7800E-01
16	0.1935E 01	0.1878E 01	0.4689E 00	0.1251E 02	0.1251E 02	0.6692E 00	0.7265E-01
17	0.2172E 01	0.2112E 01	0.4989E 00	0.2243E 01	0.2243E 01	0.7612E 00	0.6809E-01
18	0.2425E 01	0.2365E 01	0.5000E 00	0.0	-0.3978E-02	-0.4900E-02	0.6422E-01
19	0.2691E 01	0.2631E 01	0.5000E 00	0.0	0.2473E-02	0.8255E-03	0.6096E-01
20	0.2971E 01	0.2911E 01	0.5000E 00	0.0	-0.3711E-02	-0.5435E-04	0.5823E-01
21	0.3263E 01	0.3203E 01	0.5000E 00	0.0	0.1437E-03	-0.1585E-03	0.5599E-01
22	0.3566E 01	0.3506E 01	0.5000E 00	0.0	0.6285E-03	0.9587E-04	0.5419E-01
23	0.3878E 01	0.3818E 01	0.5000E 00	0.0	-0.2230E-03	-0.5328E-06	0.5279E-01
24	0.4197E 01	0.4137E 01	0.5000E 00	0.0	0.4268E-03	-0.3248E-04	0.5178E-01
25	0.4521E 01	0.4461E 01	0.5000E 00	0.0	0.4920E-03	0.2546E-04	0.5114E-01
26	0.4848E 01	0.4788E 01	0.5000E 00	0.0	-0.5324E-03	0.8391E-04	0.5087E-01
27	0.5175E 01	0.5115E 01	0.5000E 00	0.0	-0.2378E-02	0.5825E-04	0.5098E-01
28	0.5501E 01	0.5441E 01	0.5000E 00	0.0	-0.1788E-02	-0.1216E-03	0.5148E-01
29	0.5822E 01	0.5762E 01	0.5000E 00	0.0	0.2081E-02	-0.2990E-03	0.5242E-01
30	0.6136E 01	0.6076E 01	0.5000E 00	0.0	0.8595E-02	-0.2767E-03	0.5383E-01
31	0.6440E 01	0.6380E 01	0.5001E 00	0.0	0.8029E-02	0.3416E-03	0.5579E-01
32	0.6732E 01	0.6672E 01	0.5001E 00	0.0	-0.2662E-02	0.9352E-03	0.5840E-01
33	0.7010E 01	0.6950E 01	0.5000E 00	0.0	-0.2203E-01	0.1499E-02	0.6179E-01
34	0.7271E 01	0.7211E 01	0.4999E 00	0.0	-0.1938E-01	-0.2769E-02	0.6614E-01
35	0.7513E 01	0.7454E 01	0.4999E 00	0.0	0.5385E-01	-0.7781E-02	0.7172E-01
36	0.7735E 01	0.7676E 01	0.5003E 00	0.0	0.8941E-01	0.6040E-02	0.7888E-01
37	0.7936E 01	0.7876E 01	0.5004E 00	0.0	-0.7667E-01	0.2291E-01	0.8812E-01
38	0.8114E 01	0.8054E 01	0.4990E 00	0.0	-0.2152E 01	0.6643E 00	0.1001E 00
39	0.8269E 01	0.8209E 01	0.4847E 00	0.0	-0.8398E 01	0.7227E 00	0.1159E 00
40	0.8401E 01	0.8341E 01	0.4586E 00	0.0	-0.1383E 02	0.7626E 00	0.1368E 00
41	0.8513E 01	0.8453E 01	0.4263E 00	0.0	-0.1848E 02	0.8251E 00	0.1642E 00
42	0.8605E 01	0.8545E 01	0.3918E 00	0.0	-0.2244E 02	0.8863E 00	0.1992E 00
43	0.8681E 01	0.8621E 01	0.3578E 00	0.0	-0.2579E 02	0.9660E 00	0.2404E 00
44	0.8745E 01	0.8686E 01	0.3246E 00	0.0	-0.2871E 02	0.9442E 00	0.2793E 00
45	0.8803E 01	0.8743E 01	0.2916E 00	0.0	-0.3106E 02	-0.1939E 01	0.2977E 00
46	0.8860E 01	0.8800E 01	0.2550E 00	0.0	-0.1086E 02	-0.6596E 02	0.2790E 00
47	0.8924E 01	0.8864E 01	0.2550E 00	0.0	0.1355E-03	-0.1205E-01	0.2431E 00
48	0.8998E 01	0.8938E 01	0.2550E 00	0.0	-0.2549E-05	-0.2950E-05	0.2096E 00
49	0.9084E 01	0.9024E 01	0.2550E 00	0.0	-0.1286E-07	-0.2236E-07	0.1786E 00
50	0.9186E 01	0.9126E 01	0.2550E 00	0.0	-0.5914E-10	0.1232E-09	0.1501E 00
51	0.9308E 01	0.9248E 01	0.2550E 00	0.0	-0.4389E-11	0.6637E-11	0.1240E 00
52	0.9457E 01	0.9397E 01	0.2550E 00	0.0	0.2231E-11	0.1034E-11	0.1004E 00
53	0.9644E 01	0.9584E 01	0.2550E 00	0.0	0.4848E-13	-0.1016E-12	0.7937E-01
54	0.9884E 01	0.9824E 01	0.2550E 00	0.0	-0.5846E-13	0.1246E-13	0.6076E-01
55	0.1020E 02	0.1014E 02	0.2550E 00	0.0	0.4784E-14	0.3016E-14	0.4464E-01
56	0.1065E 02	0.1059E 02	0.2550E 00	0.0	0.1875E-15	0.1476E-15	0.3100E-01
57	0.1132E 02	0.1126E 02	0.2550E 00	0.0	0.4834E-16	0.1178E-16	0.1984E-01
58	0.1244E 02	0.1238E 02	0.2550E 00	0.0	0.0	0.0	0.1116E-01
59	0.1468E 02	0.1462E 02	0.2550E 00	0.0	0.0	0.0	0.4961E-02
60	0.2140E 02	0.2134E 02	0.2550E 00	0.0	0.0	0.0	0.1240E-02
61	0.1000E 31	0.1000E 31	0.2550E 00	0.0	0.0	0.0	0.1000E-29

(b) Tangential coordinates.

Figure 24.- Continued.

ITERATION NO. 1

IT	DPMAX	ID	JD	RMAX	IR	JR	ISUB	ISUP	RAVG	RF1	QF3	NS	SEC/CYC
1	0.402E-01	45	31	0.312E 02	1	31	1	0	0.150E 00	1.400	0.100	0	0.203
2	0.243E-01	44	31	0.162E 02	46	31	1	0	0.119E 00	1.400	0.100	1	0.213
3	0.202E-01	44	31	0.115E 02	45	31	1	0	0.104E 00	1.400	0.100	1	0.210
4	0.173E-01	44	31	0.112E 02	46	31	1	0	0.977E-01	1.400	0.100	5	0.207
5	0.153E-01	44	31	0.102E 02	46	31	1	0	0.941E-01	1.400	0.100	10	0.200
6	0.145E-01	43	31	0.958E 01	46	31	1	0	0.915E-01	1.400	0.100	14	0.190
7	0.134E-01	43	31	0.904E 01	46	31	1	0	0.824E-01	1.400	0.100	15	0.203
8	0.123E-01	42	31	0.856E 01	46	31	1	0	0.789E-01	1.400	0.100	18	0.207
9	0.117E-01	42	31	0.815E 01	46	31	1	0	0.756E-01	1.400	0.100	21	0.213
10	0.103E-01	42	31	0.779E 01	46	31	1	0	0.766E-01	1.400	0.100	25	0.207
11	0.870E-02	42	31	0.749E 01	46	31	1	0	0.752E-01	1.400	0.100	28	0.200
12	0.796E-02	45	31	0.723E 01	46	31	1	0	0.697E-01	1.400	0.100	33	0.207
13	0.784E-02	45	31	0.703E 01	46	31	1	0	0.676E-01	1.400	0.100	37	0.213
14	0.795E-02	42	29	0.688E 01	46	31	1	0	0.667E-01	1.400	0.100	39	0.193
15	0.797E-02	42	31	0.676E 01	46	31	1	0	0.690E-01	1.400	0.100	47	0.213
16	0.752E-02	43	31	0.660E 01	46	31	1	0	0.679E-01	1.400	0.100	51	0.210
17	0.695E-02	44	31	0.638E 01	46	31	1	0	0.637E-01	1.400	0.100	57	0.213
18	0.666E-02	46	31	0.618E 01	46	31	1	0	0.610E-01	1.400	0.100	61	0.200
19	0.651E-02	45	31	0.604E 01	46	31	1	0	0.599E-01	1.400	0.100	70	0.210
20	0.639E-02	45	31	0.591E 01	46	31	1	0	0.601E-01	1.400	0.100	75	0.200

RMAX= 0.59E 01, COVR= 0.33E-01

(c) Iteration history.

Figure 24.- Continued.

ITERATION NO. 1

PLOT OF CP AT EQUAL XI-INCREMENTS

I	XB	YB	FM	QS	CP
1	0.0	0.0	0.0	0.0	1.2192
2	0.068	0.017	0.908	1.007	-0.0148
3	0.138	0.035	0.632	0.728	0.5159
4	0.212	0.053	0.698	0.798	0.3901
5	0.290	0.073	0.725	0.826	0.3394
6	0.376	0.094	0.740	0.841	0.3097
7	0.470	0.117	0.751	0.853	0.2881
8	0.573	0.143	0.761	0.862	0.2699
9	0.688	0.172	0.769	0.871	0.2528
10	0.815	0.204	0.778	0.880	0.2354
11	0.955	0.239	0.788	0.890	0.2166
12	1.110	0.278	0.799	0.901	0.1950
13	1.279	0.320	0.813	0.915	0.1684
14	1.463	0.366	0.832	0.934	0.1318
15	1.662	0.416	0.869	0.970	0.0591
16	1.878	0.469	1.054	1.142	-0.2858
17	2.112	0.499	1.211	1.276	-0.5516
18	2.365	0.500	1.052	1.141	-0.2829
19	2.631	0.500	0.926	1.025	-0.0501
20	2.911	0.500	0.917	1.016	-0.0319
21	3.203	0.500	0.911	1.010	-0.0208
22	3.506	0.500	0.907	1.007	-0.0140
23	3.818	0.500	0.905	1.005	-0.0097
24	4.137	0.500	0.904	1.003	-0.0068
25	4.461	0.500	0.903	1.002	-0.0050
26	4.788	0.500	0.902	1.002	-0.0037
27	5.115	0.500	0.901	1.001	-0.0028
28	5.441	0.500	0.901	1.001	-0.0022
29	5.762	0.500	0.901	1.001	-0.0020
30	6.076	0.500	0.901	1.001	-0.0024
31	6.380	0.500	0.902	1.002	-0.0036
32	6.672	0.500	0.903	1.003	-0.0058
33	6.950	0.500	0.905	1.004	-0.0086
34	7.211	0.500	0.907	1.007	-0.0134
35	7.454	0.500	0.913	1.013	-0.0253
36	7.676	0.500	0.929	1.027	-0.0544
37	7.876	0.500	0.974	1.070	-0.1402
38	8.054	0.499	1.096	1.178	-0.3592
39	8.209	0.495	1.247	1.291	-0.6082
40	8.341	0.459	1.345	1.341	-0.7521
41	8.453	0.426	1.346	1.310	-0.7530
42	8.545	0.392	1.141	1.125	-0.4362
43	8.621	0.358	0.899	0.899	0.0022
44	8.686	0.325	0.758	0.754	0.2741
45	8.743	0.292	0.561	0.558	0.6460
46	8.800	0.255	0.438	0.505	0.8515
47	8.864	0.255	0.450	0.528	0.8326
48	8.938	0.255	0.559	0.650	0.6484
49	9.024	0.255	0.639	0.735	0.5035
50	9.126	0.255	0.702	0.802	0.3837
51	9.248	0.255	0.754	0.855	0.2831
52	9.397	0.255	0.797	0.899	0.1996
53	9.584	0.255	0.831	0.933	0.1323
54	9.824	0.255	0.858	0.959	0.0809
55	10.144	0.255	0.877	0.978	0.0446
56	10.592	0.255	0.889	0.989	0.0216
57	11.264	0.255	0.895	0.996	0.0088
58	12.384	0.255	0.899	0.999	0.0028
59	14.624	0.255	0.900	1.000	0.0006
60	21.343	0.255	0.900	1.000	0.0000
61	********	0.255	0.900	1.000	0.0

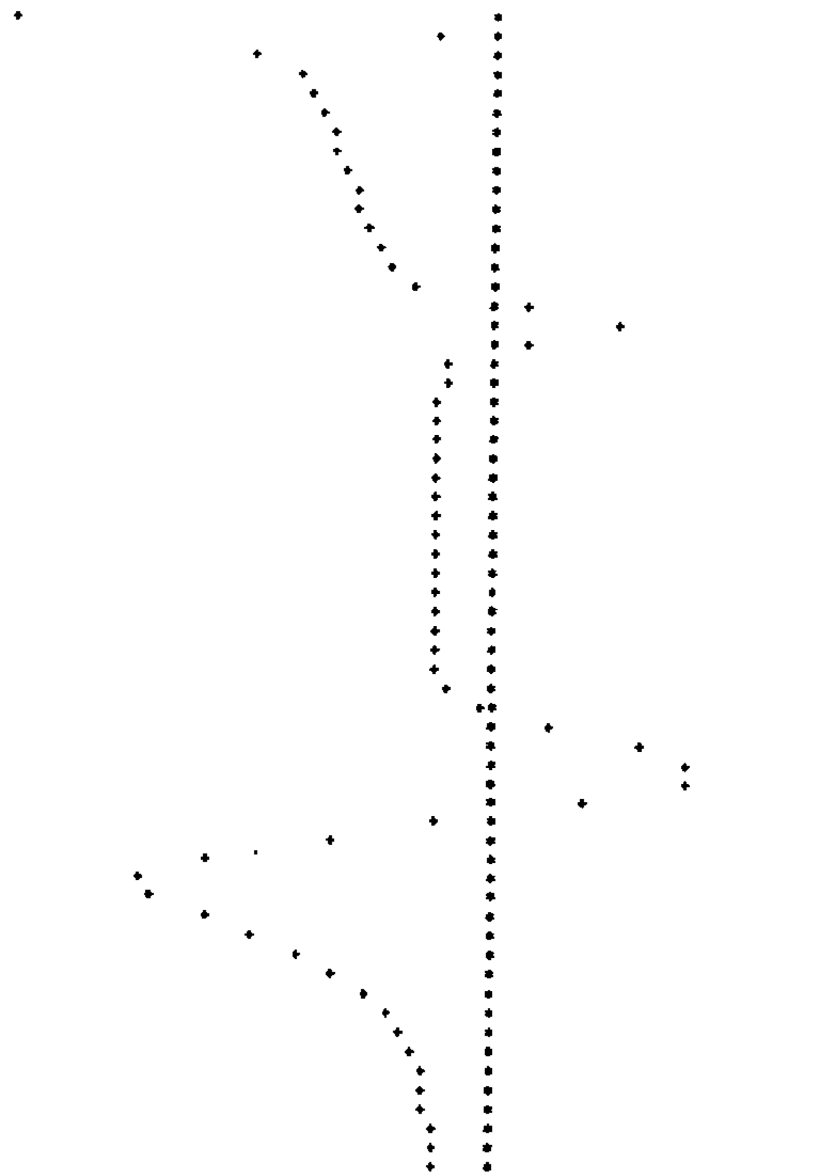

TOTAL BODY DRAG COEFFICIENT= 0.21993

AFTERBODY DRAG COEFFICIENT= 0.16222

(d) Tabulated solution and plot of C_p.

Figure 24.– Concluded.

TABLE I. RELATION BETWEEN EXTERNAL DATA SETS AND INPUT/OUTPUT LOGICAL UNIT NUMBERS

Data File (fig. 16)	Logical Unit	
	Input	Output
1	14	9
2	13	8
3	12	2
4	15	10
5	11	3

TABLE II. BASIC INPUT DATA

ITEM NO.	VARIABLES	FORMAT
1	TITLE (Three cards)	20A4
2	NRSTRT,NPRINT,N3,ILIM,IITER	5I5
	If NRSTRT $\neq$ 0 and N3 $\neq$ 0, skip to item 12	
	If NRSTRT $\neq$ 0 and N3 $\neq$ 0 stop. No further input is necessary	
3	LPROG,N1,N2,IBL,IUNIT,MIT	6I5
4	GAM,AMINF	
	If LPROG = 1 skip to item 13	
5	IXY	I5
	If IXY = 0, skip next card	I5
6	XO,YO (IXY cards)	2F10.0
7	IMAX,JMAX,MHALF,KLOSE,LREADP	5I5
8	DNDZO,XIXM,XM,DSDXIM,XBT,DMAX,XZNEW	7F10.0
9	PLUMIN	L5
	If PLUMIN = FALSE, skip next card	
10	GAMAP,PTPPFS,AMP,THETAP,TTP,GMP,DELCZ	7F10.0
	If LPROG = -1, skip remaining cards	
11	LSEP	L5
	If LSEP = FALSE, skip next card	
12	XSEP,THETS	2F10.0
	If NRSTRT $\neq$ 0 stop. No further input is necessary	

TABLE II. (Concluded)

ITEM NO.	VARIABLES	FORMAT
13	IOPT,K,LVAR1,LSHAPE,LIC,LDSTAR,LSHPBL	7I5
	If LPROG ≠ 1 or if LPROG = 1 and both IOPT = 1 and LVAR1 = 2, skip items 14 and 15	
14	NVAR	I5
15	XVAR,VAR	2F10.0
16	EL,PT,TT,TWONTT,VISC,RGAS,SCON,DFACT	8F10.0
17	XZ,RLEN,XT,DXP,HLIM	5F10.0
	If LSHAPE ≠ 0, skip next card	
	If LIC = 1, input CFC1 and DELTA1	
	If LIC = 2, input CFC1 and DELST1	
18	CFC1,DELTA1 (or DELST1)	2F10.0
	If IOPT = 1, skip next card	
19	UE1,DUEDX	2f10.0
	If LSHPBL = 0 and LPROG = 0, skip items 20 and 21	
20	NR	I6I5
21	XRP,RL	2F10.0

TABLE III. SUMMARY OF INPUT DATA FOR RESTARTING

ITEM NO.	VARIABLES	FORMAT
1	TITLE (Three cards)	20A4
2	NRSTRT,NPRINT,N3,ILIM,IITER	5I5
	If N3 = 0 stop. No further cards are necessary	
3	XSEP,THETS	2F10.0

NOMENCLATURE

A	cross sectional area of inviscid plume
A_{nj}	coefficients in equations (47), (48), (54), (56), (60), (116) and (124)
A'_{nj}	coefficients in equations (124) and (125)
A^*	cross sectional area at a sonic throat
a	speed of sound
a_{nj}	coefficients in equations (61) to (63)
B_n	coefficients in equations (47), (48), (54), (56), (116), and (126).
b_n	coefficients in equations (61), (62) and (64)
C	Chapman-Rubesin parameter, equation (31)
C_c	parameter defined by equation (82)
C_f	skin-friction coefficient
c_p	specific heat at constant pressure
D	factor in mixing layer temperature profile, equation (81)
f	weighting function defined by equation (39)
G_n	integral functions defined by equations (49) and (123)
g	acceleration of gravity
H_i	transformed shape factor, equation (66)
I_n	integral functions defined by equations (50) and (58)
J	conversion factor used in equations (33) and (35)
J_n	integral functions defined by equations (51), (52), and (59)
K	entrainment fraction, equation (74)
$\overline{K}$	factor defined by equation (53)

NOMENCLATURE (Continued)

k	factor in equations (8) and (9)
L	reference length
M	Mach number
m	Mach number function $\frac{1}{2}(\gamma-1)M^2$
P_n	functions defined by equations (120) to (122)
p	pressure
q_p	velocity in inviscid exhaust plume, equation (11)
R	gas constant
R_n	functions defined by equations (117) to (119)
r	radius
S	temperature function, equations (17) and (84)
S_n	temperature function at nozzle exit, equation (80)
S_s	temperature function in fully developed mixing layer, equation (83)
s	rms error of boundary-layer-edge velocity, equation (5)
s_θ	rate of change of s with θ_s, equation (6)
s_x	rate of change of s with x_s, equation (7)
T	temperature
T_s	constant in Sutherland's viscosity relation, equation (31)
t	factor in transformed boundary-layer equations, equation (26)
U,V	transformed velocity components, equations (28) to (30)
U_β	wake velocity factor, equation (40)
U_τ	friction velocity, equation (41)
u,v	velocity components of physical flow field, figure 4

NOMENCLATURE (Continued)

u_n	velocity function at nozzle exit, equations (75) and (76)
u_s	velocity function in fully developed mixing layer, equations (77) and (78)
$\tilde{u},\tilde{v}$	transformed velocity components, equations (22) and (23)
X,Y	transformed coordinates, equations (28) to (30)
x,y	coordinates of physical flow field, figure 4
x_p	axial location of minimum u_e downstream of boattail
x_s	axial location of separation point
$\tilde{x},\tilde{y}$	transformed coordinates, equations (18) and (19)
Y^+	coordinate of logarithmic part of boundary layer, equation (42)
α	damping factor for viscid-inviscid iterations, equation (4)
β	eddy-viscosity factor, equations (15), (16), (43), and (45)
β_T	value of β for fully turbulent flow
β_t	value of β in transition zone between laminar and turbulent flow
γ	ratio of specific heats
δ	boundary layer thickness
δ_c	thickness of nozzle internal boundary layer or thickness of inner part of mixing layer
δ_i	transformed boundary layer thickness
δ_{u_1}	value of δ for external boundary layer at nozzle exit
δ^*	boundary layer displacement thickness, $\int_o^\delta (1 - \frac{\rho u}{\rho_e u_e})\frac{r}{r_w}\, dy$

NOMENCLATURE (Concluded)

δ_k^* boundary layer displacement thickness, $\int_0^\delta (1 - \frac{u}{u_e}) dy$

ε eddy viscosity for mixing layer, equation (86)

$\bar{\varepsilon}$ constant in eddy viscosity of mixing layer, equation (86)

θ_s angle of separated displacement surface with the axis, equation (2)

κ factor in transition region eddy viscosity, equation (46)

μ molecular viscosity

ν μ/ρ

ρ density

τ shear stress

SUBSCRIPTS

c refers to inviscid core, inner edge of mixing layer

e refers to boundary layer or mixing layer external edge

I refers to inviscid flow

o refers to free stream reference conditions

t refers to stagnation conditions

V refers to viscous flow

w refers to the solid surface or the inviscid plume boundary

x,y denotes differentiation with respect to x, or y

SUPERSCRIPT

' denotes differentiation with respect to y/δ